SECTION 6: ZONES OF INFLUENCE OF EMISSIONS

OBJECTIVES

The principal objective of this subtask is to estimate the areas of upwind influence for the core and other monitoring sites during PM episodes.

APPROACH

Three methods were employed. First, the gridded concentration fields, described in Section 5, were examined to identify concentration gradients. The gradients were qualitatively evaluated to identify approximate distances over which concentration peaks diminished to both urban and regional background levels. The gridded concentration fields were also compared with maps of emission densities.

Second, a series of regressions of site concentrations versus emissions densities were carried out. Emission densities were determined for a variety of scales of spatial averaging and the averaging scales that provided the best fits between concentrations and emissions were identified. The regressions included PM_{10} mass versus primary PM_{10} emissions, PM_{10} mass less secondary aerosol concentrations versus primary PM_{10} emissions, PM_{10} carbon mass versus emissions from motor vehicles and residential fuel combustion, and PM_{10} geological-species mass versus emissions from sources of geological materials (including agricultural activities, paved and unpaved road dust, construction, and other categories).

The third method employed a dispersion model. Daily peak particulate concentrations at the core sites during selected fall and winter dates were identified. We used a Gaussian puff model (Petersen and Lavdas, 1986) in a "backwards" mode, as described more fully under "Methods" below, to delineate the upwind boundaries of the zones in which emission sources contributed to the observed concentrations during the specified time periods.

METHODS

The methods used for generating concentration contours from the saturation networks are fully described in Section 5. The plots shown in Appendix C, as well as plots for individual days, were examined to approximately identify the magnitudes of concentration gradients and the distances separating network maxima and minima.

Gridded emission files (4 km x 4 km resolution) were obtained from the ARB, as described in Section 2. Daily summary files were used to obtain estimates of point, area, motor vehicle, and total primary PM emissions for each grid cell, as well as daily emissions of gas-phase precursor species, such as NO_x. The hourly emission files, disaggregated by 113 source categories, were reaggregated to provide daily gridded estimates of PM components, including geological materials as well as carbon-containing emittants (e.g., from sources such as residential fuel combustion), as described in Section 2.

For the regressions, average site concentrations were obtained for each site with data during the fall monitoring period (November 1 through 14), the winter period (December 9 through January 6), and the winter episodes (December 9 and 10 and 26 through 28 and January 4 through 6). The average concentrations were regressed against emission densities, averaged over the same sets of days, determined for various spatial scales as described below. Time averaging of concentrations was employed to reduce uncertainties in the daily concentration values.

For each site, emission densities were determined for a variety of spatial scales, beginning with the 4 km x 4 km grid cell in which the site was located, continuing with the nine-cell square whose center cell contained the site, and continuing with progressively larger scales. The emissions scales that yielded the best fit between emission densities and PM concentrations were then identified.

The upwind dispersion calculation was carried out by placing a surface-level (2 m) pseudo-source at the location of a monitoring site and computing the resulting "concentration" field. Because we reversed the time sequence and directions of the winds, each "concentration" field delineated an upwind area of influence, rather than a (downwind) plume. "Emissions" were released from each pseudo-source during the three hours corresponding to each PM peak and were tracked upwind for an additional nine hours. The "concentration" fields consisted of the predicted 12-hour mean concentrations at surface level (2 m) at a 50 x 50 grid of points spaced at 1 km intervals. Calculations were carried out specifying three deposition velocities: 0, 0.1, and 1 cm sec^{-1}. Results for the latter two are taken here to be indicative of the transport of primary fine and coarse particulate, respectively.

The puff model uses as input two-dimensional wind fields derived from surface observations, which were taken from wind fields provided by the ARB. We used the standard deviation of wind direction (sigma theta), as recorded at the surface monitors, to determine dispersion. Mixing heights were obtained from T&B Systems. As described in Section 2, the mixing heights determined by T&B Systems from the Bakersfield and Fresno soundings were sometimes substantially different from those that had been obtained from the diffusion break calculation of the IMS95 meteorological model. For consistency, we have used the mixing heights from T&B Systems (the modeled mixing heights were available only for the January episode).

Table 44 shows which sites and dates were selected for analysis based on peak particulate levels. The last column indicates for which cases model calculations were completed or were not completed because of missing data. The peak hour shown in the table is the beginning hour of each 3-hour peak.

Table 44. Summary of dispersion calculations.

DATE	SITE	PEAK	STATUS
12/25/95	Bakersfield	2100	site meteorological data missing
		600	site meteorological data missing
	Kern	900	completed
		1800	completed
	Fresno	2300	site meteorological data missing
	SW Chowchilla	900	completed
12/26/95	Bakersfield	1500	completed
	Kern	900	completed
		1800	completed
	Fresno	2100	completed
	SW Chowchilla	1500	completed
12/27/95	Bakersfield	1800	completed
	Kern	1500	completed
	Fresno	2100	site meteorological data missing
	SW Chowchilla	1200	completed
1/4/96	Bakersfield	900	completed
	Kern	2100	completed
	Fresno	2100	completed
	SW Chowchilla	1500	completed
1/5/96	Bakersfield	0	completed
		2100	completed
	Kern	900	completed
	Fresno	0	completed
		1800	site meteorological data missing
	SW Chowchilla	1500	site meteorological data missing

DATE	SITE	PEAK	STATUS
1/6/96	Bakersfield	1800	completed
	Kern	1200	completed
	Fresno	0	site meteorological data missing
		2100	site meteorological data missing
	SW Chowchilla	1200	site meteorological data missing
11/12/95	all sites	---	Incomplete—no mixing heights available
12/9/95 12/10/95	all sites	---	not completed

RESULTS

Spatial Concentration Gradients

Plots depicting gridded contours of PM_{10} mass, crustal, carbon, and secondary species concentrations, prepared for each saturation domain as described in Section 5, were examined for each episode day. In addition, days were averaged to produce mean gridded contour plots, which may be found in Appendix C. A summary of the results was prepared by qualitatively examining the mean contour plots, as well as plots for individual days (see Table 45).

Table 45. Summary of gradients observed in saturation monitoring networks.

Characteristic	Variable	Network			
		Bakersfield	Corcoran	Fresno	Kern
Dimensions	East-west (km)	30	20	25	17
	North-south (km)	10	36	32	10
	Area (km^2)	300	720	800	170
Range of mean site concentrations during episodes	Mass	48-66	100-175	45-78	34-40
	Crustal	2-7	32-58	2-7	1.4-1.7
	Carbon	13-24	14-30	18-35	No data
	Secondary	24-27	25-30	20-26	No data
Observed gradients ($\upsilon g\ m^{-3}\ km^{-1}$)	Mass	1	10-50	<1-4	0.2-0.6
	Crustal	<0.2	0.5-10	<0.3-1	0.02
	Carbon	1	0.2-10	<0.3-3	No data
	Secondary	0.05-1	0-1	<1	No data
Usual maximum sites	Mass	B2,3,10	C5	F27	K15
	Crustal	B10	C5	F19,30,39	K15
	Carbon	B2,4	C5	F27	No data
	Secondary	B4,5	various	F39	No data
Distance between maxima and minima (km)	Mass	10-15	5-10	10-15	~10
	Crustal	10-15	5-10	5-20	~10
	Carbon	~10	5-10	5-10	No data
	Secondary	5-10	10-25	5-10	No data

As shown in Table 45, the saturation networks range in size from 10 to 20 km along the shorter dimension and from 17 to 36 km along the longer. While they are large enough to cover the urban areas of Bakersfield, Fresno, and Corcoran, the three urban networks probably are not large enough to include sites whose concentrations represent regional background values. This conclusion may be justified by noting that the minima in the Bakersfield and Fresno networks exceed the maxima in the Kern network (see Table 45). Thus, the minima observed in the Bakersfield and Fresno networks should be considered as urban background, rather than regional background. The distances between the maxima and minima therefore represent the scales over which local maxima decay to the urban background level. However, emissions may also contribute to the regional background over larger scales than can be observed in the networks.

The gradient of PM_{10} mass in the Corcoran network is 10 to 50 $\upsilon g\ m^{-3}\ km^{-1}$ (see Table 45). Therefore, substantial concentration changes occurred over distances of the order of 1 km, implying that nearby emission sources often influenced site concentrations substantially. In contrast, gradients of PM_{10} mass during the winter in the other three networks ranged from less than one to a few $\upsilon g\ m^{-3}\ km^{-1}$, implying either more uniform emissions influences, lower deposition rates, broader dispersion, or a combination of theses factors, relative to the fall data.

From Table 45, it may be seen that the distance between network minima and maxima PM_{10} mass is about 5 to 10 km in the fall (Corcoran network) and 10 to 15 km in the winter (remaining three networks). Similar distances are found for the crustal and carbon components. Thus, the distance scale for the decay from peak to urban background values was about 5 to 10 km in Corcoran and 10 to 15 km elsewhere. However, the range of influence of emission sources may be greater than these scales since, as noted earlier, the network domains are not large enough to capture the decay from urban background levels to regional background levels.

The network concentration maxima, typically found at or close to the sites listed in Table 45, are located in or adjacent to the grid cells having the highest emission densities (see Appendix D). In the Bakersfield network, sites B01, B12, B04, and B07 are located in the grid cell with the highest primary PM emissions. PM mass maxima typically occurred at sites B04, B02 or B03 (located in grid cells adjacent to the highest emission density-cell), or B10, which was also associated with maxima in crustal components.

In the Fresno network, PM mass maxima typically occurred at sites F27, F21, F20, or F41. These sites are located one grid cell west of the cell having the highest emissions of primary PM (see Appendix D). However, they are within the cell having the highest PM emissions from motor vehicles (see Appendix D). Since motor vehicle emissions probably correlate with population density, the maximum Fresno sites appear to be close to the maximum emissions from motor vehicles and other sources of fine PM, such as residential fuel combustion. The measurements show that the winter PM mass was dominated by carbon and secondary species, occurring on the fine fraction (see Section 7). Hence, the closer similarity of the pattern of PM concentrations to motor vehicle emission density, rather than to total PM emissions, is not unexpected.

In the Corcoran network, maximum PM concentrations occurred at site C05, adjacent to the railroad tracks and located in the industrial area on the east side of the city. A second maximum was observed near sites C13 and C18, between Corcoran and Hanford. These three maximum sites are located in grid cells having the highest area-source emissions, but one cell west of the grid cells having the highest total PM emissions. The difference between the area-source and total emissions is due to point sources within two grid cells. Since site C05 is situated within a few hundred meters of several major point sources, it appears that the emission grid resolution is too coarse to capture the exact location of the point sources, or the sources may have been

displaced by one grid cell. In either case, the Corcoran concentration maxima occur close to the maximum emissions.

The spatial coincidence of network concentration maxima with areas of high emission density, with some variation fom day to day, indicates that pollutant transport was limited in all saturation networks. A more quantitative analysis of the relationship between emissions and concentrations is presented in the next subsection.

Regressions of Concentrations Against Emission Densities

Regressions of average concentrations against emission densities, determined for a variety of spatial scales, were carried out as described previously. As noted, emissions were determined for each site beginning with the 4 km x 4 km grid cell in which the site was located, continuing with the nine-cell square whose center cell contained the site, and continuing with progressively larger scales. Therefore, the mean distances from the site to the outer boundary of each progressively larger square of emissions increased according to the following series: 2 km (1-cell area), 6 km (9-cell area), 10 km (25-cell area), 14 km (49-cell area), 18 km (81-cell area), and so on up to 70 km. In the results that follow, we use distances rather than areas or cell numbers to identify spatial scales.

During the winter period, regressions of PM_{10} mass against primary PM emissions at the 2 km scale showed only a modest relationship between concentrations and emission densities (see Figure 48, top panel). While boundary sites and Kern saturation sites exhibited both the lowest concentrations and the lowest 2 km-scale emission densities, the Fresno and Bakersfield saturation sites spanned a wide range of 2 km scale-emission densities that did not correlate with the sites' concentrations. The best regression was obtained for the 14 km scale (see Figure 48, center panel). Correlation coefficients decreased as the emissions averaging scales increased beyond 14 km (see Figure 48, bottom panel, for the 30 km scale).

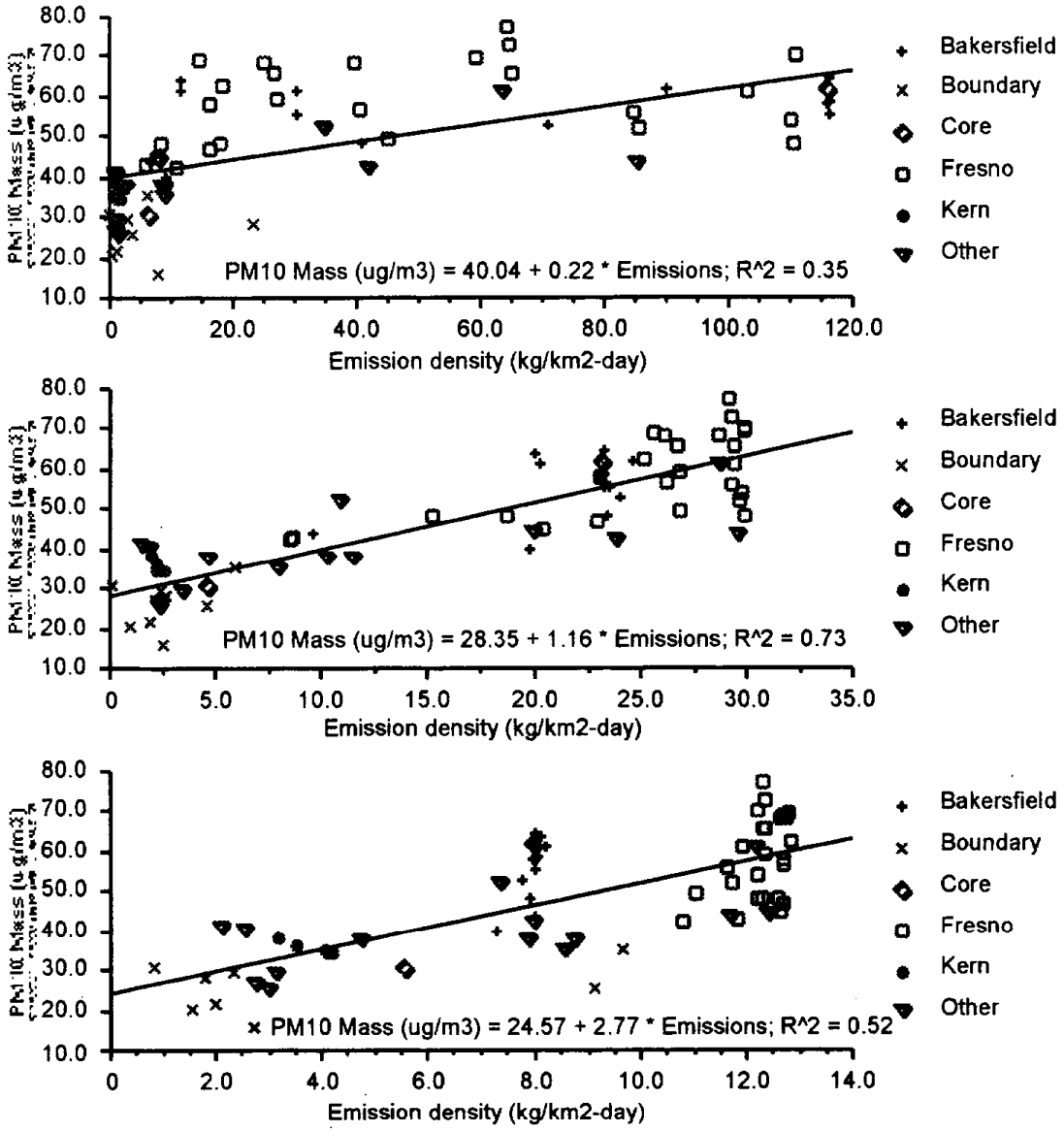

Figure 48. Regressions of PM_{10} mass against emissions density for spatial scales of 2 km (top), 14 km (middle), and 30 km (bottom). Both concentration and emissions density were averaged over winter episode days (see text).

Additional regressions were carried out to associate PM components with corrresponding emissions as follows: PM_{10} mass minus secondary-species concentrations versus primary PM emissions, PM carbon concentrations (CAR) versus the sum of motor vehicle and residential fuel combustion emissions, PM crustal component (CRU) versus emissions from source categories having emissions dominated by geological materials (e.g., paved and unpaved road dust, agricultural emissions, etc.), and PM secondary-species concentrations (SEC) versus NO_x emissions. Although fewer sites had speciated data than mass measurements, the additional regressions supported the results for mass versus primary PM emissions (see Figure 49, top panel). Except the regressions of secondary species against NO_x, which showed a distance scale on the order of 40 km, all regressions exhibited the highest correlation coefficient for a distance scale of 14 km. High correlation coefficients persist for longer distances in the case of the regressions of PM carbon and PM mass less secondary species (in the latter case, the intercept shown in Figure 49 was reduced to less than 10 $\mu g\ m^{-3}$, while the slope remained about the same as shown). However, these regressions used many fewer sites than did those for PM mass and therefore may be less reliable. In general, the regressions for the longer distance scales do not explain concentration variations among sites within each of the saturation networks (see Figure 48, bottom panel), whereas those at the 14 to 18 km scale more adequately associate saturation sites having lower concentrations with lower emission densities (Figure 48, center panel). However, the correlations for the regressions at the longer distances suggest the occurrence of some regional-scale (20 to 50 km) transport and dispersion.

Regression results were also expressed in terms of mean-square error, rather than correlation coefficient. This change did not affect the results (because the dependent variable, concentration, was not spatially averaged, the degrees of freedom are the same regardless of scale and the correlation coefficient is a function of the mean square error).

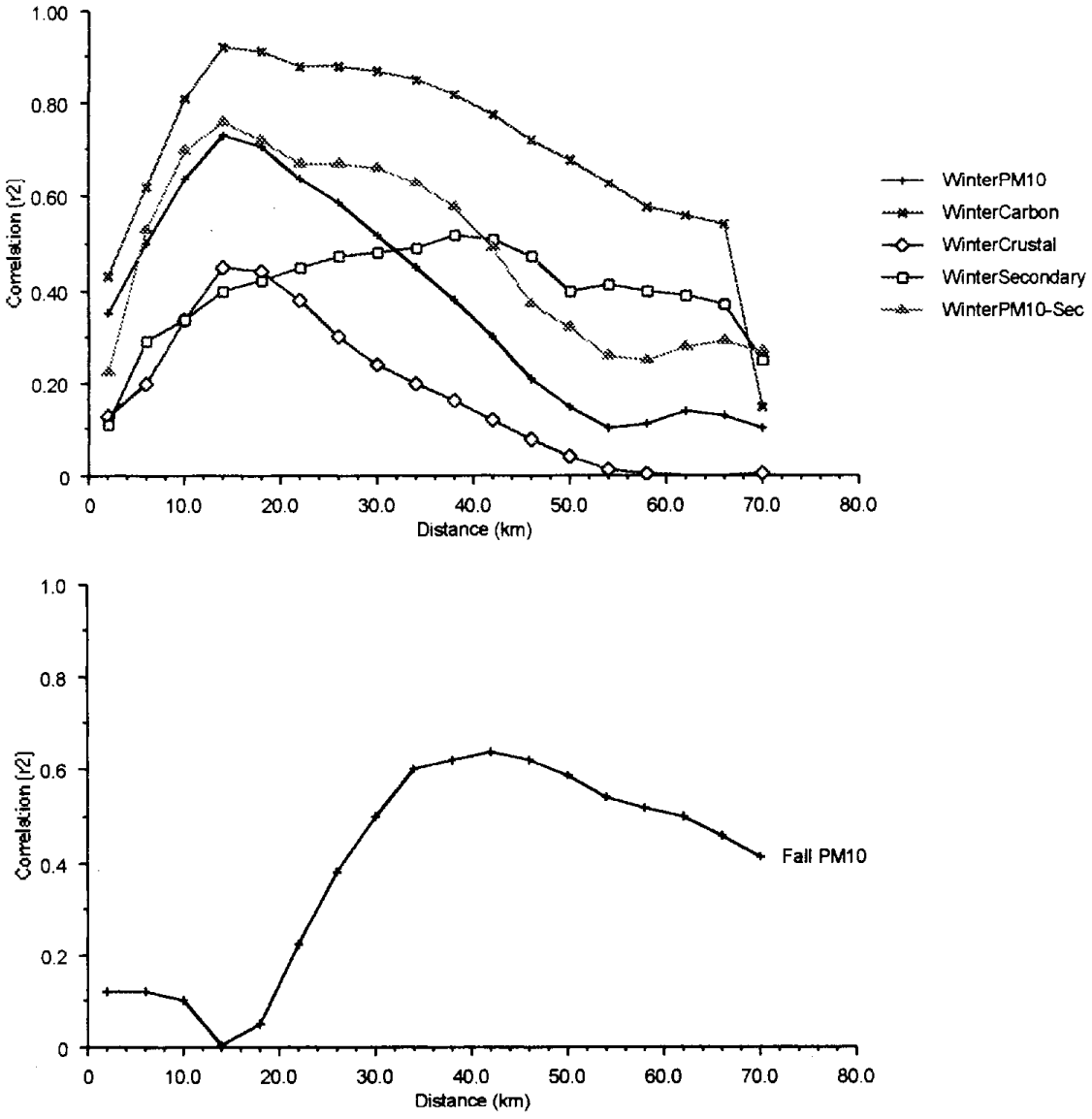

Figure 49. Correlation coefficient (r^2) of regressions versus distance scale used for spatial averaging of emissions (see text) for winter (top) and fall (bottom) data.

The winter regression results indicate that transport and dispersion of emissions occurred on a scale of about 15 km (urban scale). Local influences (neighborhood scale, 0.5 to 4 km) may have been superimposed upon the urban-scale dispersion, but the regressions are not capable of discerning such influences (emissions grid-cell resolution is only 4 km x 4 km). However, the scatter occurring in the best regressions (Figure 48, center panel) indicates that some sites were influenced by nearby emission sources. The higher mean PM_{10} concentrations in the Fresno and Bakersfield networks were 60 to 80 $\mu g\ m^{-3}$, while the urban background was about 40 $\mu g\ m^{-3}$. The regressions are also consistent with regional dispersion of PM emissions on scales exceeding 15 to 20 km, since correlation coefficients remain high for scales exceeding the 14 km scale of the best fit regressions.

The fall regression results (see Figure 49, bottom panel) exhibited a peak correlation coefficient at 42 km and no correlation at scales less than 20 km. These results might reflect weaknesses in the emission inventory. They might also define a regional scale of influence, upon which local influences (see previous discussion of concentration gradients) may have been superimposed. Urban sites (in Fresno and Bakersfield) showed lower PM_{10} concentrations in the fall than did the Corcoran sites, even though emission densities were greater in the urban areas (see Figure 50, top panel). On larger averaging scales (see Figure 50, bottom panel), the Corcoran concentrations were associated with higher emission densities, thus indicating the contribution of a regional background concentration to the overall values observed at the Corcoran sites. This contribution could have been as great as about 100 $\mu g\ m^{-3}$, which is the mean value observed at the lowest-concentration sites in the Corcoran saturation network. The variability within the Corcoran network is not explained by the regressions, thus demonstrating the significance of local source contributions (for example, the highest concentration indicated in Figure 50 occurred at site C05, which was previously shown to exhibit emission influences on the scale of 1 km).

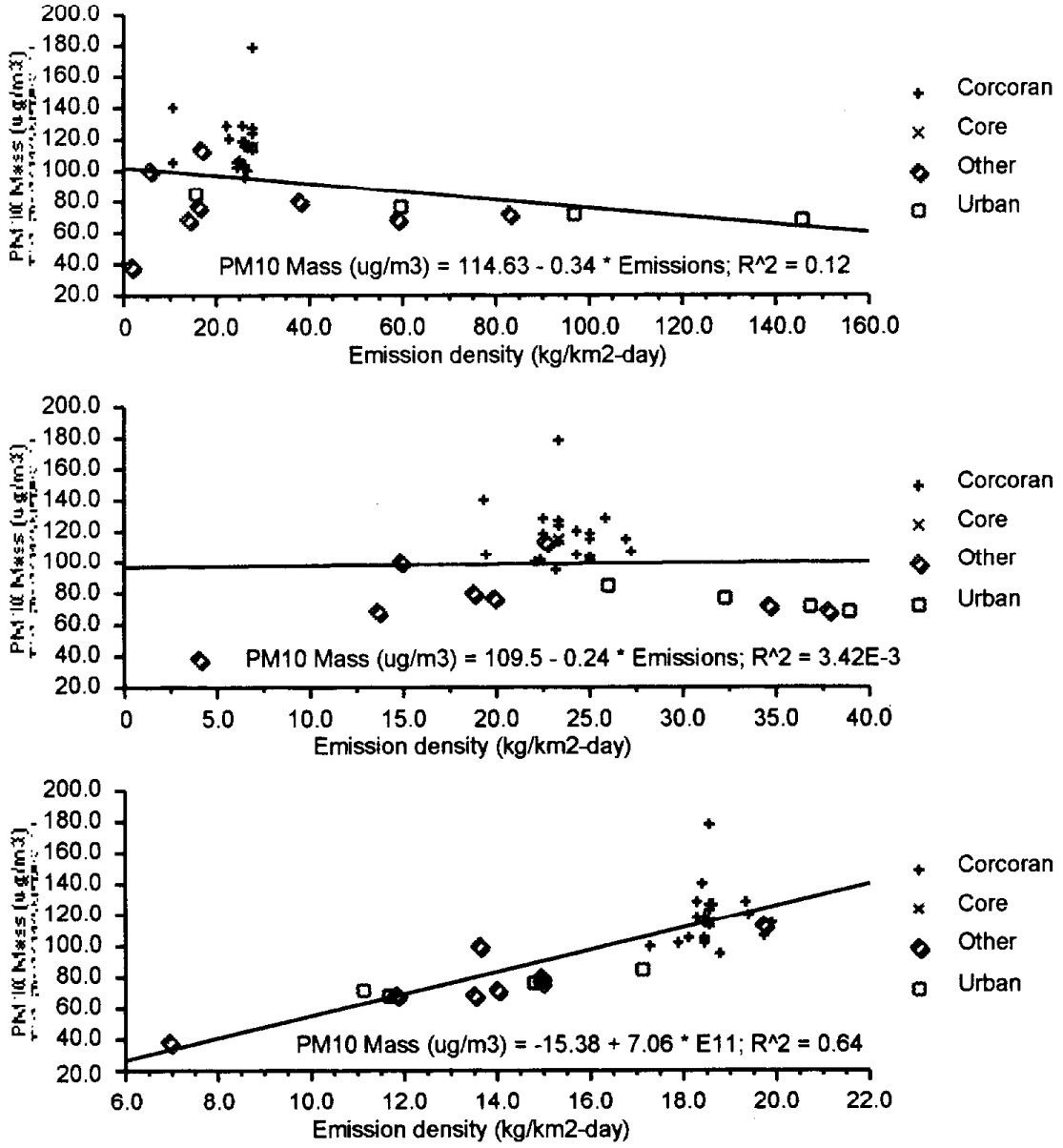

Figure 50. PM_{10} mass versus emissions density averaged over spatial scales of 2 km (top), 14 km (center) and 42 km (bottom). Both concentration and emission density were averaged over the period 1-14 November 1995.

Dispersion Model Results

Plots are included for the December 25-27 and January 4-6 episodes (see Figures 51 through 68). In these figures, the influence scale uses arbitrary units such that the sum over all points would be 100 if the back-trajectory were to remain entirely within the domain shown and the mixing height were a constant 100 m. (When mixing heights exceed 100 m during part of a simulation, the estimates of relative influence are lower as a consequence of dilution). For each case, results are shown using deposition velocities of both 0.1 and 1 cm sec^{-1}.

By themselves, the puff estimates do not indicate relative emission influence (even for chemically inert species), except for the special case of a spatially homogeneous emission field. The puff model estimates of relative influence must be combined with gridded emission estimates to generate estimates of relative source contributions, by source category. However, the model estimates do indicate ranges of influence. The puff model calculations show substantial source influence for locations less than 5 to 15 km of receptor sites and less influence, but more geographically widespread, from locations within about 15 to greater than 25 km. These ranges are somewhat less for the analyses with deposition velocities set to 1 cm sec^{-1} (corresponding to coarse particulate). The results suggest a scale of local emissions influence of a few up to about 15 km, and a scale of approximately 20 km over which emissions are more widely dispersed but still contribute to general background levels.

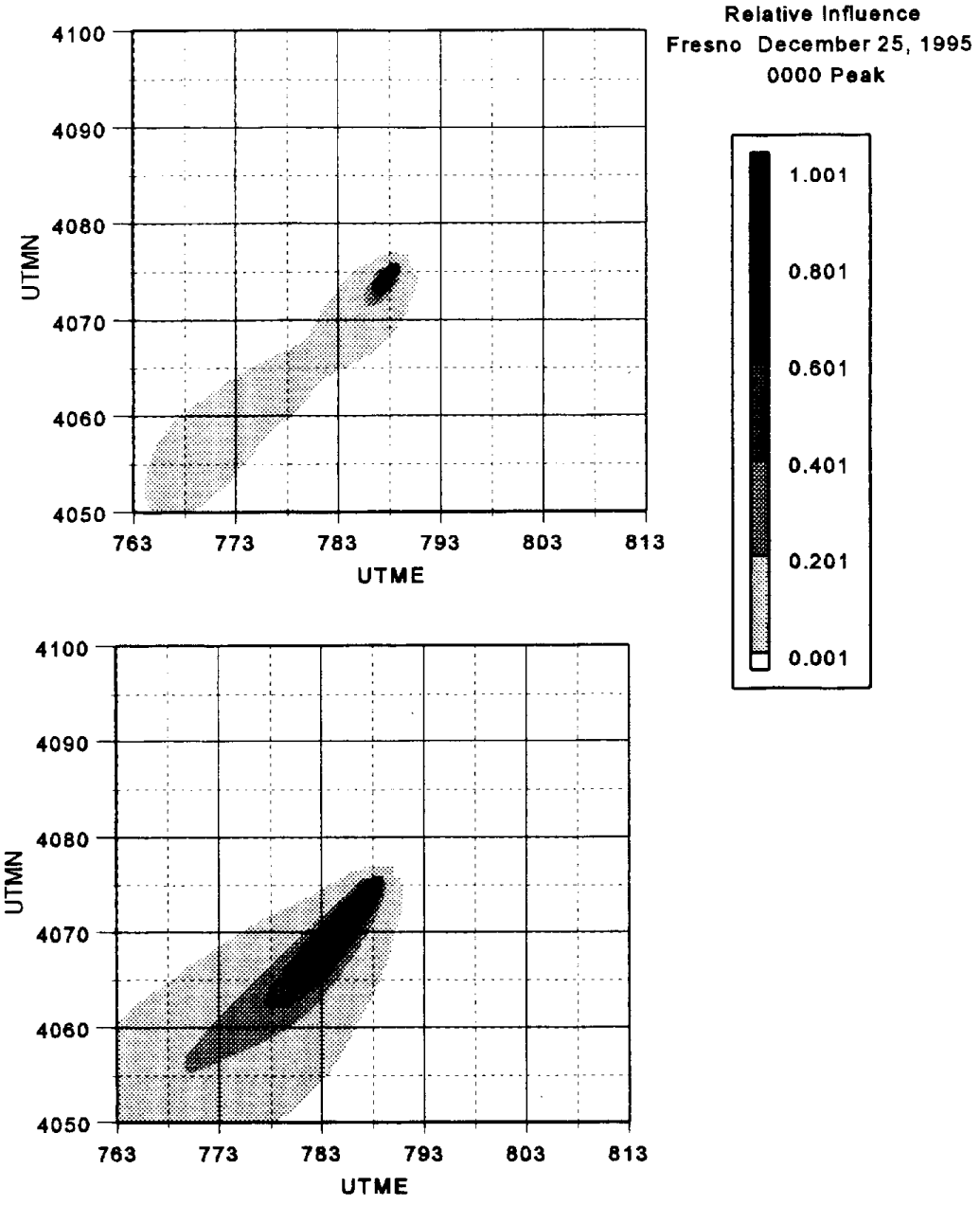

Figure 51. Relative influence of source areas on the Fresno sample collected from 0000 to 300 December 26. Top chart has deposition velocity of 1.0 cm/sec; bottom chart has deposition velocity of 0.1 cm/sec.

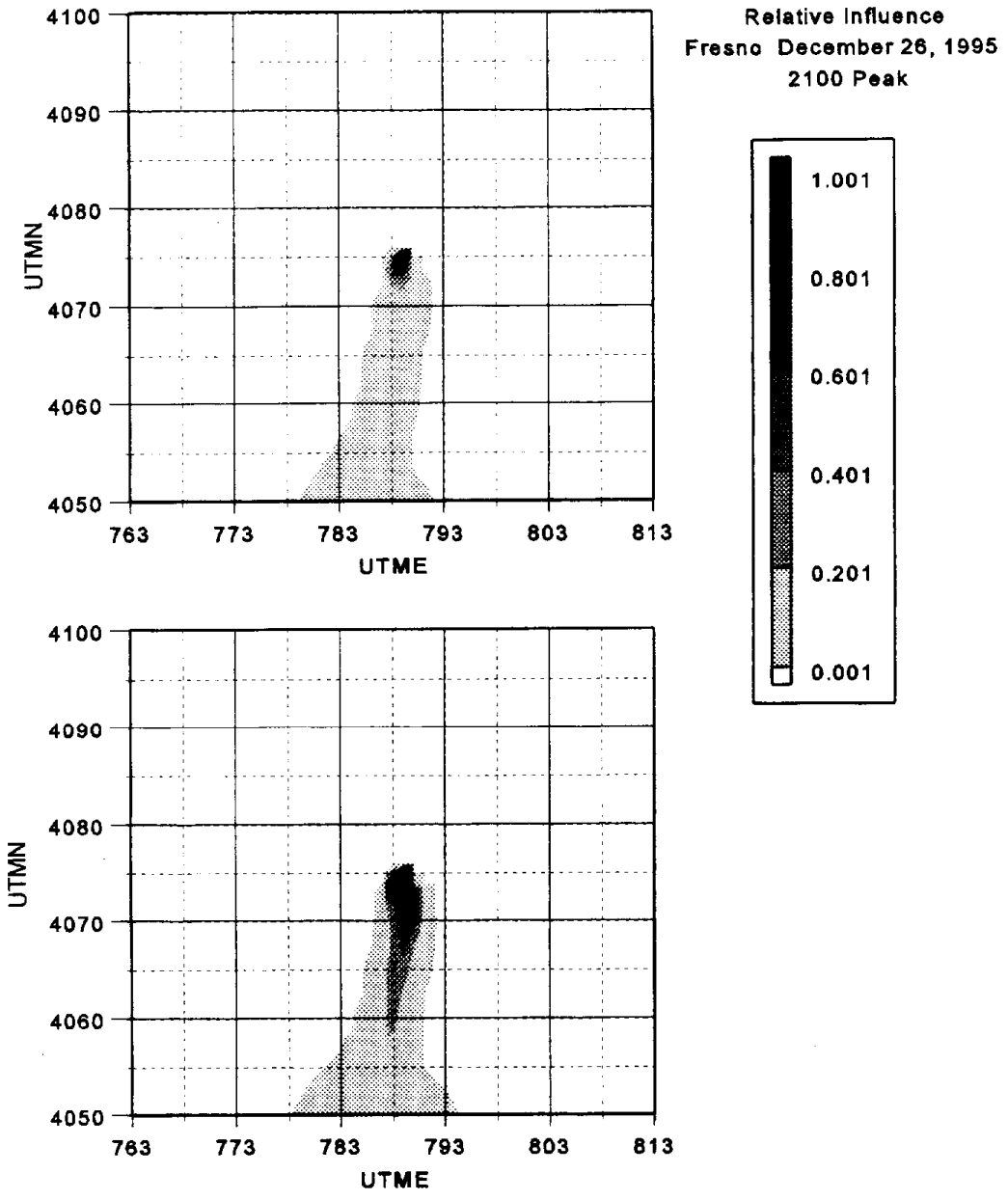

Figure 52. Relative influence of source areas on the Fresno sample collected from 2100 December 26 to 0000 December 27. Top chart has deposition velocity of 1.0 cm/sec; bottom chart has deposition velocity of 0.1 cm/sec.

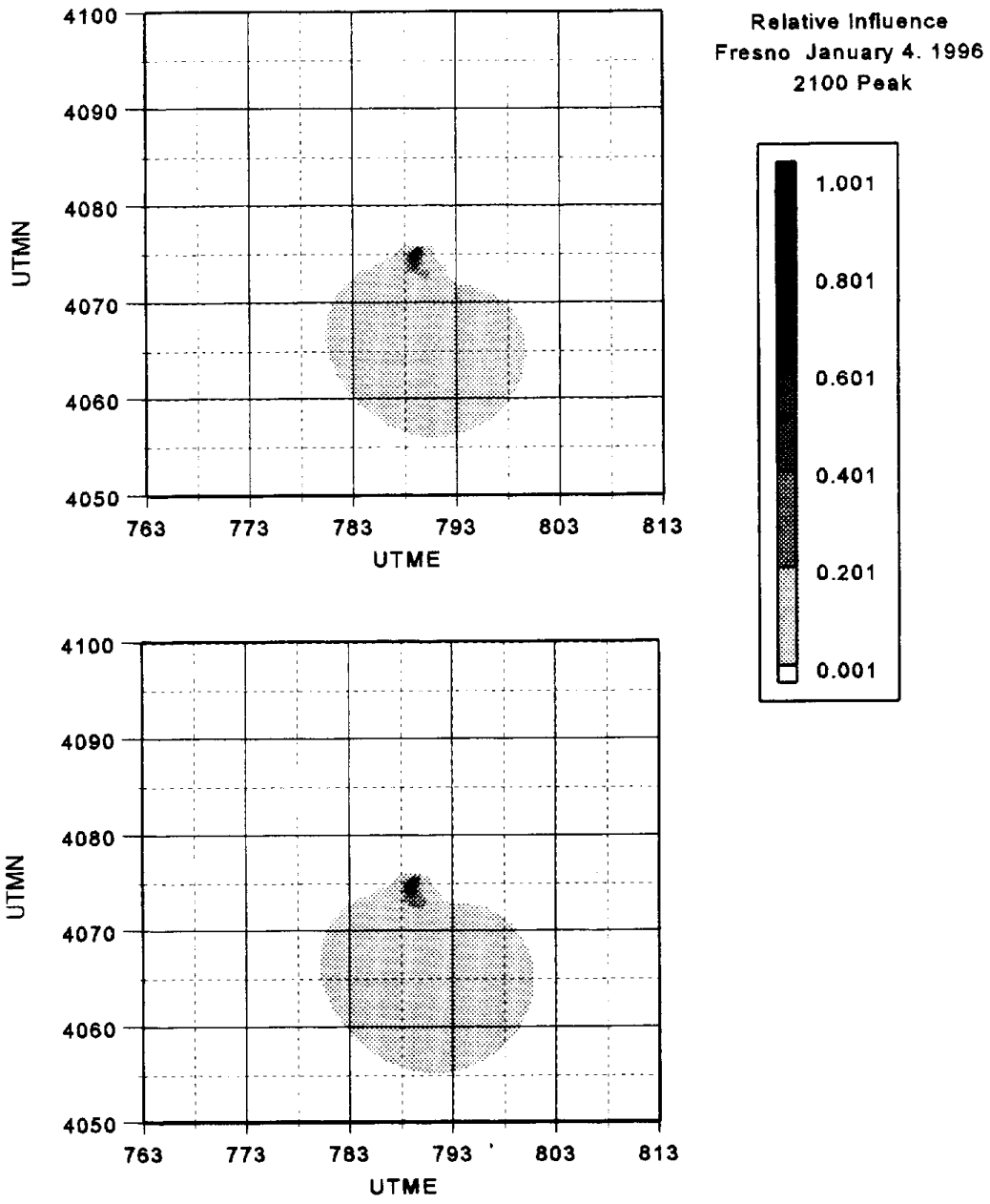

Figure 53. Relative influence of source areas on the Fresno sample collected from 2100 January 4 to 0000 January 5. Top chart has deposition velocity of 1.0 cm/sec; bottom chart has deposition velocity of 0.1 cm/sec.

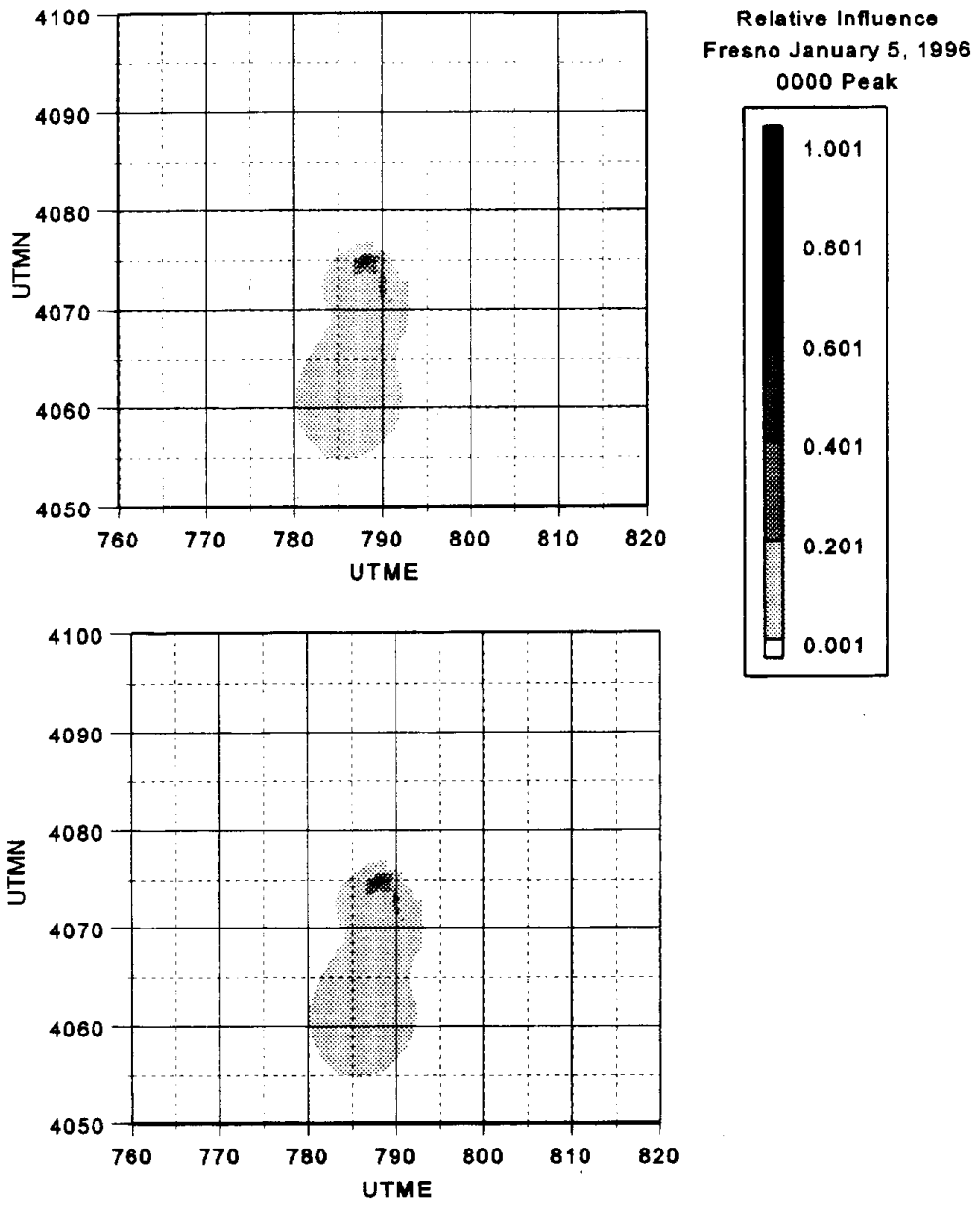

Figure 54. Relative influence of source areas on the Fresno sample collected from 0000 to 300 January 5. Top chart has deposition velocity of 1.0 cm/sec; bottom chart has deposition velocity of 0.1 cm/sec.

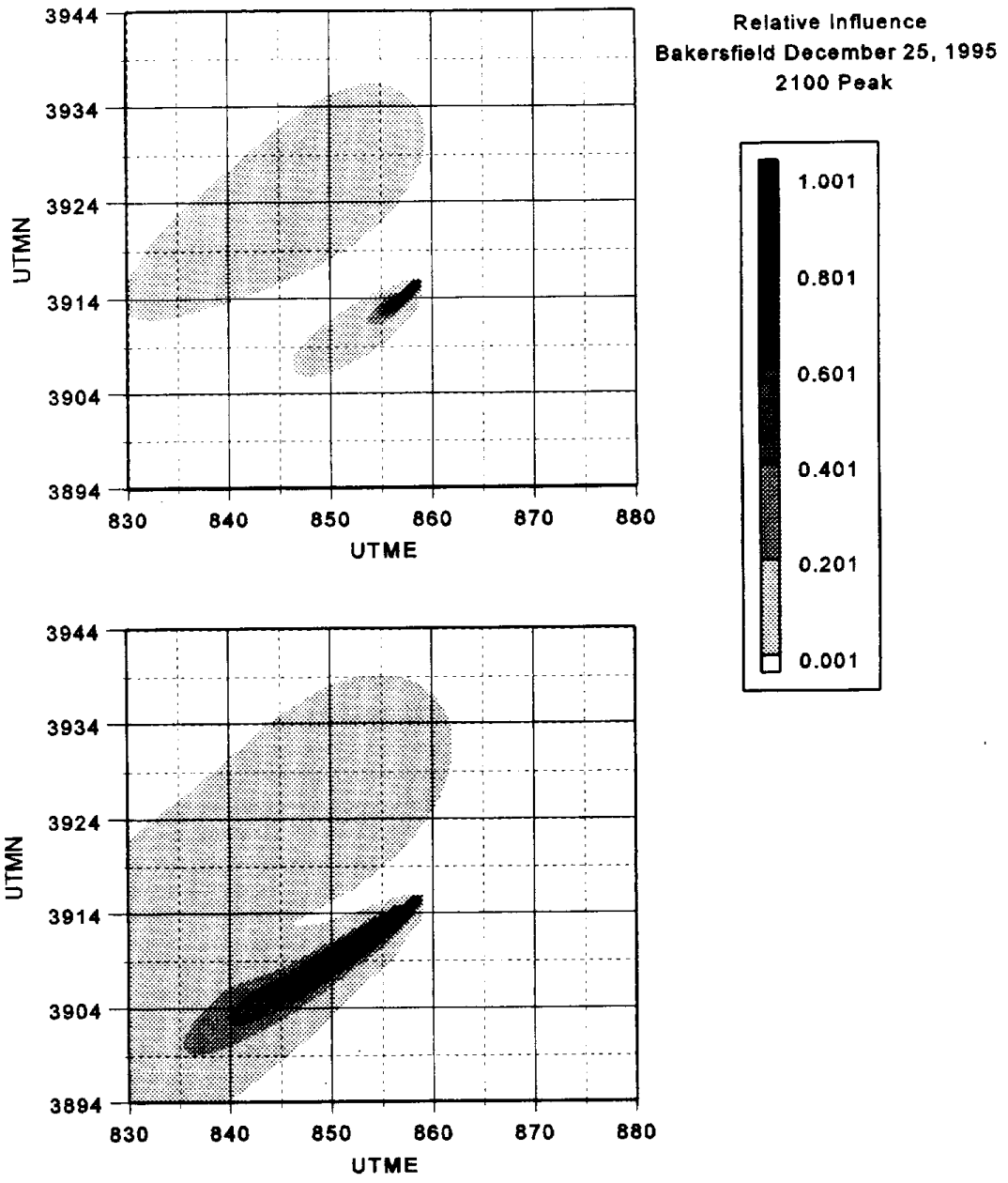

Figure 55. Relative influence of source areas on the Bakersfield sample collected from 2100 December 25 to 0000 December 26. Top chart has deposition velocity of 1.0 cm/sec; bottom chart has deposition velocity of 0.1 cm/sec.

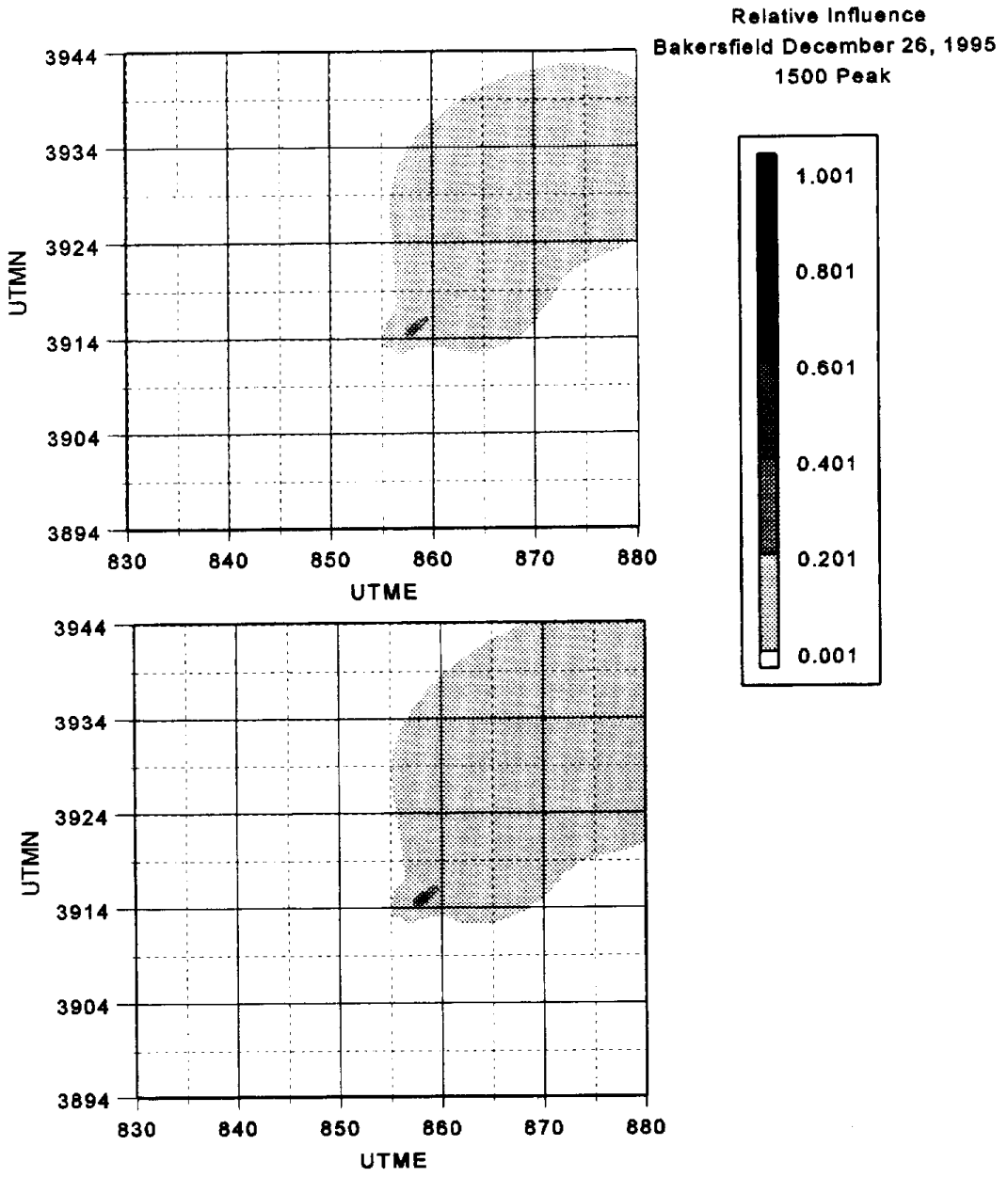

Figure 56. Relative influence of source areas on the Bakersfield sample collected from 1500 to 1800 December 26. Top chart has deposition velocity of 1.0 cm/sec; bottom chart has deposition velocity of 0.1 cm/sec.

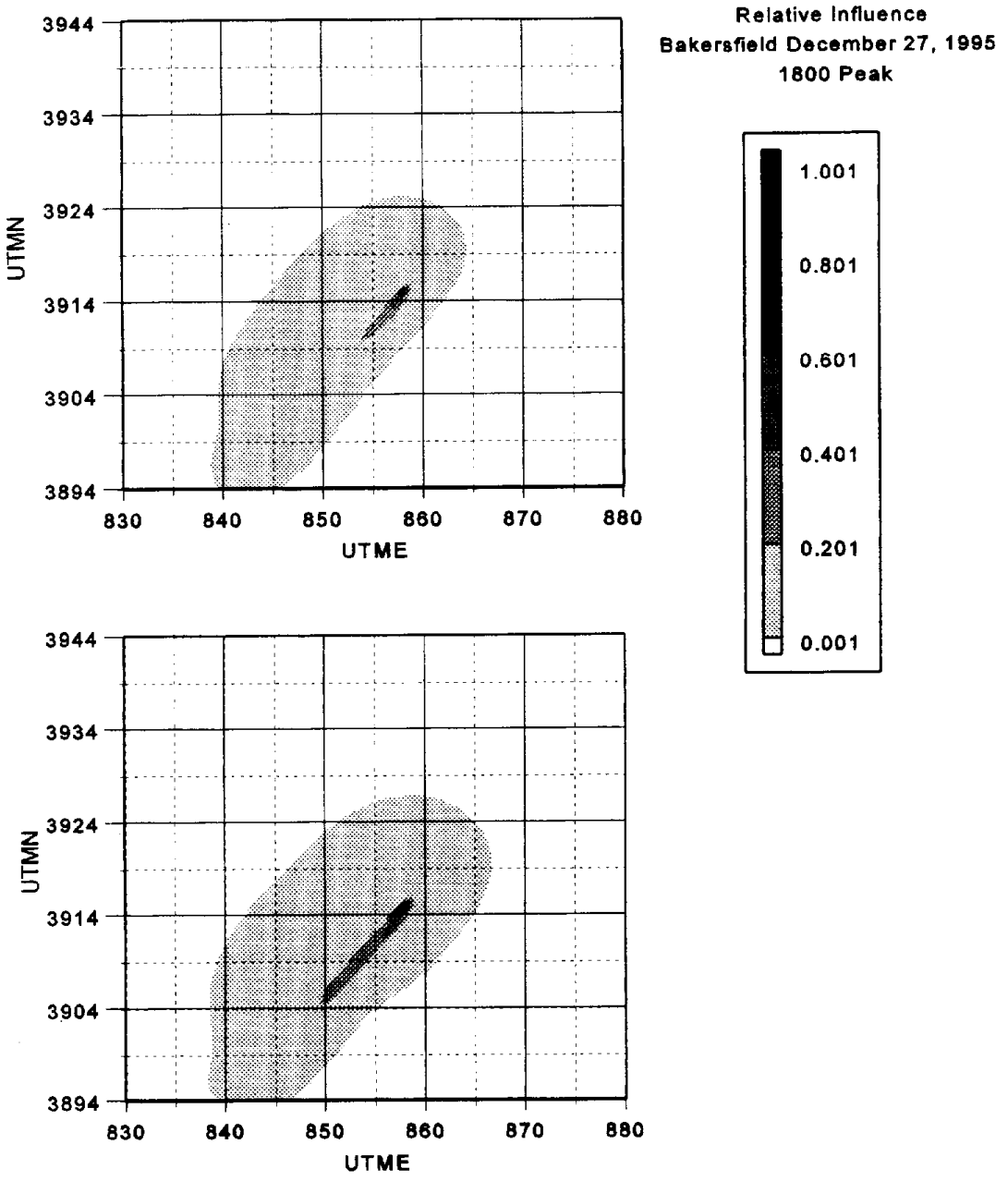

Figure 57. Relative influence of source areas on the Bakersfield sample collected from 1800 to 2100 December 27. Top chart has deposition velocity of 1.0 cm/sec; bottom chart has deposition velocity of 0.1 cm/sec.

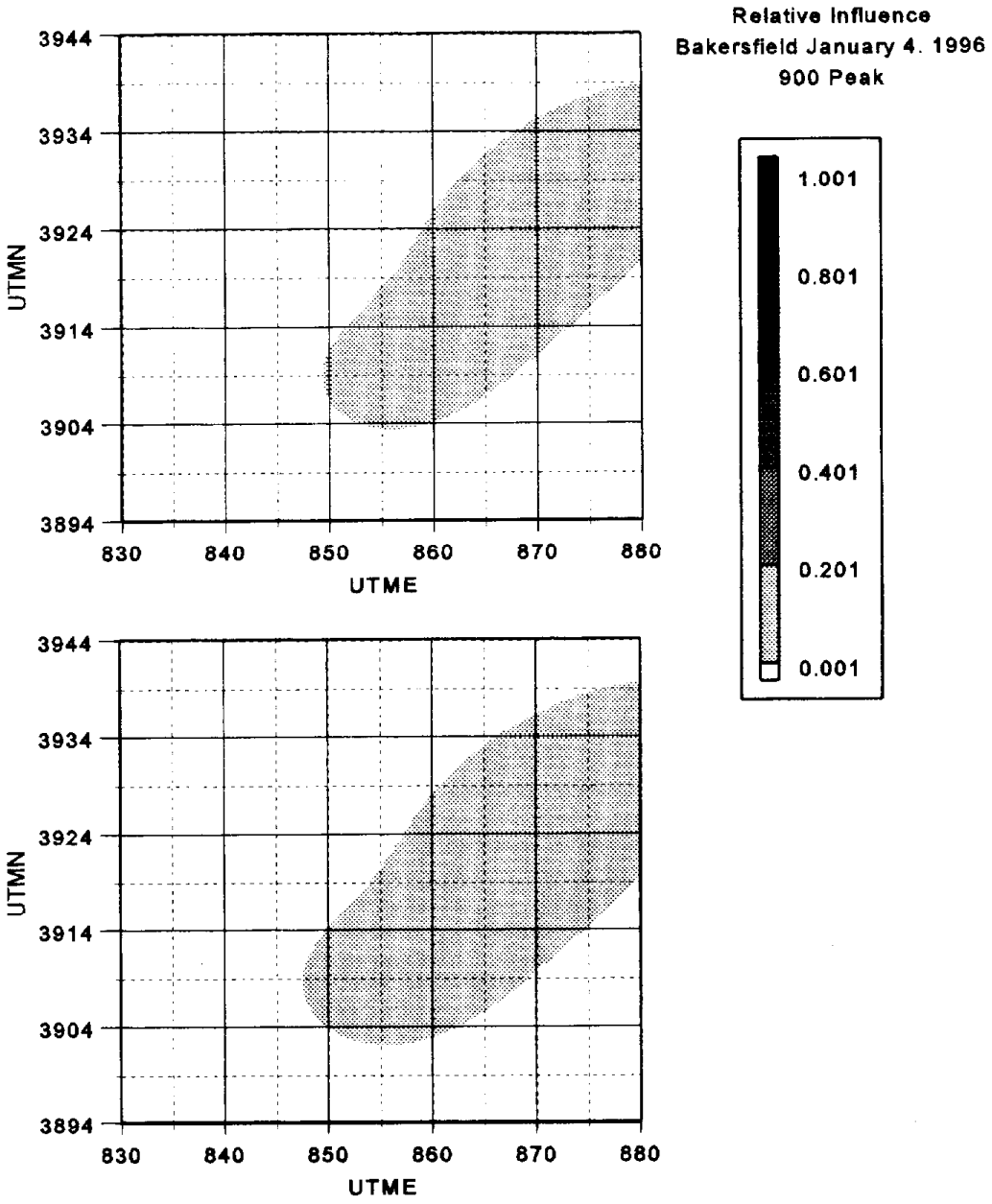

Figure 58. Relative influence of source areas on the Bakersfield sample collected from 900 to 1200 January 4. Top chart has deposition velocity of 1.0 cm/sec; bottom chart has deposition velocity of 0.1 cm/sec.

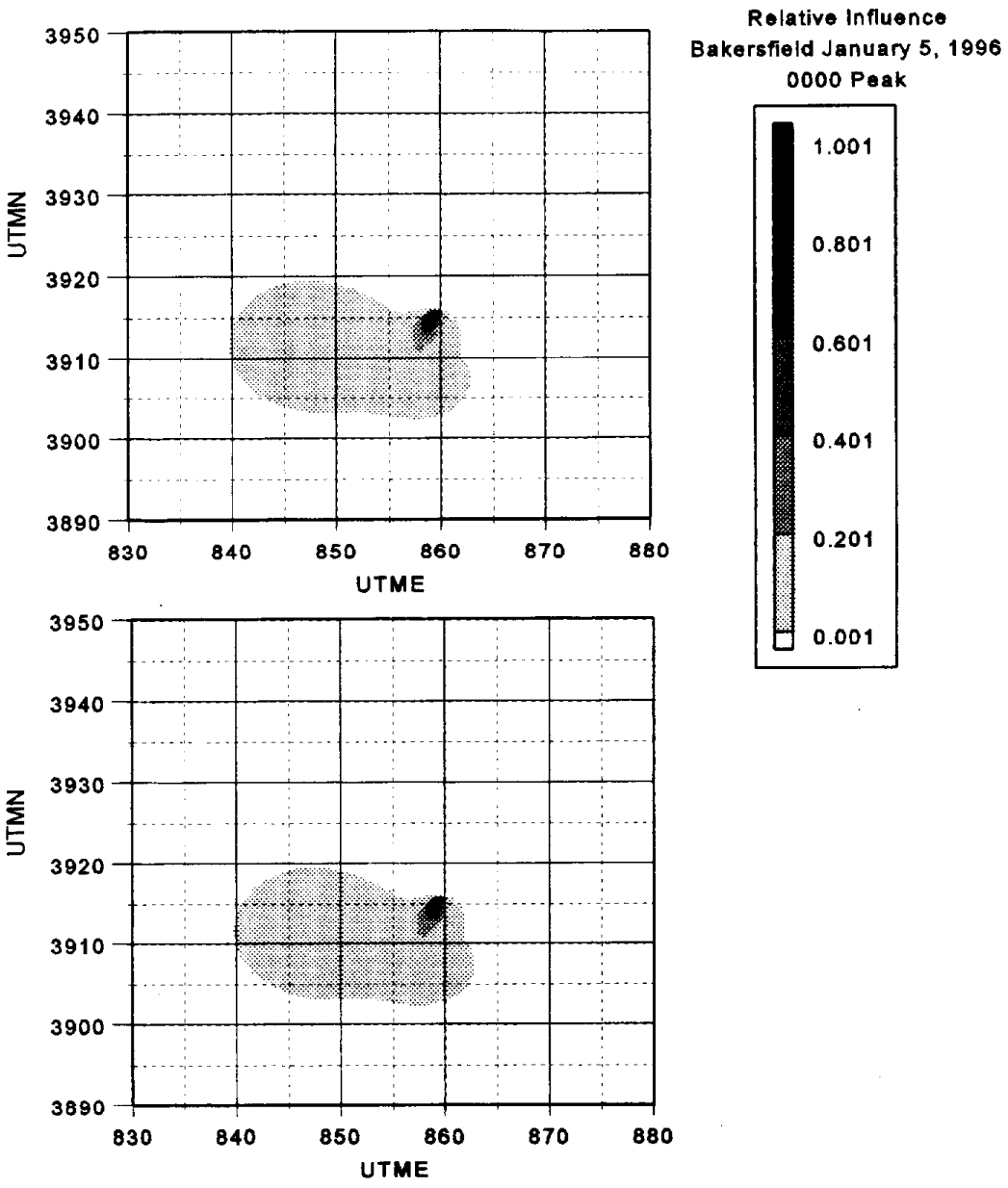

Figure 59. Relative influence of source areas on the Bakersfield sample collected from 0000 to 300 January 5. Top chart has deposition velocity of 1.0 cm/sec; bottom chart has deposition velocity of 0.1 cm/sec.

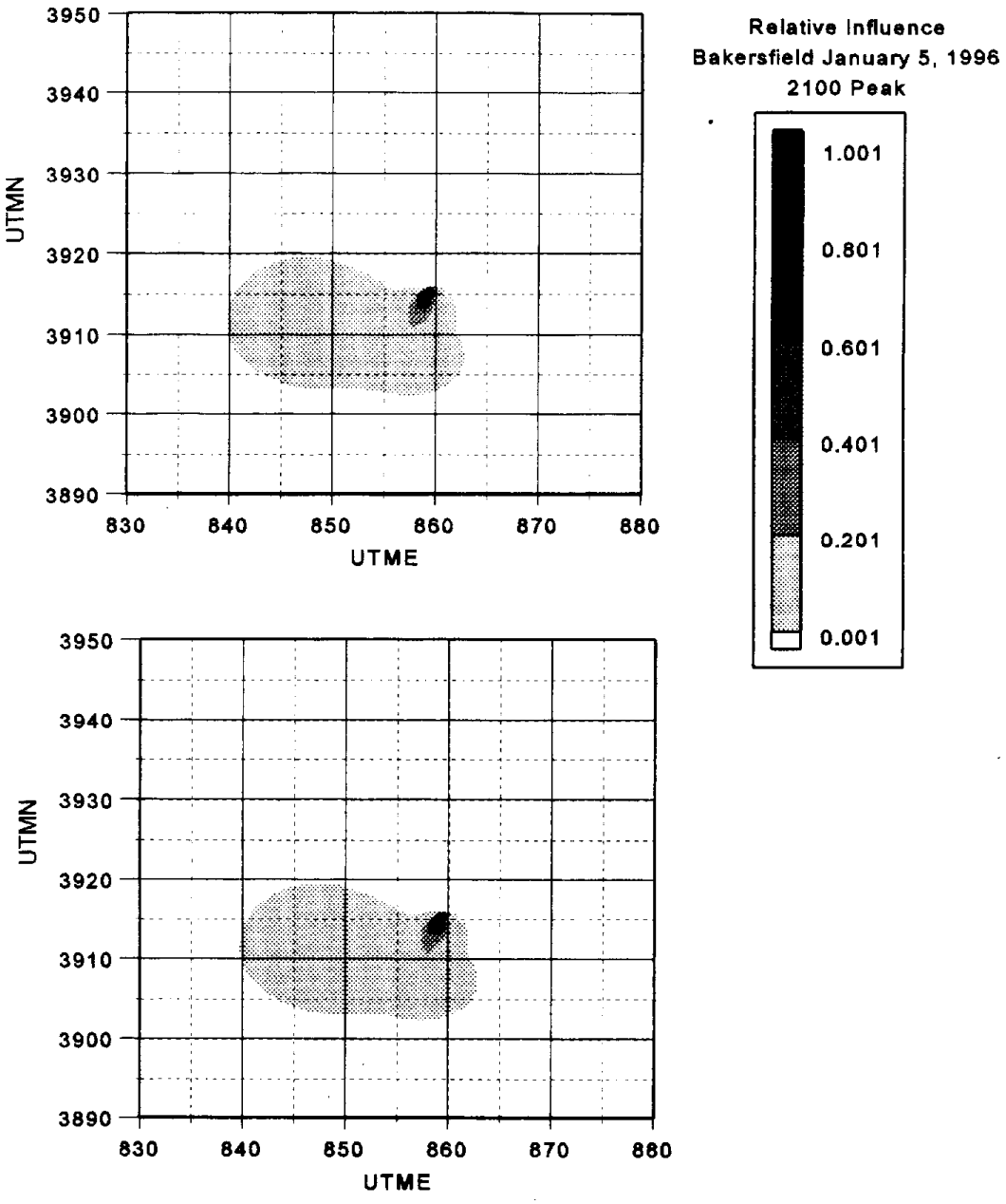

Figure 60. Relative influence of source areas on the Bakersfield sample collected from 2100 to January 5 to 0000 January 6. Top chart has deposition velocity of 1.0 cm/sec; bottom chart has deposition velocity of 0.1 cm/sec.

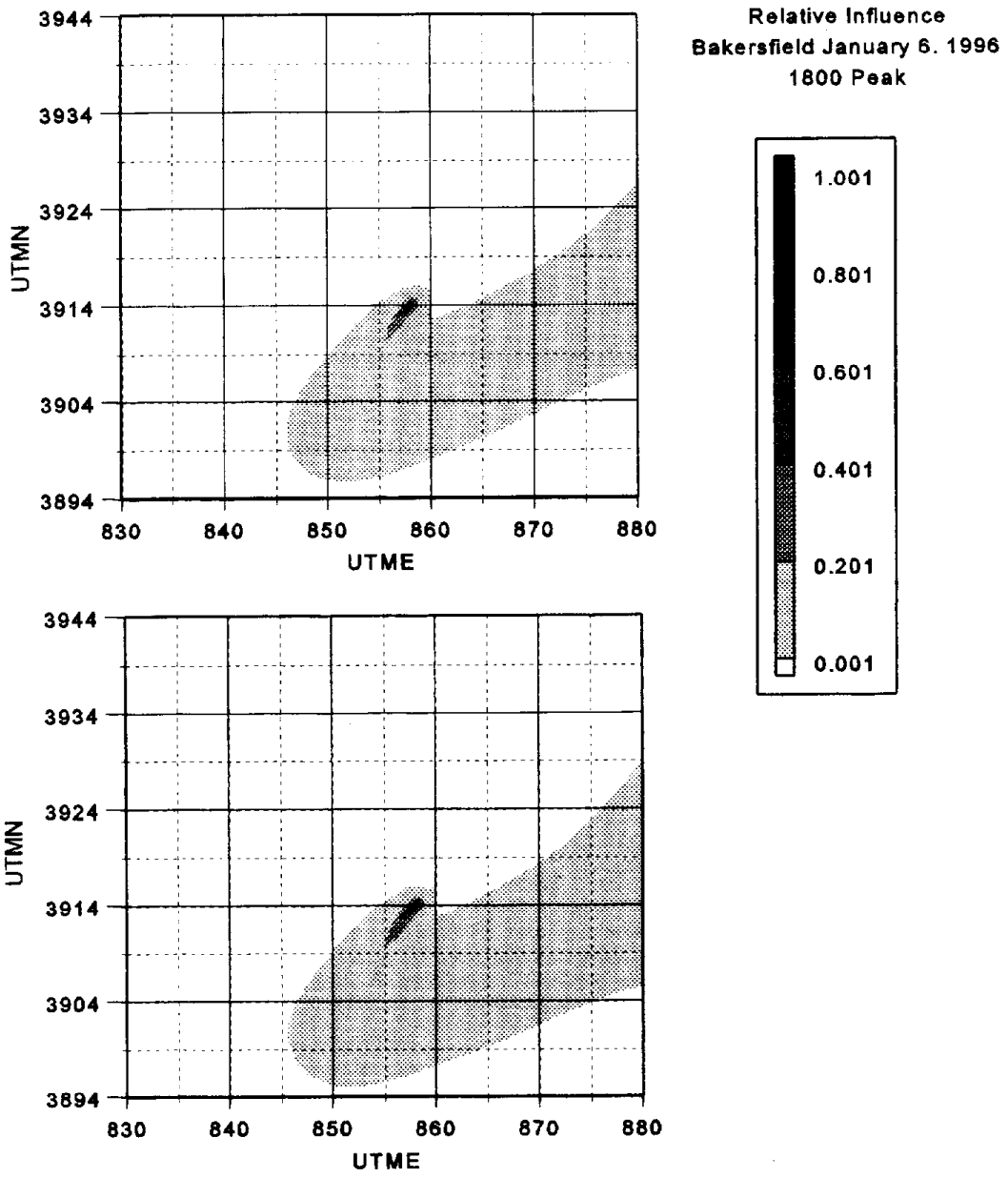

Figure 61. Relative influence of source areas on the Bakersfield sample collected from 1800 to 2100 January 6. Top chart has deposition velocity of 1.0 cm/sec; bottom chart has deposition velocity of 0.1 cm/sec.

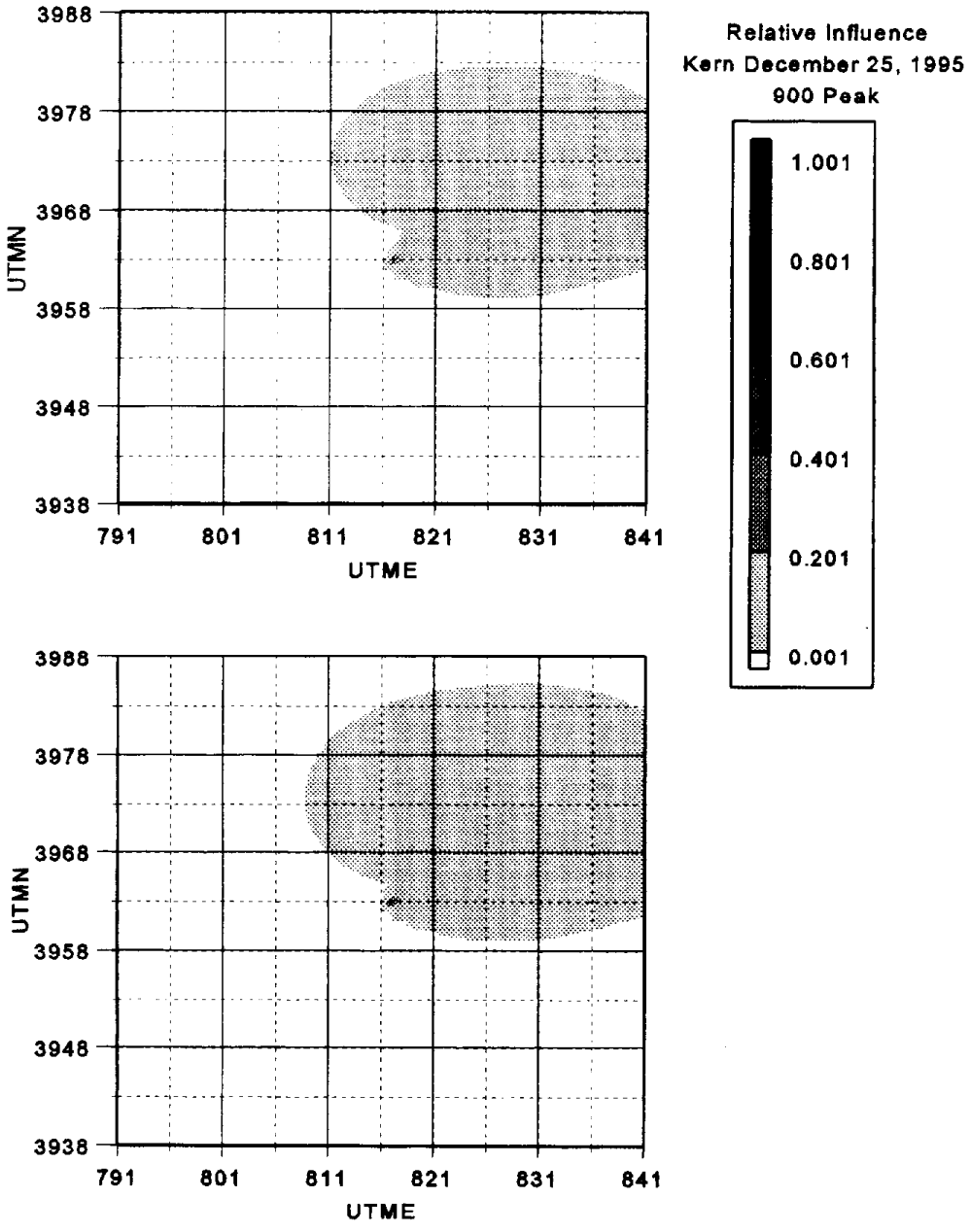

Figure 62. Relative influence of source areas on the Kern sample collected from 900 to 1200 December 25. Top chart has deposition velocity of 1.0 cm/sec; bottom chart has deposition velocity of 0.1 cm/sec.

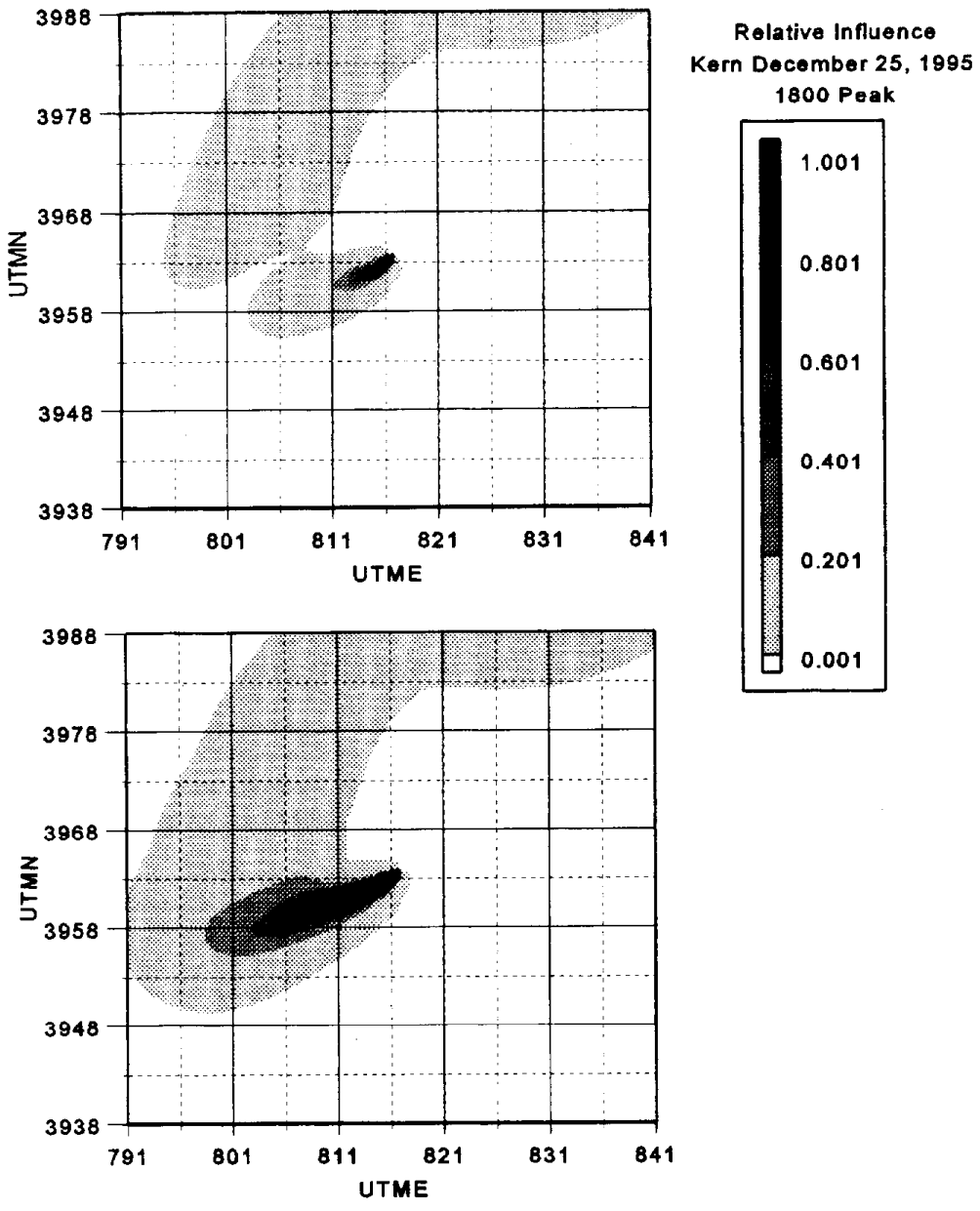

Figure 63. Relative influence of source areas on the Kern sample collected from 1800 to 2100 December 25. Top chart has deposition velocity of 1.0 cm/sec; bottom chart has deposition velocity of 0.1 cm/sec.

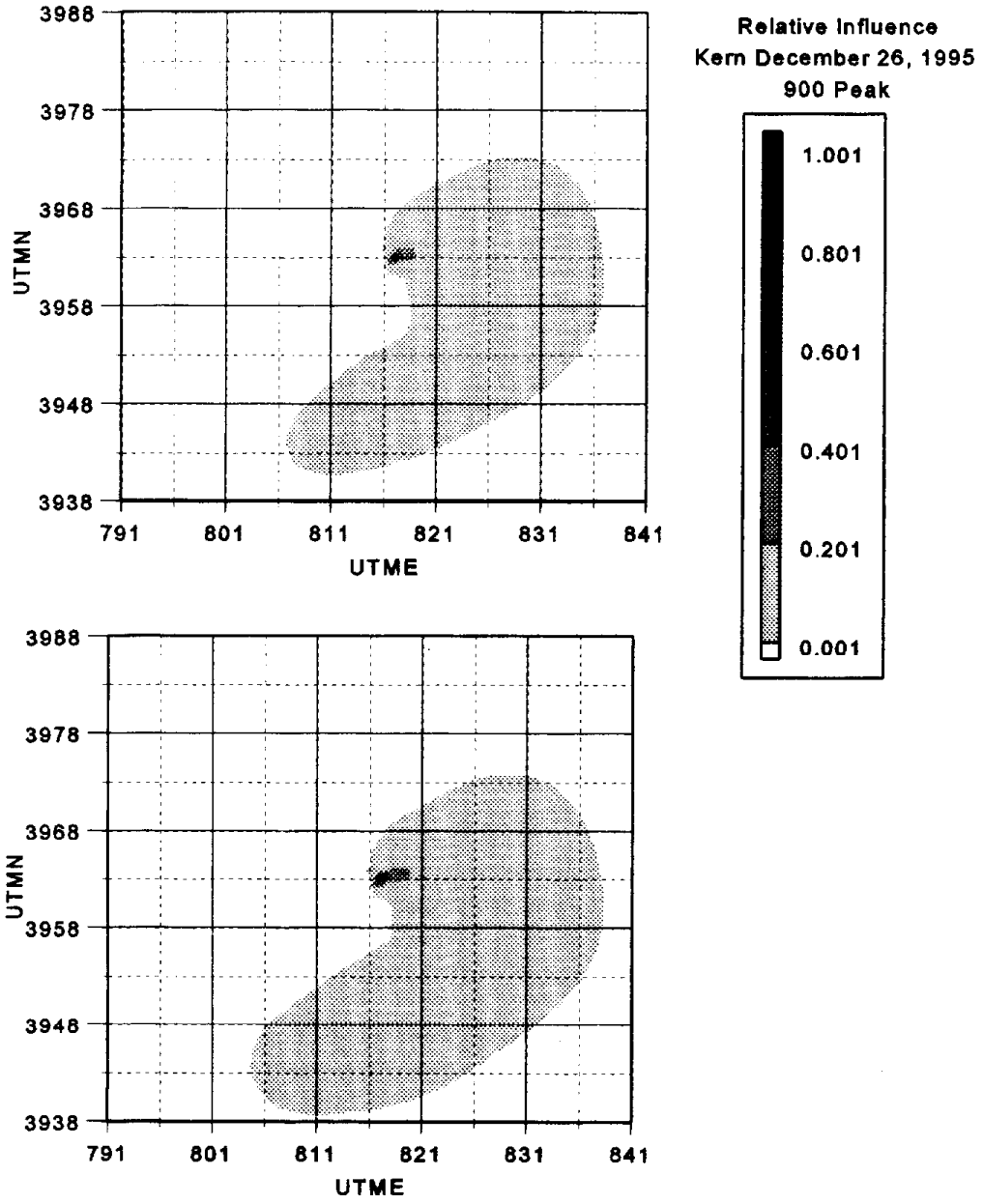

Figure 64. Relative influence of source areas on the Kern sample collected from 900 to 1200 December 26. Top chart has deposition velocity of 1.0 cm/sec; bottom chart has deposition velocity of 0.1 cm/sec.

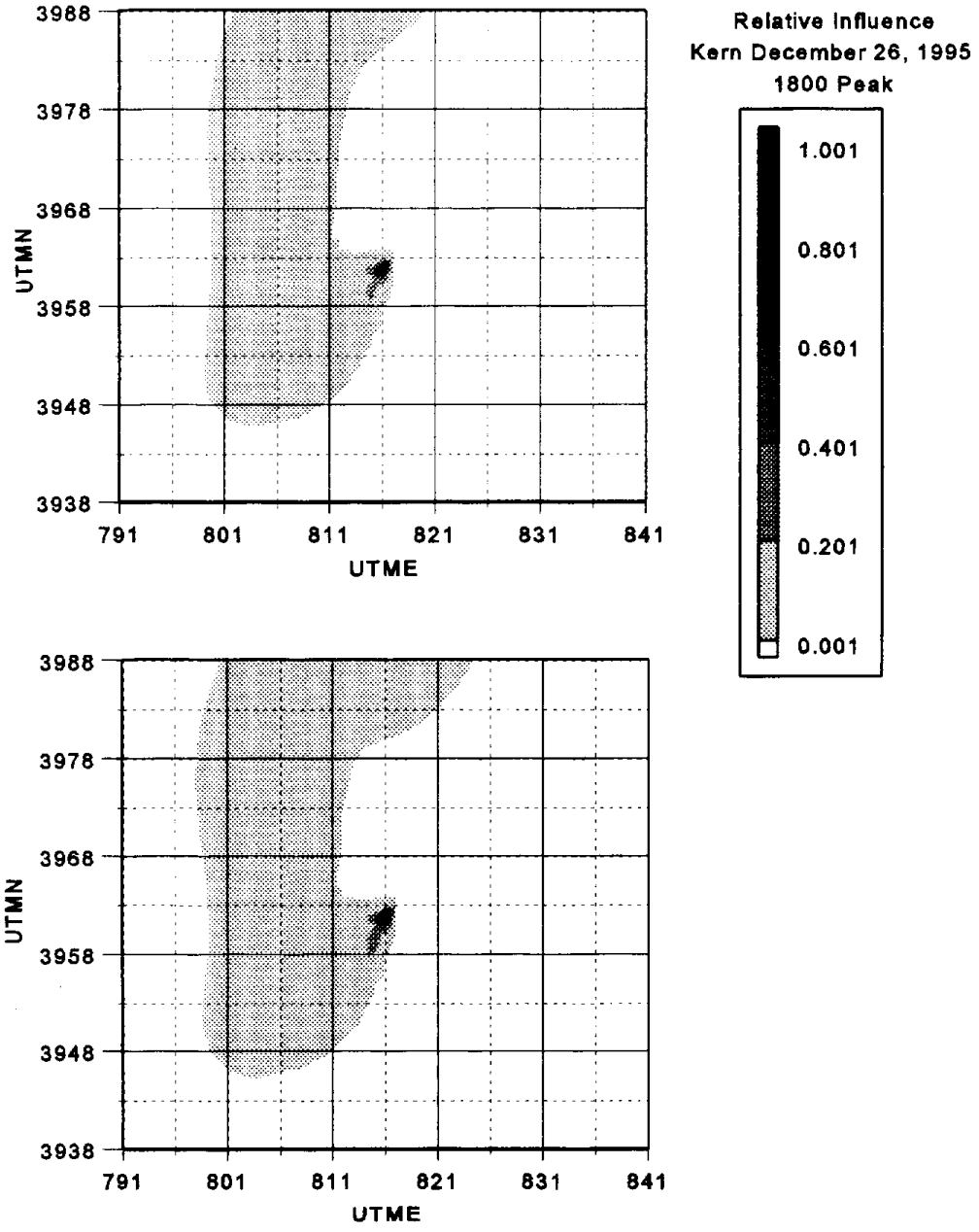

Figure 65. Relative influence of source areas on the Kern sample collected from 1800 to 2100 December 26. Top chart has deposition velocity of 1.0 cm/sec; bottom chart has deposition velocity of 0.1 cm/sec.

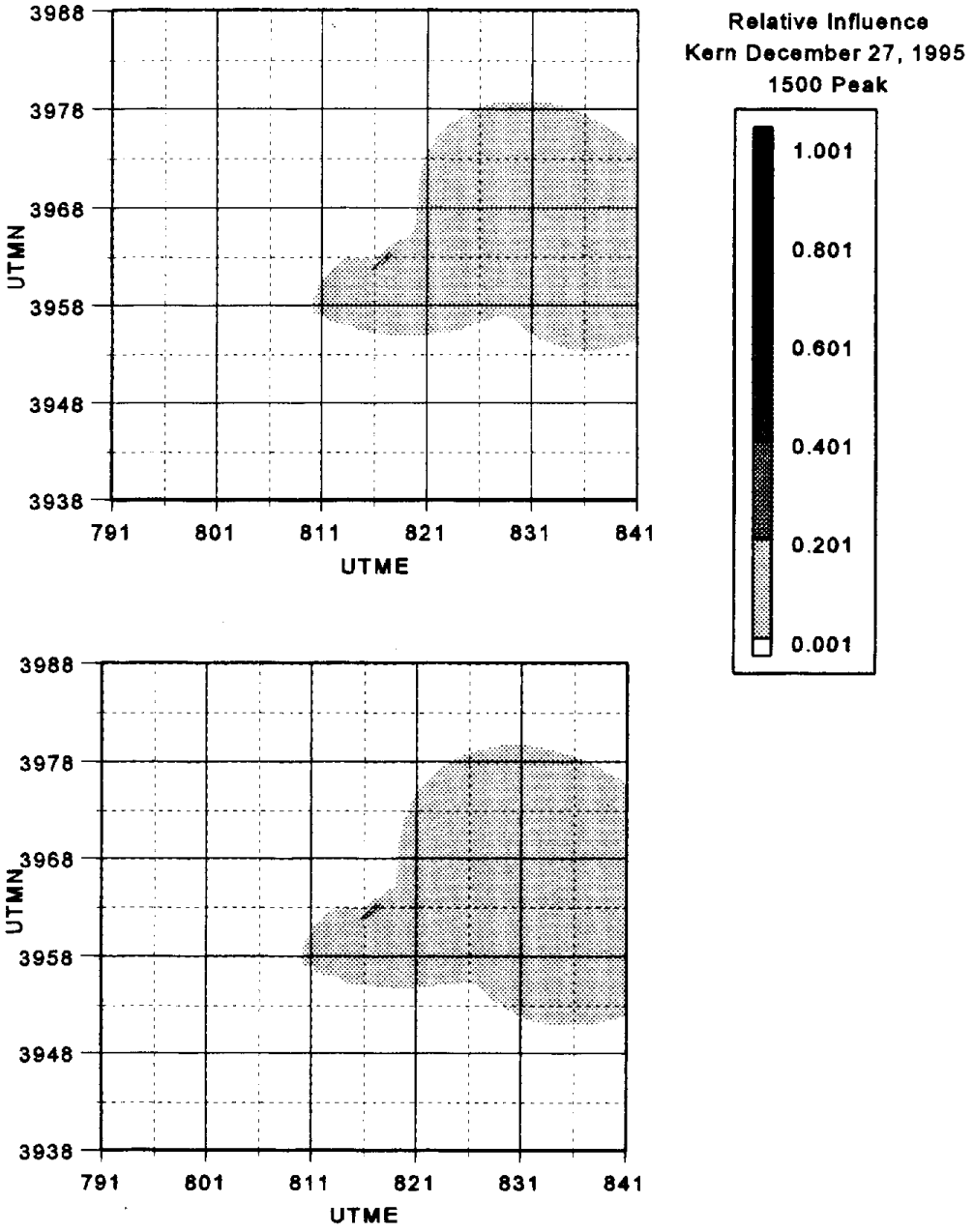

Figure 66. Relative influence of source areas on the Kern sample collected from 1500 to 1800 December 27. Top chart has deposition velocity of 1.0 cm/sec; bottom chart has deposition velocity of 0.1 cm/sec.

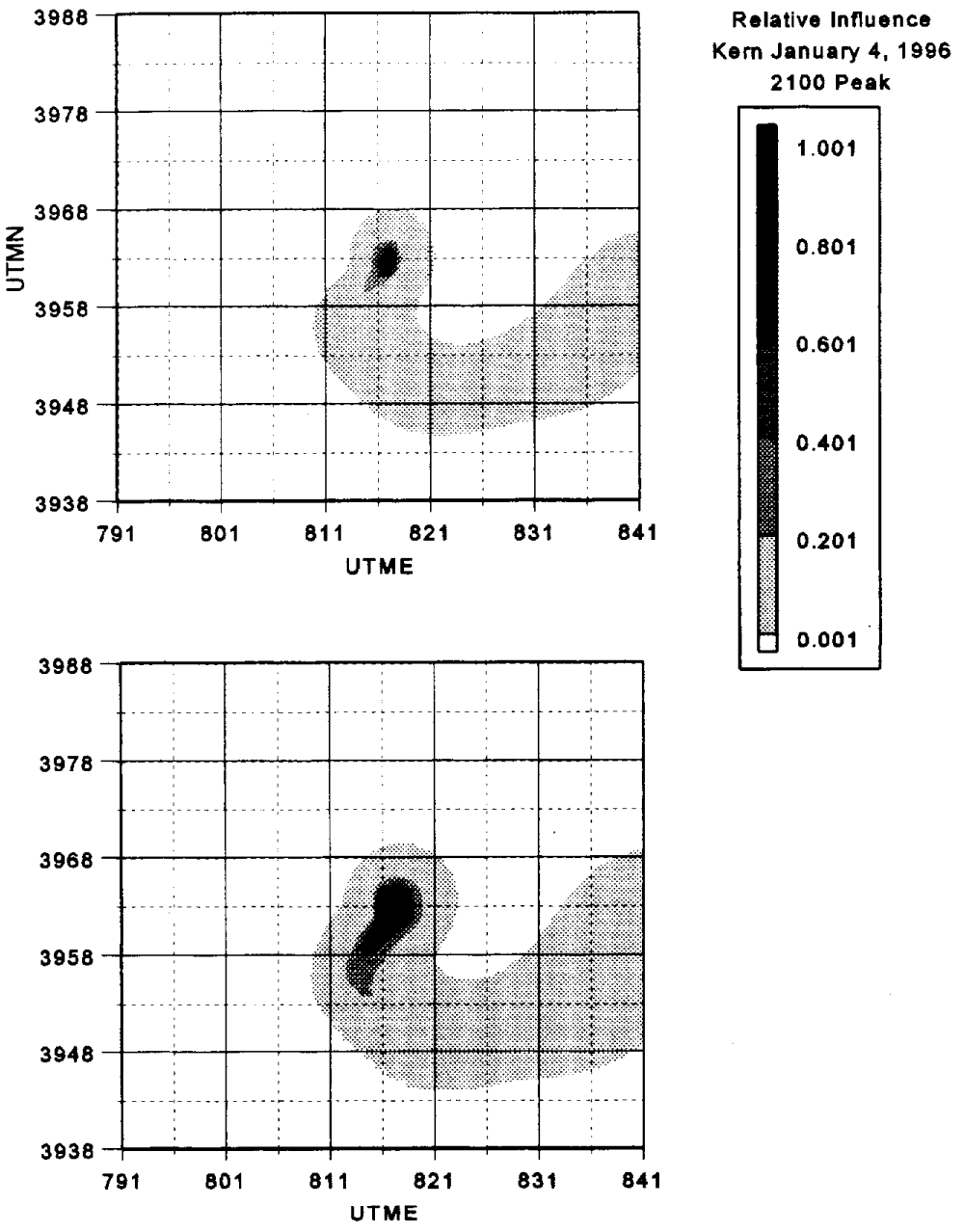

Figure 67. Relative influence of source areas on the Kern sample collected from 2100 January 4 to 0000 January 5. Top chart has deposition velocity of 1.0 cm/sec; bottom chart has deposition velocity of 0.1 cm/sec.

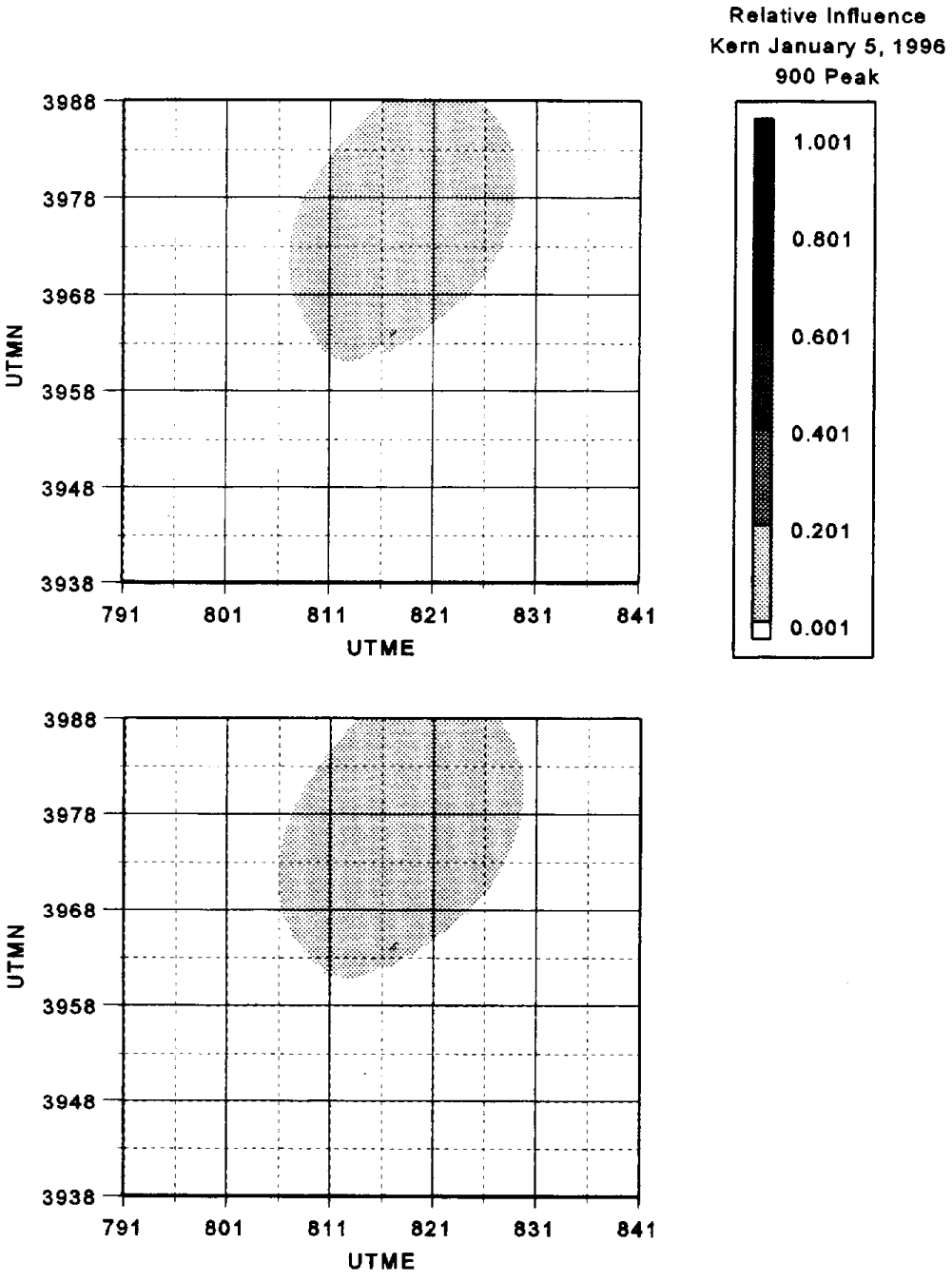

Figure 68. Relative influence of source areas on the Kern sample collected from 900 to 1200 January 5. Top chart has deposition velocity of 1.0 cm/sec; bottom chart has deposition velocity of 0.1 cm/sec.

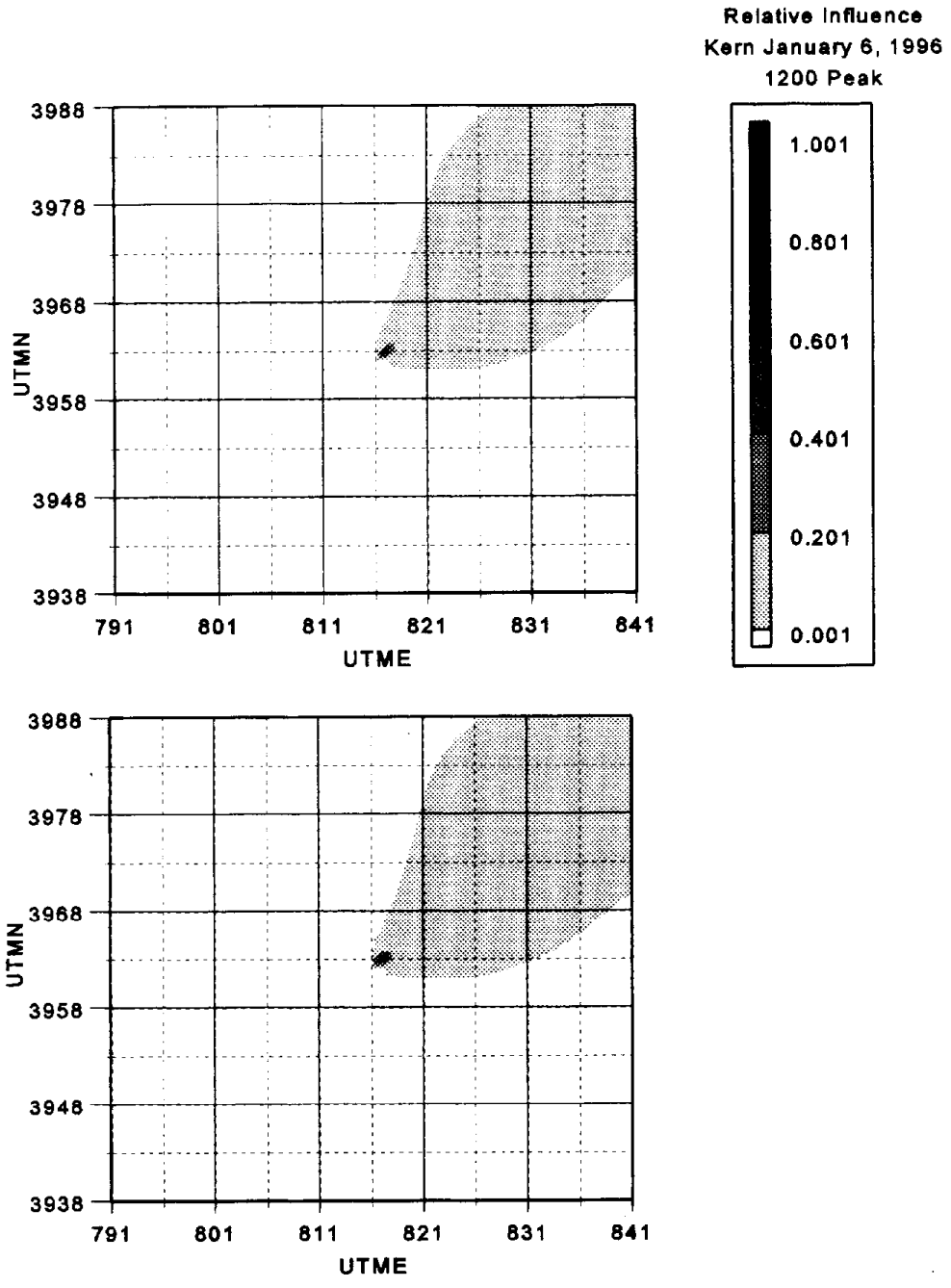

Figure 69. Relative influence of source areas on the Kern sample collected from 1200 to1500 January 6. Top chart has deposition velocity of 1.0 cm/sec; bottom chart has deposition velocity of 0.1 cm/sec.

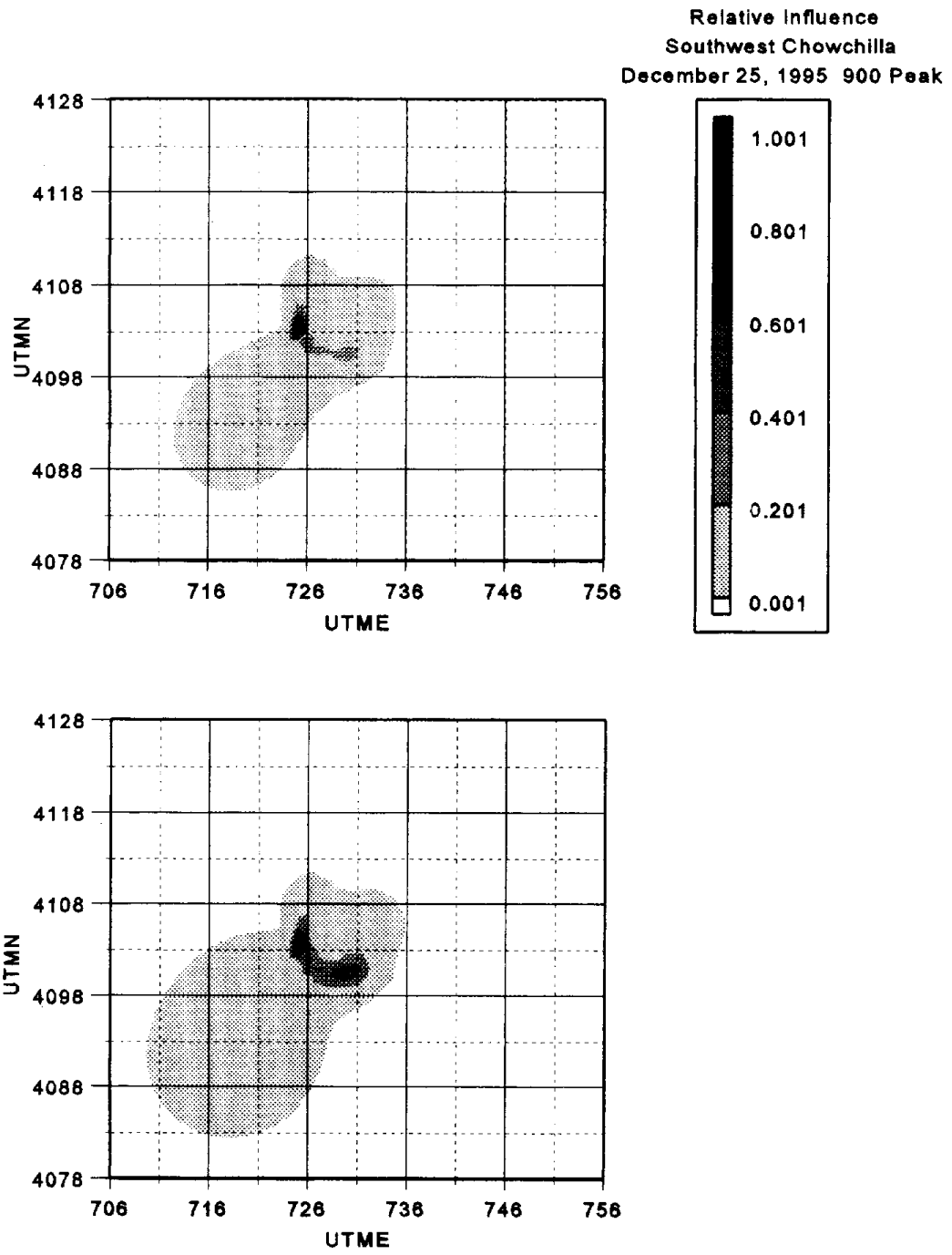

Figure 70. Relative influence of source areas on the Southwest Chowchilla sample collected from 900 to 1200 December 25. Top chart has deposition velocity of 1.0 cm/sec; bottom chart has deposition velocity of 0.1 cm/sec.

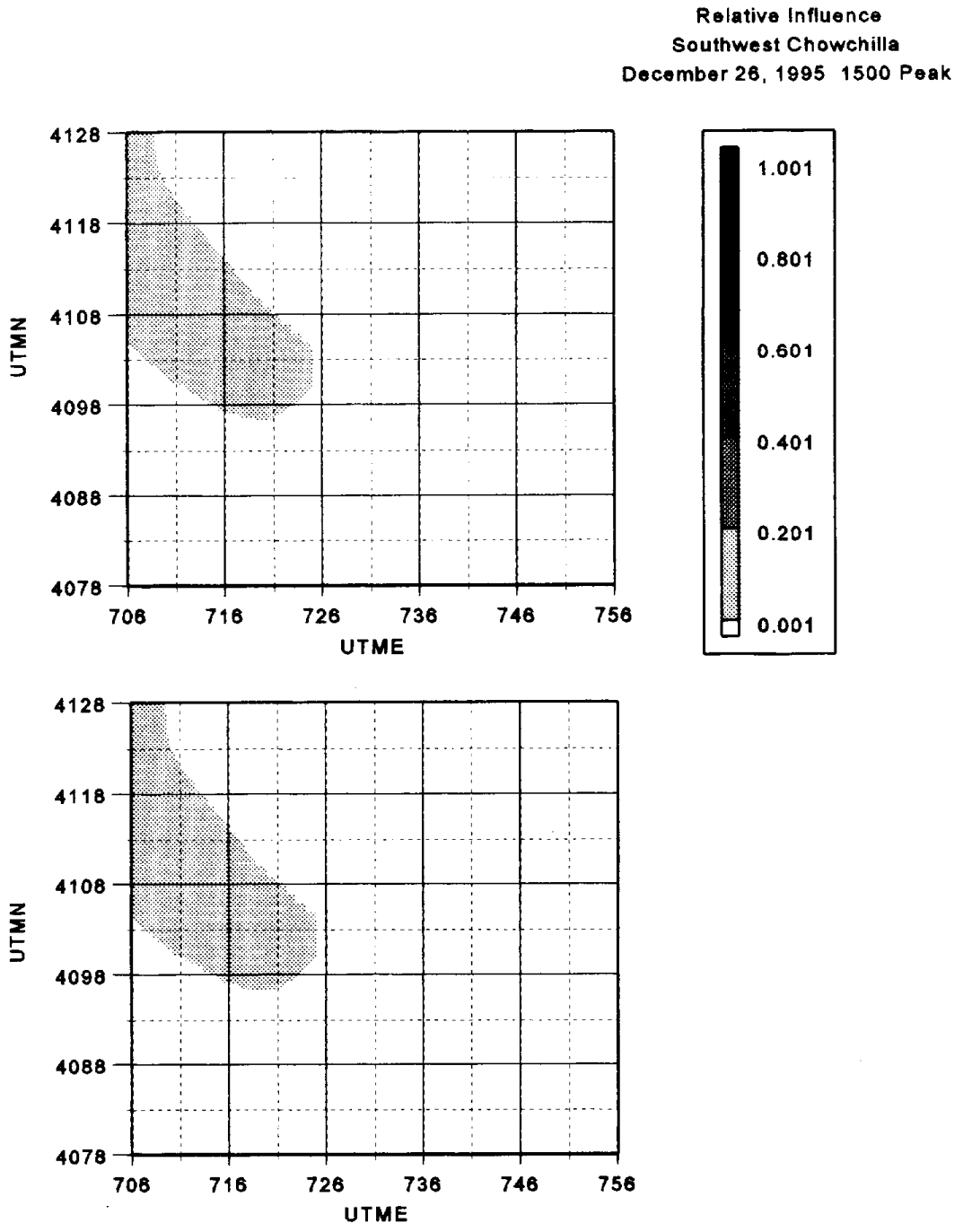

Figure 71. Relative influence of source areas on the Southwest Chowchilla sample collected from 1500 to 1800 December 26. Top chart has deposition velocity of 1.0 cm/sec; bottom chart has deposition velocity of 0.1 cm/sec.

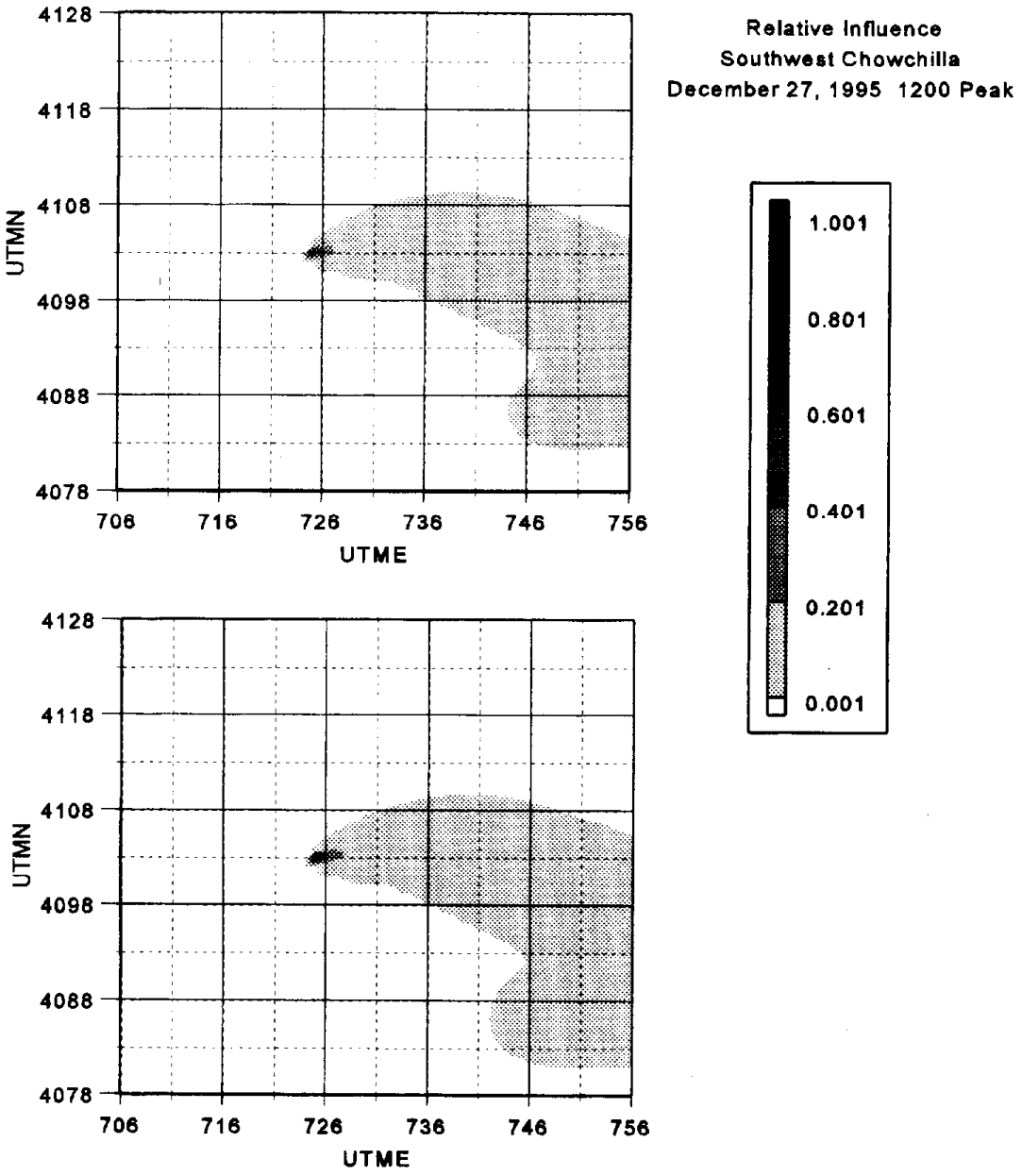

Figure 72. Relative influence of source areas on the Southwest Chowchilla sample collected from 1200 to 1500 December 27. Top chart has deposition velocity of 1.0 cm/sec; bottom chart has deposition velocity of 0.1 cm/sec.

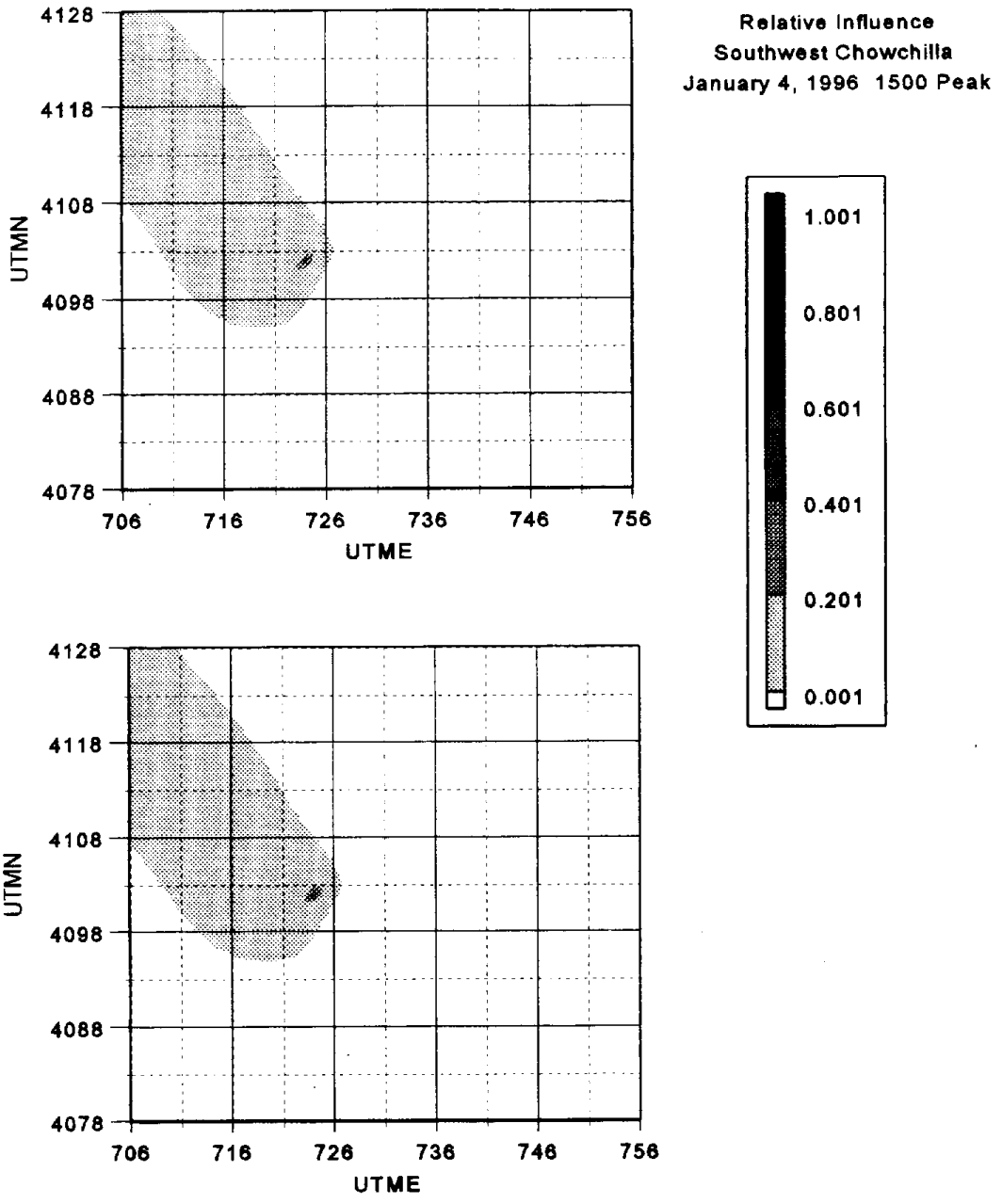

Figure 73. Relative influence of source areas on the Southwest Chowchilla sample collected from 1500 to 1800 January 4. Top chart has deposition velocity of 1.0 cm/sec; bottom chart has deposition velocity of 0.1 cm/sec.

CONCLUSION

Three methods were employed to evaluate the zones of influence of emissions. First, gridded concentration fields were examined to identify concentration gradients. The gradients were qualitatively evaluated to identify approximate distances over which concentration peaks diminished to both urban and regional background levels. The gridded concentration fields were also compared with maps of emission densities. Second, a series of regressions of site concentrations versus emissions densities were carried out. Emission densities were determined for a variety of scales of spatial averaging and the averaging scales that provided the best fits between concentrations and emissions were identified. Finally, a dispersion model was used to estimate upwind areas of influence on the core sites.

The three methods yielded consistent results. The contour plots revealed neighborhood-scale (on the order of 1 km) influences in the Corcoran domain and urban-scale (5 to 15 km) influences for all saturation networks. In the fall Corcoran study, gradients of PM_{10} mass were 10 to 50 $\upsilon g\ m^{-3}\ km^{-1}$, implying that nearby emission sources often influenced site concentrations substantially. The distance scale for the decay from peak to urban background values was about 5 to 10 km in Corcoran and 10 to 15 km in the other domains. However, the range of influence of emission sources could have been greater than these scales since the network domains were not large enough to capture the decay from urban background levels to regional background levels.

The regression results indicated that transport and dispersion of emissions occurred on a scale of about 15 km (urban scale) during winter and about 40 km (regional scale) during fall. Local influences (neighborhood scale, 0.5 to 4 km) could have been superimposed upon the urban and regional-scale dispersion, as indicated by the scatter of concentrations within each saturation network, but the regressions were not capable of discerning such influences since the emissions grid-cell resolution

was only 4 km x 4 km. The winter regressions are also consistent with regional dispersion of PM emissions on scales exceeding 15 to 20 km, since correlation coefficients remained high for scales exceeding the 14 km scale of the best fit regressions. The fall regression results showed no correlation between concentrations and emissions densities at scales less than 20 km because the urban sites (in Fresno and Bakersfield) showed lower PM_{10} concentrations than did the Corcoran sites, even though emission densities were greater in the urban areas. On a scale of about 40 km, though, the Corcoran concentrations were associated with higher emission densities, thus indicating the contribution of a regional background concentration to the overall values observed at the Corcoran sites.

The dispersion model calculations for the winter episodes showed substantial source influence for locations within less than 5 to about 15 km of receptor sites and less influence, but geographically more widespread, from locations within about 15 to greater than 25 km. The results suggest a scale of significant emissions influence of a few up to about 15 km, and a scale of approximately 20 km or more over which emissions are more widely dispersed but still contribute to general background levels. Input data for the dispersion calculation were unavailable for the fall period.

In summary, it is possible to identify neighborhood-scale (about 1 km), urban-scale (about 15 to 20 km), and regional-scale (exceeding about 20 to 25 km) emission influences during both fall and winter. During winter, the neighborhood and urban scales dominated, with a mean urban background concentration of approximately 40 $\mu g\ m^{-3}$ in the Fresno and Bakersfield networks and mean peak-site values of about 60 to 80 $\mu g\ m^{-3}$. During fall, the mean regional background in the Corcoran network was about 100 $\mu g\ m^{-3}$, with neighborhood- and urban-scale influences increasing mean concentrations at the peak sites to about 130 to 190 $\mu g\ m^{-3}$.

SECTION 7: ANALYSIS OF DIURNAL CONCENTRATION VARIATIONS

OBJECTIVES

The original objective of this section was to contribute to the analysis of the zones of influence of emissions by relating diurnal profiles of PM concentrations and for the sites with 3-hour averaging times to diurnal profiles of specific emission sources and daily emissions activities. As will be demonstrated, the analysis of diurnal patterns was of less use for understanding zones of influence than were the methods described in the previous section. However, several useful findings emerged from the examination of diurnal patterns and are therefore presented in this section.

APPROACH

The emission files were first reviewed to identify diurnal patterns of emissions. Correlations between CO, NO_x, and other motor vehicle emissions were considered.

Ambient concentration measurements were also reviewed to distinguish diurnal profile patterns. The correlations between measured particulate carbon and other species concentrations were evaluated. The effects of changes in mixing height throughout the day on particulate concentrations were considered. Chemical Mass Balance (CMB) analyses were obtained and diurnal patterns were determined.

RESULTS

Diurnal Patterns of Emissions

Diurnal emissions for 13 November and 5 January show identical patterns, although the levels are much higher in November, as can be seen in Figure 74. The profile of total emissions is dominated by point area sources, consisting primarily of coarse particulate and exhibiting a high plateau from 8 a.m. to 4 p.m. The uncertainty of actual emissions is unknown, but may be quite large. The combustion-related categories of motor vehicles, residential fuel combustion, and waste burning are small

compared to the total (the sum of these categories plus point sources are shown as "other" in Figure 74); however, combustion processes generate fine particulate (from condensation reactions) and secondary particulate (e.g., conversion of NO_x to HNO_3 and subsequent reaction with ammonia to generate particulate ammonium nitrate). Their diurnal emission profiles are shown more clearly in Figure 75.

Within the urban areas of Fresno and Bakersfield, the point, motor vehicle, and residential fuel combustion categories are a larger fraction of the total PM emissions than is the case for the domain-wide emissions shown in Figure 74. During winter, residential fuel combustion constitutes about 25 percent of the nighttime and 15 percent of the daytime primary PM emissions in Fresno and Bakersfield (not plotted).

During fall, emissions in the Corcoran area are dominated by area sources (about 90 percent) and point sources (about 10 percent), producing a diurnal pattern similar to that shown for the domain-wide case (Figure 74, top panel).

As shown in Figure 75, the estimated emissions from point sources and waste burning decrease from fall to winter, while emissions from residential fuel combustion increase. The commute profile is evident in the motor vehicle category. Emissions from residential fuel combustion show low diurnal variation, with a morning peak coincident with the morning peak in motor vehicle emissions and an evening peak that lags the evening peak in motor vehicle emissions by about two hours. Emissions from point sources and waste burning are estimated to show daytime peaks from about 9 a.m. to 4 p.m. The waste burning profiles are discontinuous between hour 24 and hour 1. The sum of waste burning, residential fuel combustion, and motor vehicle emissions (which are all potential sources of particulate carbon) exhibits a diurnal profile largely driven by the profile of motor vehicle emissions, but having a sharper morning peak at 9 a.m. and a lesser decline during the mid-morning hours.

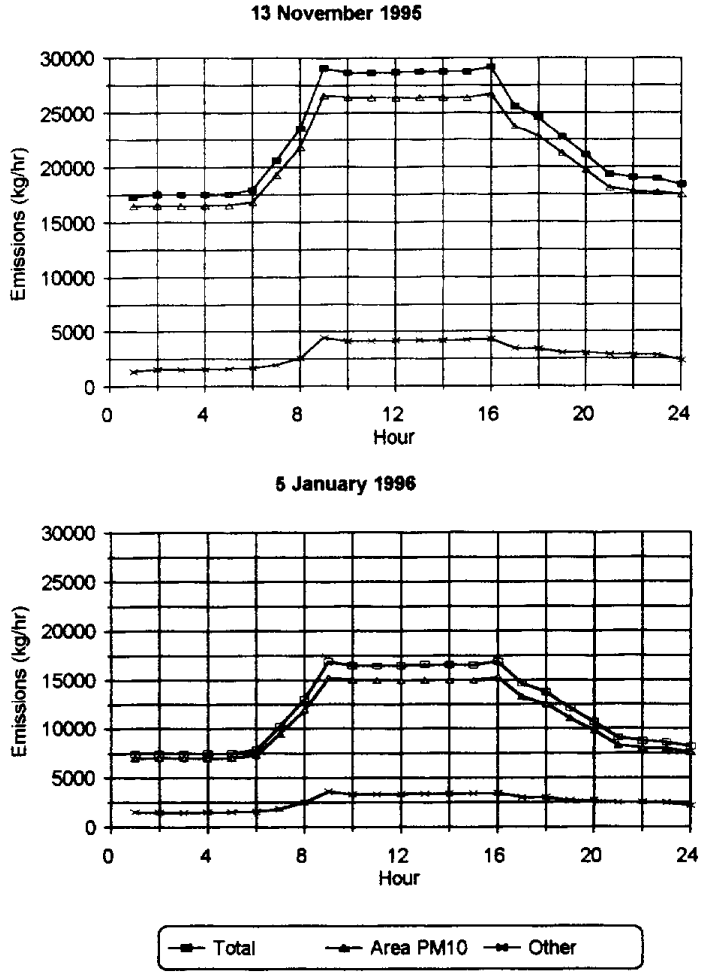

Figure 74. Domain-wide hourly emissions of PM_{10} for November 13, 1995 (top) and January 5, 1996 (bottom) showing total, area, and other sources. "Other" includes point sources, motor vehicles, residential fuel combustion, and waste burning; the latter two are also included in the "area" category.

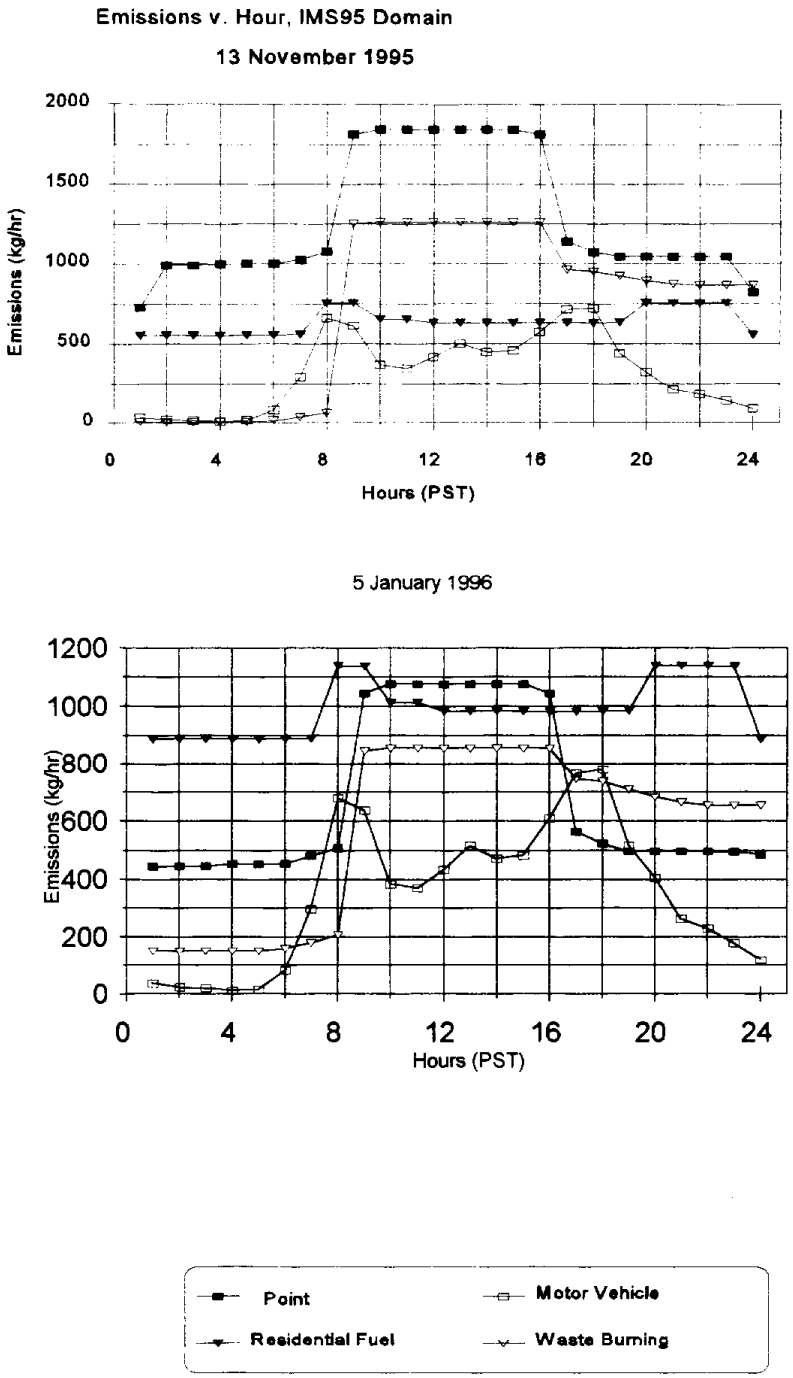

Figure 75. Domain-wide hourly PM_{10} emissions from motor vehicles, residential fuel combustion, waste burning, and point sources for November 13, 1995 (top) and January 5, 1996 (bottom).

Diurnal Patterns of Ambient Concentrations

The ambient concentration measurements also exhibit distinct diurnal profiles, as shown in Figures 76 through 79. Several features of these plots are of note:

- $PM_{2.5}$ mass is about 75 percent of the PM_{10} mass. The $PM_{2.5}$ carbon and secondary (nitrate plus ammonium plus sulfate) components are 80 to 100 percent of the PM_{10} carbon and secondary concentrations.

- At Bakersfield and Fresno, both PM_{10} and $PM_{2.5}$ mass are dominated by the carbon and secondary components, with secondary exceeding carbon during day and carbon exceeding secondary at night. At Kern and Chowchilla, the secondary components dominate during all hours.

- At Bakersfield and Fresno, both PM_{10} and $PM_{2.5}$ mass concentrations begin to rise at about 3:00 p.m. (the 1500-1800 sample) and reach maxima between 1800 and midnight. At Kern and Chowchilla, peaks occur during the day.

- The evening peaks in mass at Bakersfield and Fresno are driven by carbon.

- A daytime rise in the secondary species is evident at all sites.

- Organic carbon concentrations exceed elemental carbon by factors of 2:1 to 3:1. At each site, elemental and organic carbon follow the same profile, but the profiles at Bakersfield and Fresno differ from those at the rural sites.

- CO and NO_x are nearly perfectly correlated and, at Bakersfield and Fresno, exhibit morning and evening peaks.

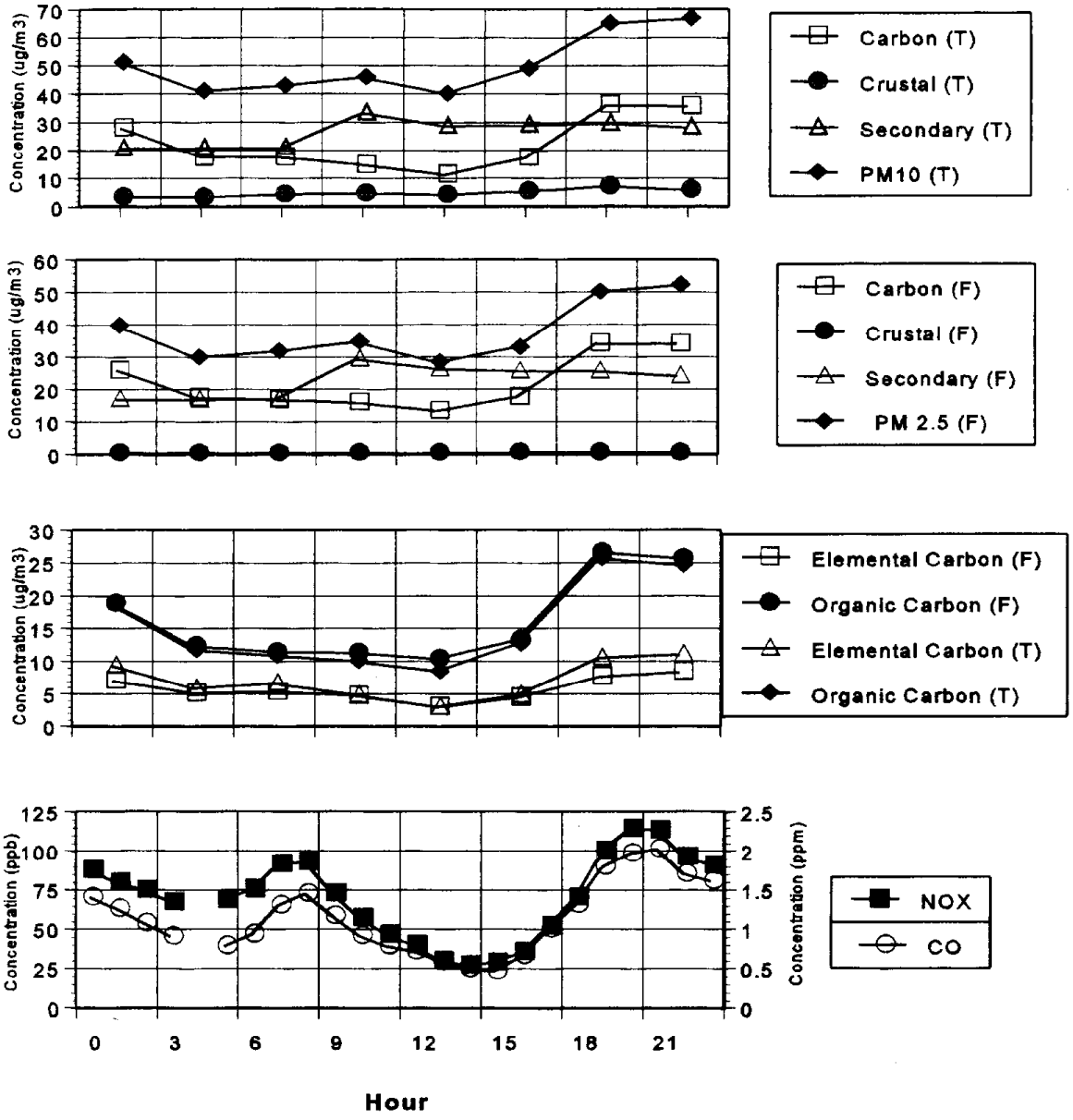

Figure 76. Diurnal averages of particulate, CO, and NO_x concentrations in Bakersfield for the period December 9, 1995-January 6, 1996. Particulate samples are 3-hour averages commencing at hours 0, 3, etc. Carbon, crustal, and secondary concentrations are averages of 5 to 8 days during the period.

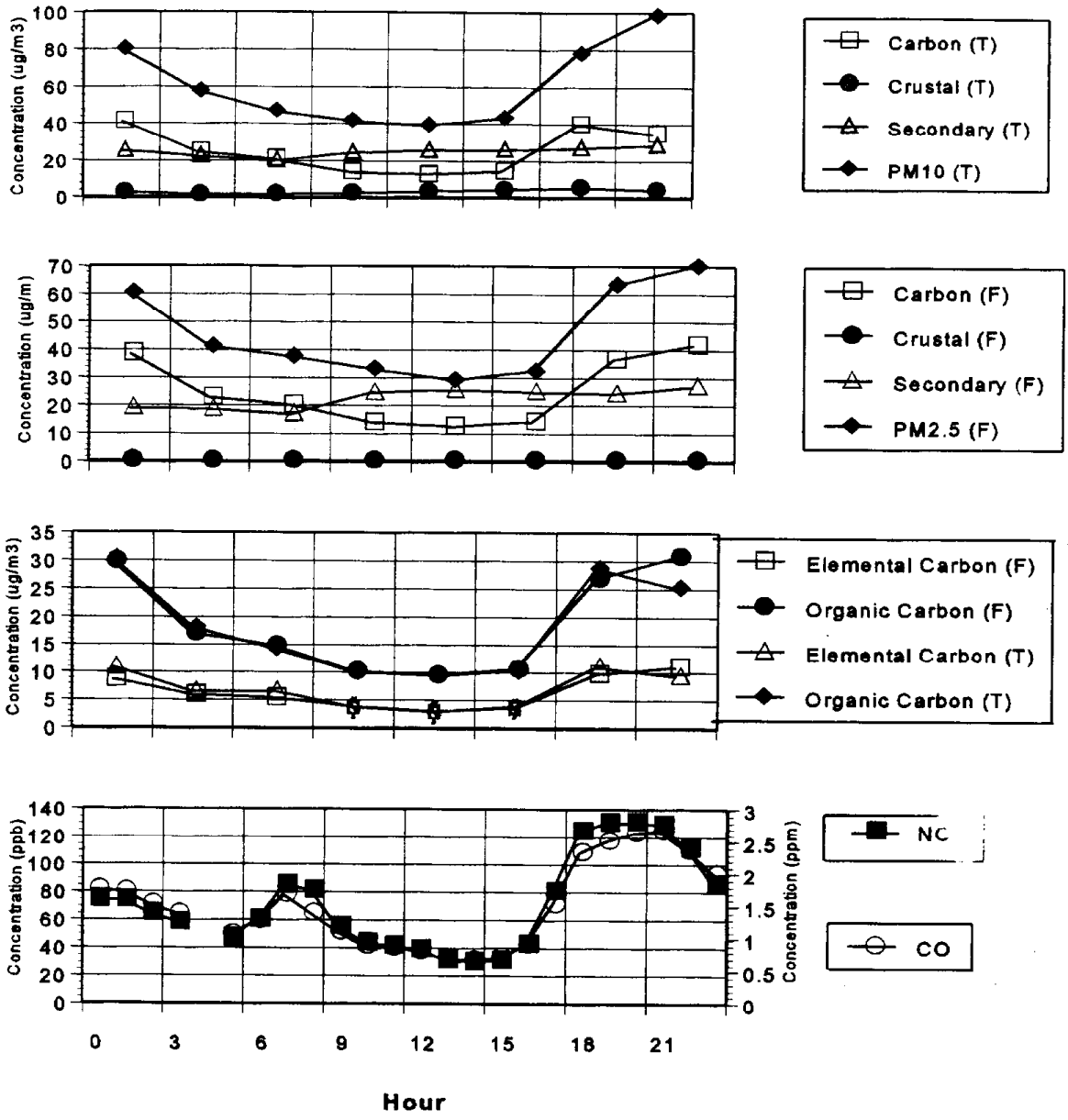

Figure 77. Diurnal averages of particulate, CO, and NO_x concentrations in Fresno for the period December 9, 1995-January 6, 1996. Particulate samples are 3-hour averages commencing at hours 0, 3, etc. Carbon, crustal, and secondary concentrations are averages of 5 to 8 days during the period.

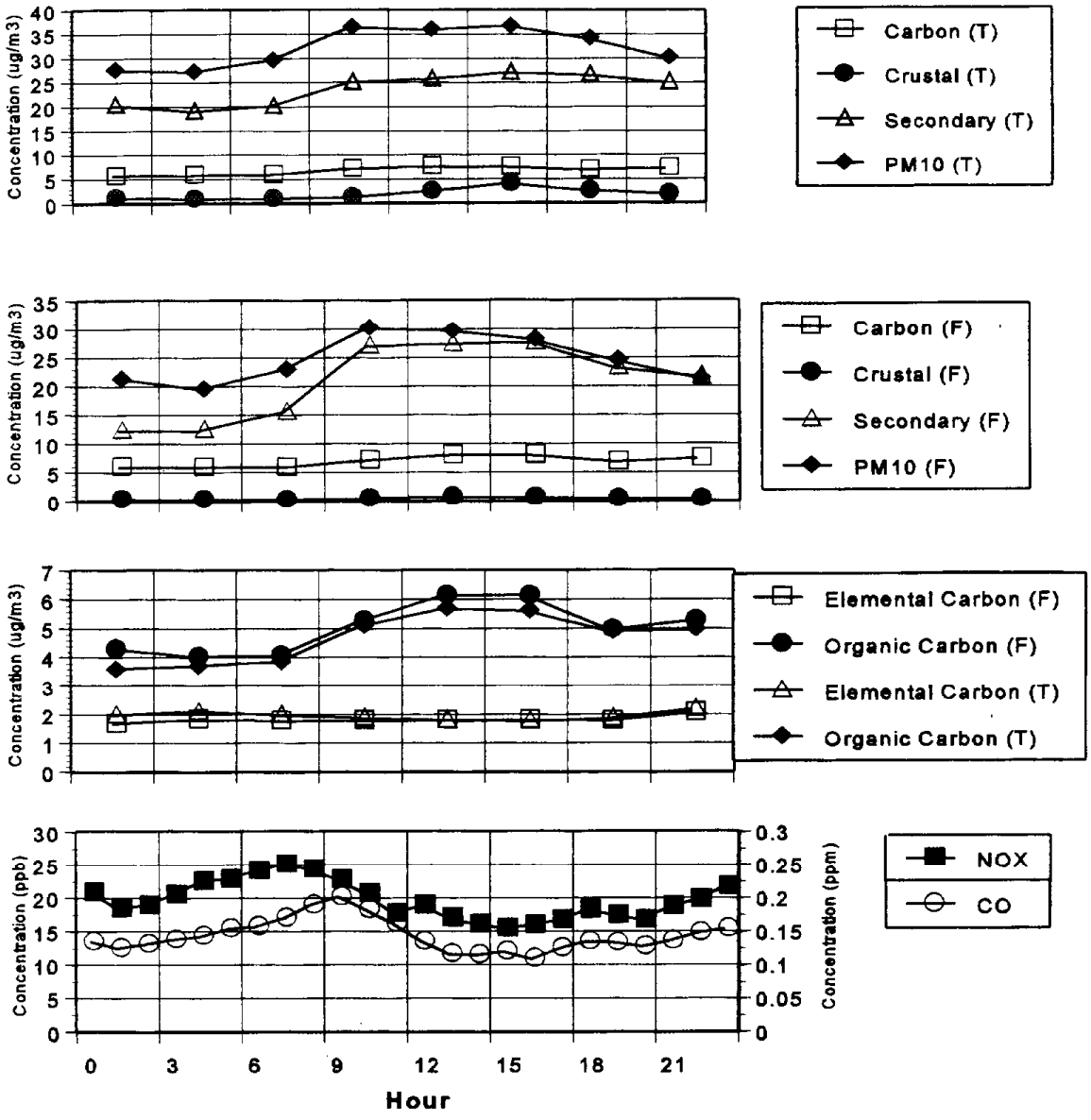

Figure 78. Diurnal averages of particulate, CO, and NO_x concentrations in Kern for the period December 9, 1995-January 6, 1996. Particulate samples are 3-hour averages commencing at hours 0, 3, etc. Carbon, crustal, and secondary concentrations are averages of 5 to 8 days during the period.

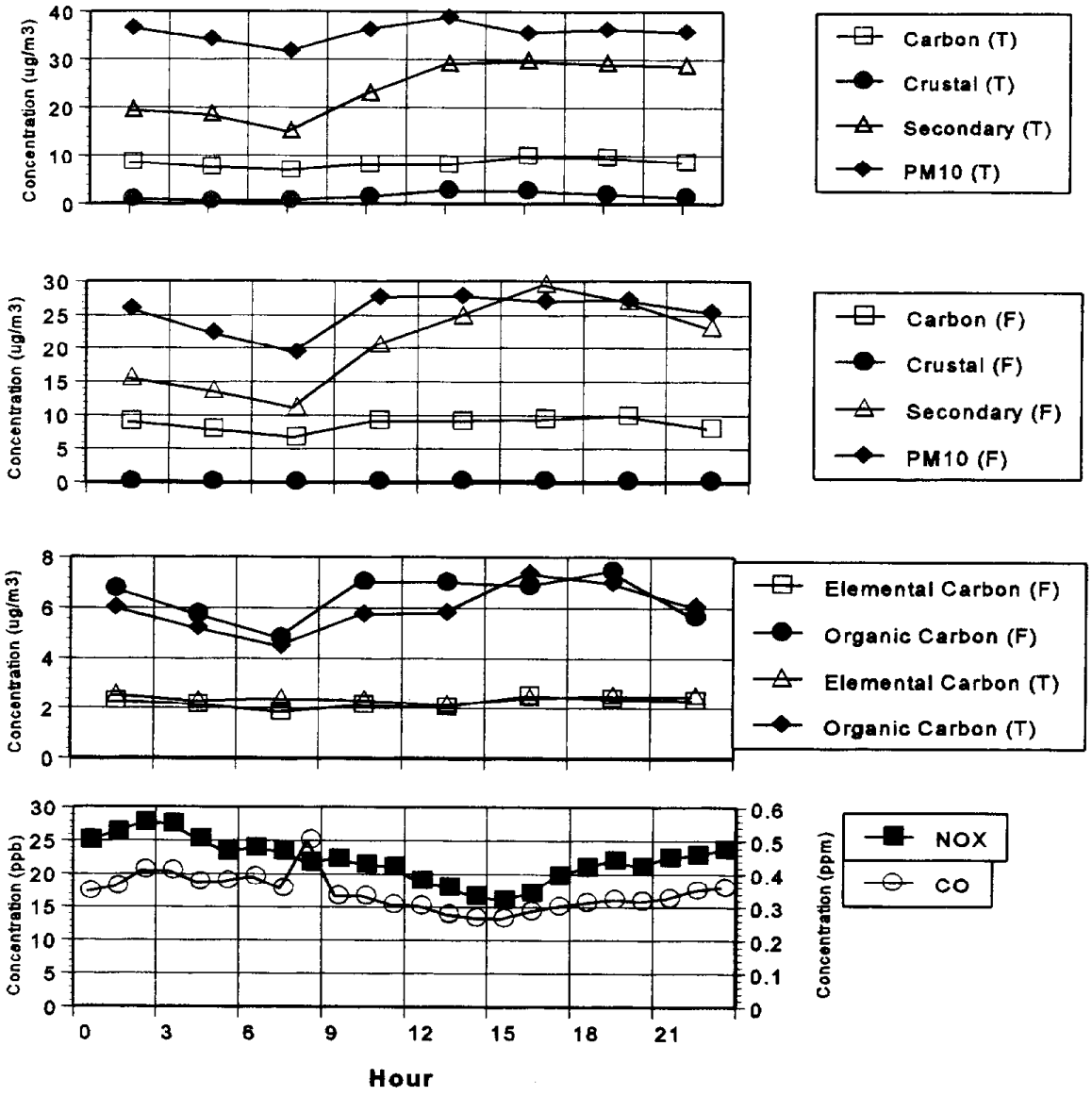

Figure 79. Diurnal averages of particulate, CO, and NO_x concentrations in Southwest Chowchilla for the period December 9, 1995-January 6, 1996. Particulate samples are 3-hour averages commencing at hours 0, 3, etc. Carbon, crustal, and secondary concentrations are averages of 5 to 8 days during the period.

Regression Relationships

The correlation between particulate carbon and CO concentrations is high, as shown in the diurnal profiles of Figure 80 and the regression plot of Figure 81. (In Figure 80, CO concentrations were averaged for the same three-hour sampling periods and the same nine days that particulate carbon measurements were made. It should be noted that the CO and NO_x monitors at Kern and Southwest Chowchilla were collocated with the particulate samplers. At Bakersfield, the particulate samplers were situated on a property adjacent to where the CO and NO_x samplers operated. At Fresno, the particulate samplers were separated from the CO and NO_x monitors by about one-half mile.) At both Fresno and Bakersfield, CO and particulate carbon show nearly identical diurnal profiles, while at Kern and Chowchilla, CO and particulate carbon profiles are both flat. These results are consistent with having strong local sources of CO and particulate carbon near the Fresno and Bakersfield sites, but not the Kern and Chowchilla samplers. Moreover, the similarity of the CO and particulate carbon profiles strongly suggests that CO and particulate carbon share a common emissions source, which is also a source of NO_x, since NO_x correlates highly with CO (see Figures 76-79).

The ratio of particulate carbon to CO does not vary much among the four locations (see Figure 81). The y-intercept is small (5.2 $\mu g\ m^{-3}$) but statistically significant (standard error of 0.5 $\mu g\ m^{-3}$). The intercept may simply result from sampling and analytical uncertainties (for example, elimination of the point where CO concentration is about 9 ppm reduces the intercept to 4.2 $\mu g\ m^{-3}$). However, the positive intercept is also consistent with the presence of a source category of particulate carbon that is distinct from the CO source. Regression of particulate carbon against soluble potassium yields an equally good fit (see Figure 82), though at higher concentrations the Bakersfield carbon values are overpredicted while the Fresno values are underpredicted. Multiple regression of fine carbon against both CO and soluble potassium (Figure 82, bottom panel) improves the fit and reduces the over or

underprediction of carbon concentrations. The intercept (4.1 $\mu g\ m^{-3}$) may result from sampling and analytical uncertainties, but is also consistent with the presence of an additional source category of particulate carbon (e.g., secondary organic aerosol). When the regressions were stratified by hour, the intercepts ranged from 2.7 $\mu g\ m^{-3}$ to 3.8 for hours 2100 through 0600 and from 5 to 6.4 $\mu g\ m^{-3}$ for hours 0900 through 1800; the larger intercepts during daytime hours are consistent with photochemical production of secondary organic aerosol.

If CO and soluble potassium can be taken as indicators of specific source types, the multiple regression (Figure 82, bottom panel), together with the observed values of CO and soluble potassium, indicate that the source associated with soluble potassium on average contributed slightly more than half the particulate carbon, whereas the source associated with CO contributed just under half (the nonzero intercept becomes a consideration for the lower concentrations). Soluble potassium is generally considered a useful tracer of wood smoke (e.g., Lewis et al, 1988; Calloway et al, 1989). Motor vehicles are sources of CO and NO_x, as well as combustion-derived PM. However, potassium is not unique to woodsmoke, nor is CO unique to motor vehicle emissions, and potassium and CO are also correlated, so the results of the multiple regression must be viewed with caution. The regression suggests a somewhat greater contribution from woodsmoke than do chemical mass balance (CMB) analyses of the IMS95 samples, which indicate approximately equal contributions from mobile sources and burning at the Fresno and Bakersfield core sites and greater contributions from mobile sources than from burning (by about 50 to 100 percent) at the Kern and Chowchilla core sites and the Fresno and Bakersfield saturation sites (Magliano, 1997). However, the CMB estimates of the relative contributions of mobile sources and burning are complicated by the presence of excess organic carbon on most samples, which is frequently of a magnitude comparable to either the mobile source or burning contributions (Magliano, 1997). The sites with the lowest excess organic carbon tend to show higher relative contributions from motor vehicles than from woodsmoke.

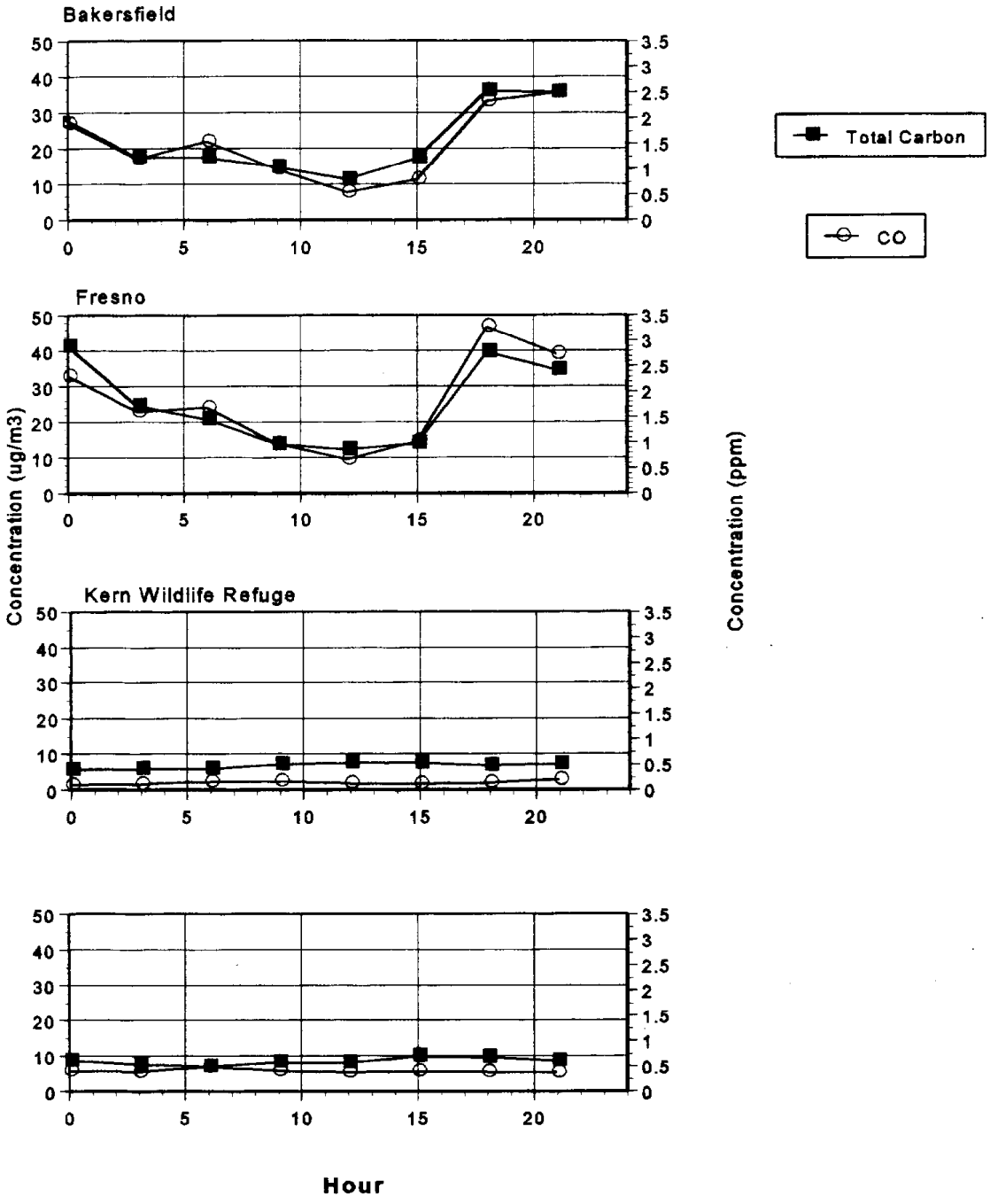

Figure 80. Diurnal average carbon monoxide (CO) and total carbon (elemental plus organic carbon, PM_{10}) concentrations as 3-hour averages at four locations.

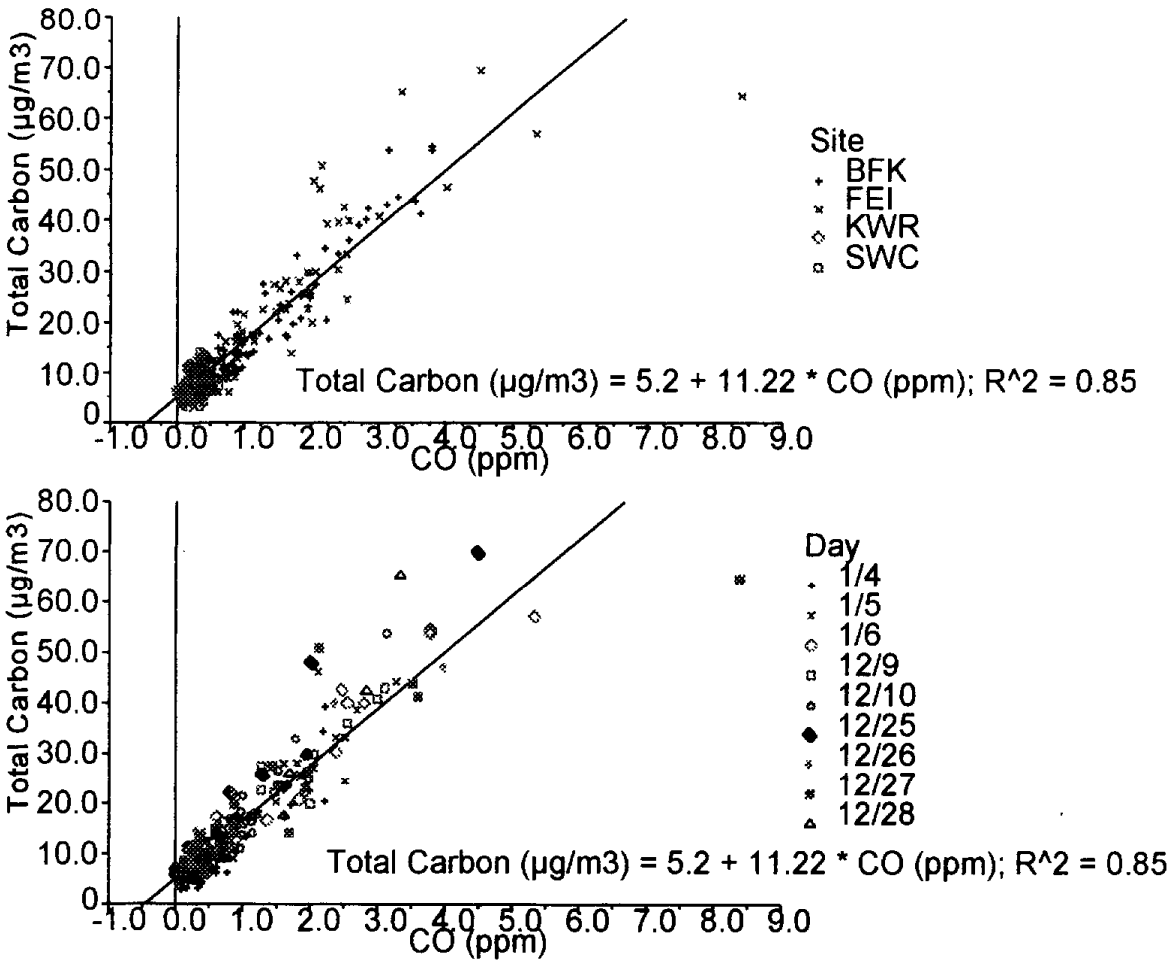

Figure 81. Three-hour average particulate carbon (elemental plus organic, PM_{10}) versus CO split by site (top) and day (bottom).

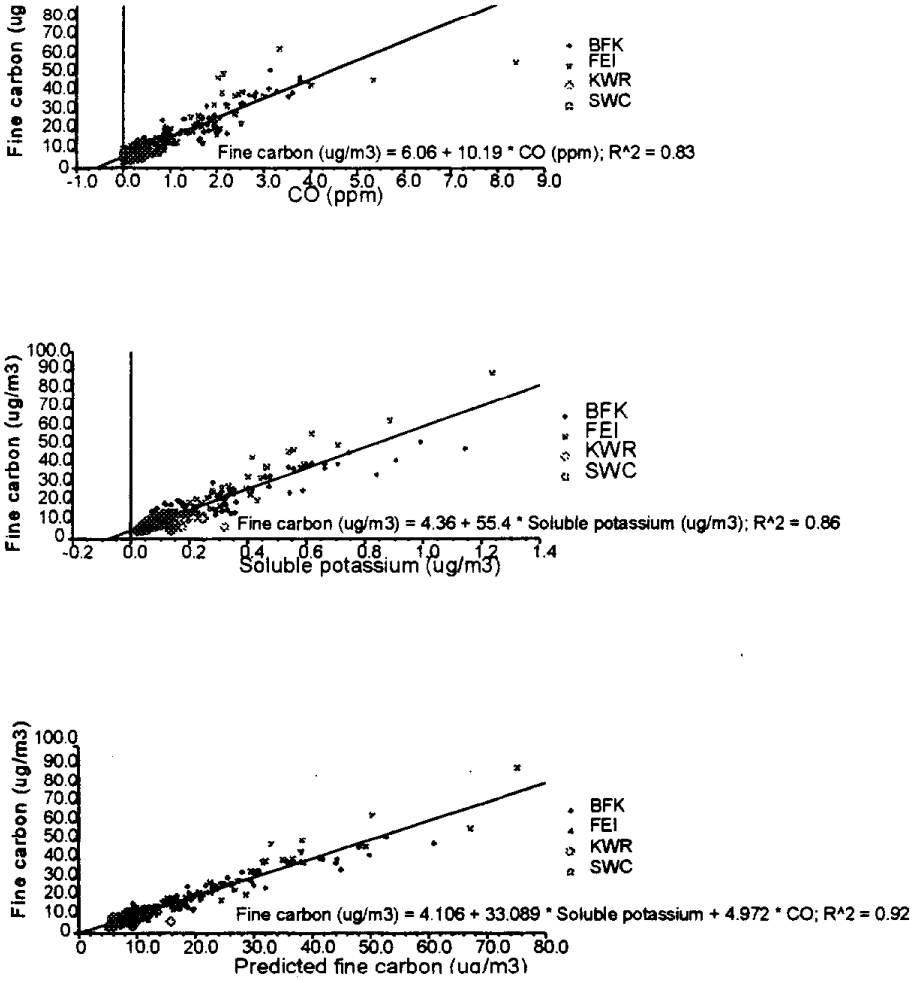

Figure 82. Three-hour average fine carbon concentration versus CO (top), soluble potassium (center), and predicted carbon from multiple regression of carbon against CO and soluble potassium (bottom).

Some additional regression relationships support the association of CO with motor vehicle emissions in the study area. Various alkenes and aromatics correlate highly with CO (see Figures 83-85). (Hydrocarbon and carbonyl samples were collected only at Bakersfield and Fresno, and only from 6:00 - 9:00 a.m. and 3:00 - 6:00 p.m.). Benzene and acetylene, for example, correlate strongly with CO. Alkanes, which are often associated with evaporative emissions, do not. MTBE, which is a gasoline additive, correlates both with exhaust components (e.g., CO) and with alkanes (see Figure 85), indicating that both are indeed related to motor vehicle emissions.

Alkenes and aromatics also correlate moderately with particulate carbon concentrations (Figure 86). These correlations are statistically significant, though not as strong as those of alkenes and aromatics with CO, or those between CO and particulate carbon. Some factors that might affect the correlations shown in Figure 86 are: (1) measurement uncertainties for both particulate carbon and the gas-phase species may be about 20 percent, (2) the VOC samples were collected only at 6:00 a.m. and 3:00 p.m., thus limiting the number of samples available, (3) samples were collected at Bakersfield and Fresno only (the Bakersfield and Fresno samples in Figure 81 showed more scatter than did those from Kern and Chowchilla), and (4) gas- and particulate-phase species are subject to different physical processes (note, however, that this consideration also applies to the correlation betwe : CO and carbon, which is greater than the correlations between alkenes and carbon or between aromatics and carbon).

Alkane concentrations were greater in Bakersfiekd than Fresno (Figure 83). Regressions of ethane against acetylene yielded mean ratios of ethane-to-acetylene of about 3:1 in Bakersfield and 1:1 in Fresno (not shown). Acetylene is usually considered an indicator of motor vehicle emissions, while ethane occurs in the global background and may also derive from oil production activities.

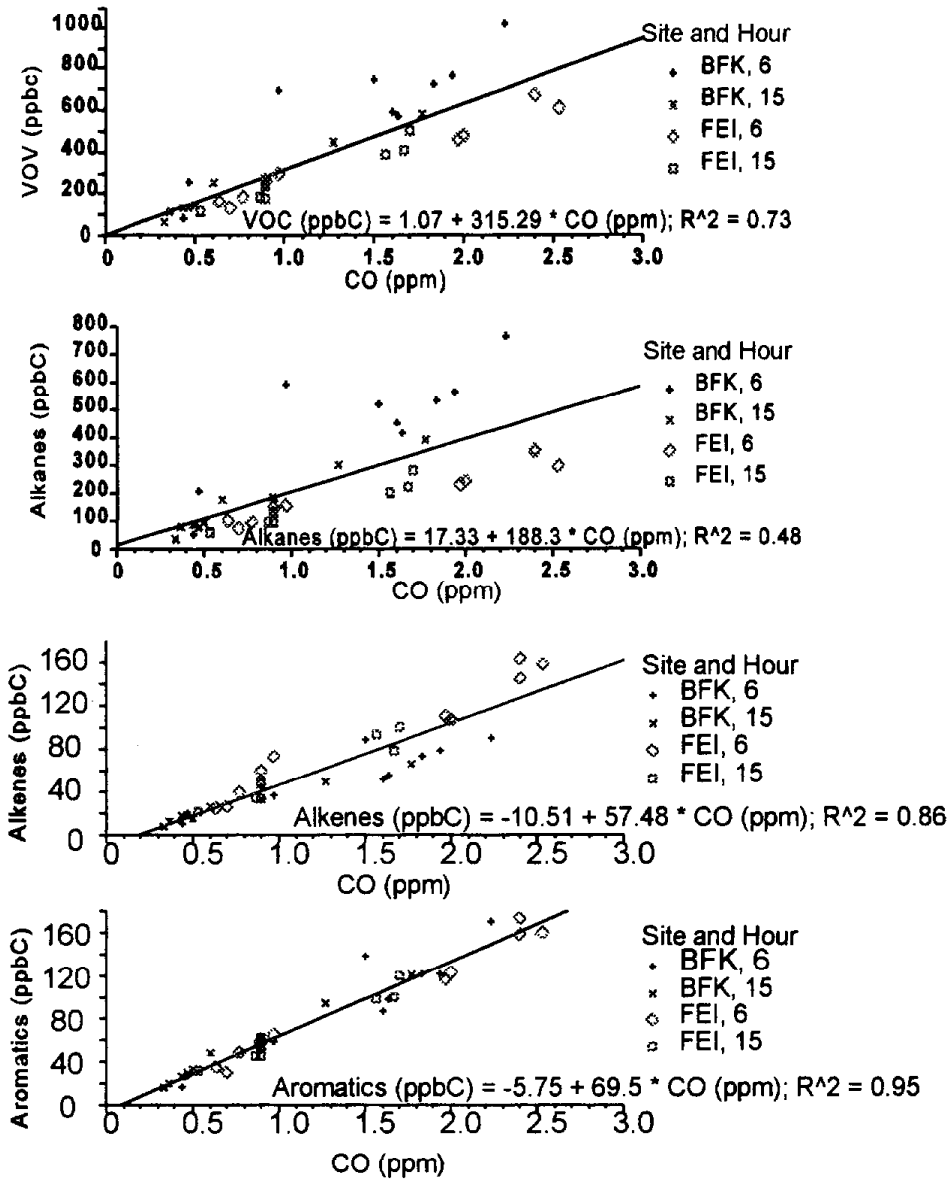

Figure 83. Hydrocarbon (VOC), alkane, alkene, and aromatic versus CO concentrations from 6:00 to 9:00 a.m. and 3:00 to 6:00 p.m. at Bakersfield and Fresno.

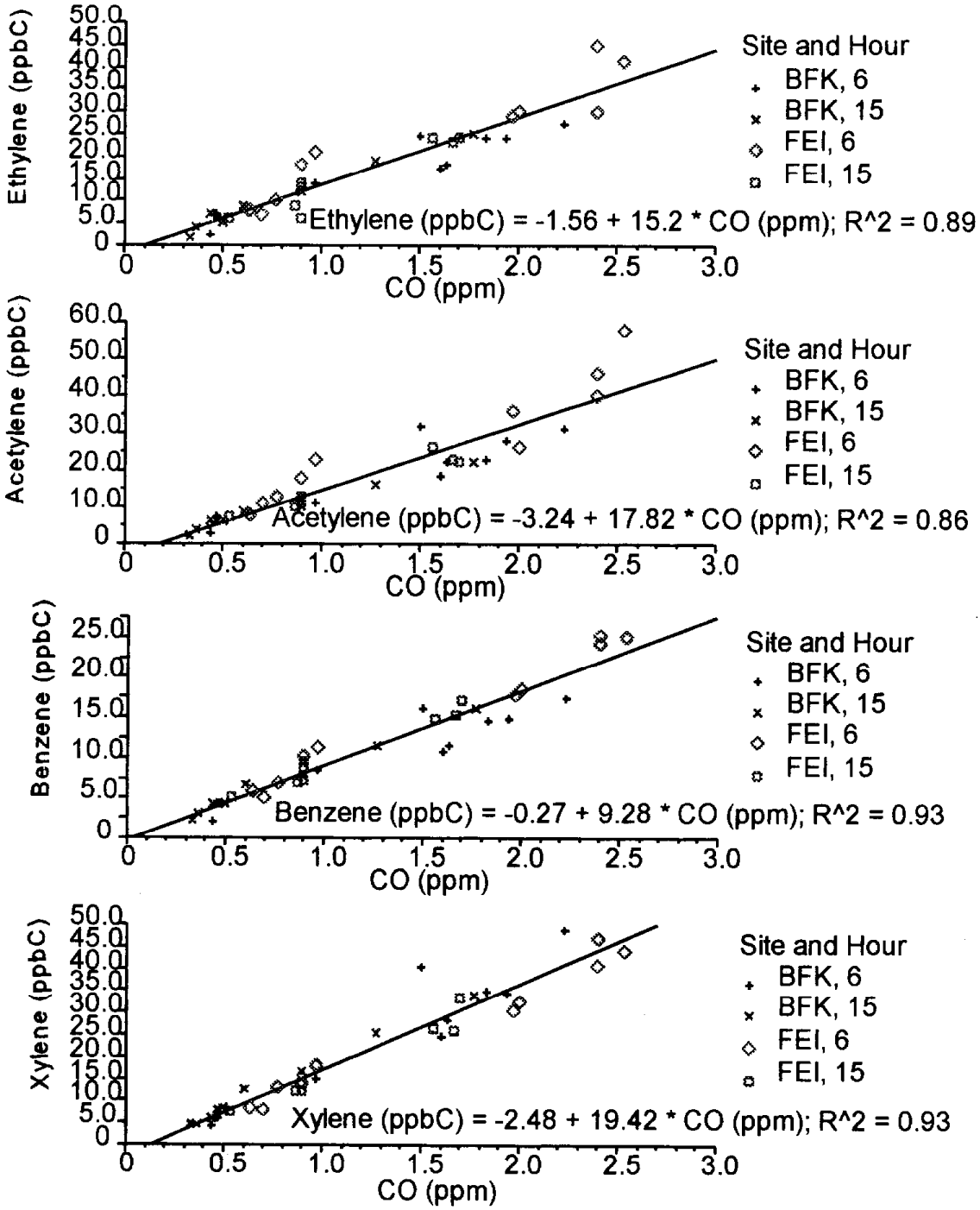

Figure 84. Ethylene, acetylene, benzene, and xylene versus CO concentrations from 6:00 to 9:00 a.m. and 3:00 to 6:00 p.m. at Bakersfield and Fresno.

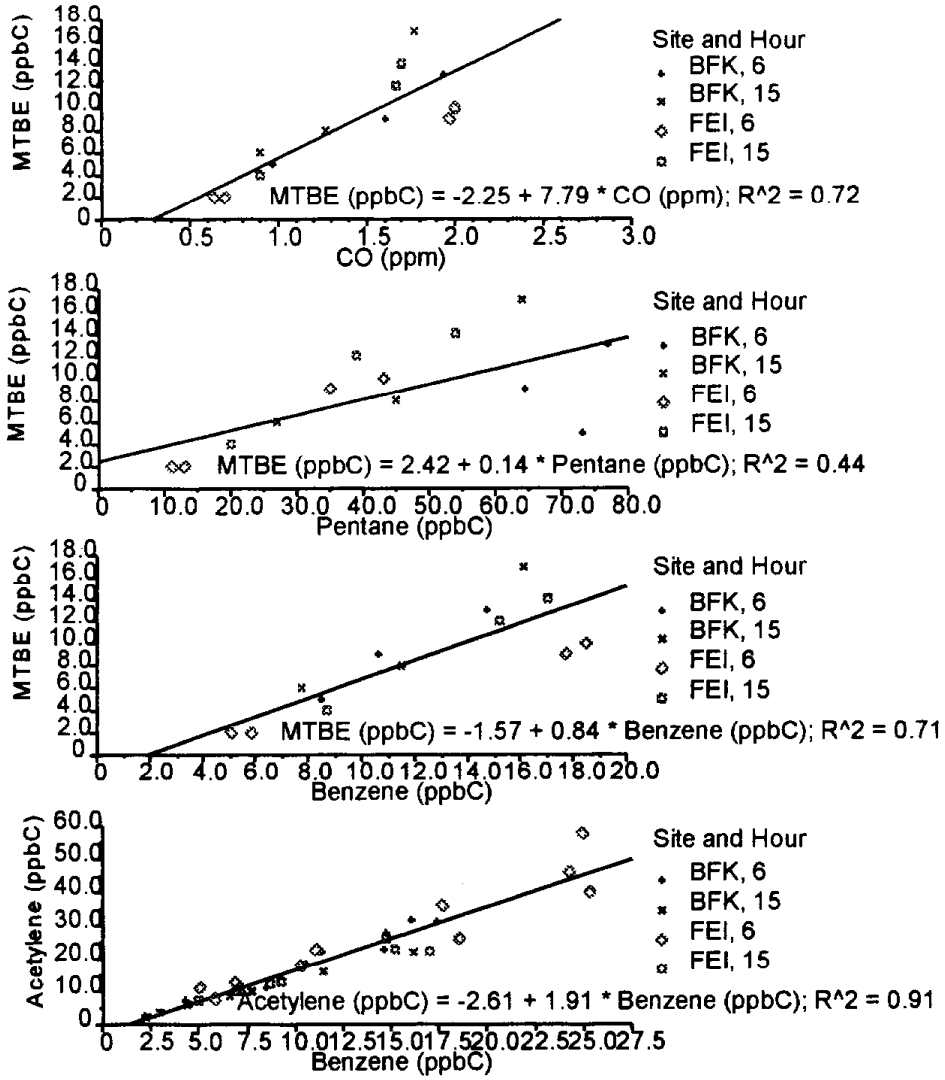

Figure 85. Acetylene and MTBE versus CO, pentane, and benzene from 6:00 to 9:00 a.m. and 3:00 to 6:00 p.m. at Bakersfield and Fresno.

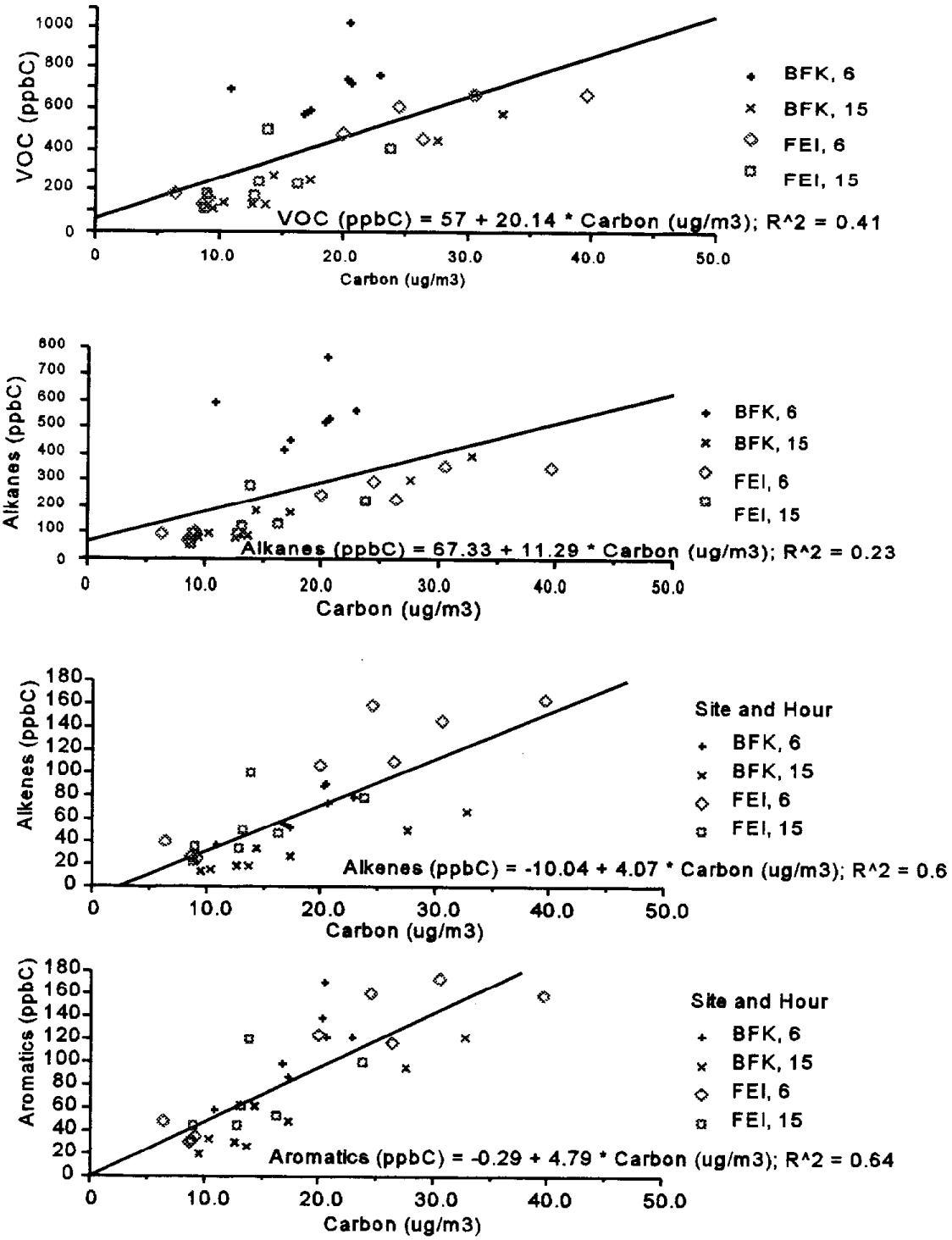

Figure 86. Hydrocarbon (VOC), alkane, alkene, and aromatic concentrations versus particulate carbon (elemental plus organic, PM_{10}) at Bakersfield and Fresno, 6:00 to 9:00 a.m. and 3:00 to 6:00 p.m.

Factor analysis was used to further delineate chemical species that tended to covary. The number of samples was limited (28 from Bakersfield and Fresno), thus limiting the number of species that could be included. The results should be viewed as indicative, rather than definitive. Three factors accounted for 92 percent of the variance. Oblique rotation showed that the factors grouped rather simply into primary emissions, including alkenes and aromatics (CO, NO_x, organic carbon, elemental carbon, benzene, ethylene, acetylene, m-xylene, and p-xylene), C2-C5 alkanes (ethane, propane, i-butane, n-butane, i-pentane, n-pentane), and species having a photochemical source (formaldehyde, acetaldehyde, and acetone) (see Table 46).

Table 46. Oblique solution primary pattern matrix for 28 samples from Bakersfield and Fresno. Cell entries are the regression coefficients relating each species to each factor. Units are ppb for all species except CO (ppm), elemental carbon (EC), and organic carbon (OC), which are $\mu g\ m^{-3}$.

Species	Factor 1	Factor 2	Factor 3
NOx	.741	.294	-.239
CO	.920	.096	.040
EC	.777	.174	.086
OC	.837	-.185	.152
Acetone	-.001	.148	.940
Benzene	1.001	-.054	.072
Ethane	.033	.950	-.010
Ethylene	.989	-.034	.030
Acetylene	1.067	-.148	-.122
Propane	-.217	1.075	-.028
i-butane	-.076	1.029	.036
n-Butane	0.000	.997	.031
i-Pentane	.341	.743	.030
n-Pentane	.072	.950	.010
m-Xylene	.834	.239	-.007
o-Xylene	.836	.232	.005
HCHO	.087	-.110	.916
CH3CHO	-.131	.027	.996

Diurnal Patterns of Mixing Height

The earlier discussion ignored the effects of changes in mixing height on ambient concentrations. Hourly mixing heights (see Section 2) were averaged over the period December 9, 1995 through January 6, 1996 for both Bakersfield and Fresno. As shown in Figure 87, daily mixing heights increased steadily from early morning (400 hours) through midday (1300 hours). After the midday hour, mixing heights decreased steadily through the night (2200 hours).

As an approximation, the diurnal concentrations were adjusted to account for differences due to mixing height as follows. For each 3-hour period, the concentration was multiplied by the ratio of the associated mixing height to the peak daily mixing height. While this adjustment corrects for differences due to dilution, it does not account for aloft concentrations of species, and therefore represents only a hypothetical concentration corresponding to dilution of surface concentrations into clean air with mixing heights equal to the daily maximum. As such, it is only a partial correction.

Figures 88 and 89 show that in both Fresno and Bakersfield, the adjusted diurnal particulate concentrations rise throughout the afternoon, with secondary species peaking in the noon sample (as expected for photochemically-driven reactions) and particulate carbon concentrations peaking in the 6:00 p.m. sample (roughly coincident with the evening commute traffic). These figures also show that CO and NO_x exhibit three peaks at approximately 900, 1200 and 2000 hours, which approximately coincide with the diurnal pattern of motor vehicle emissions shown earlier.

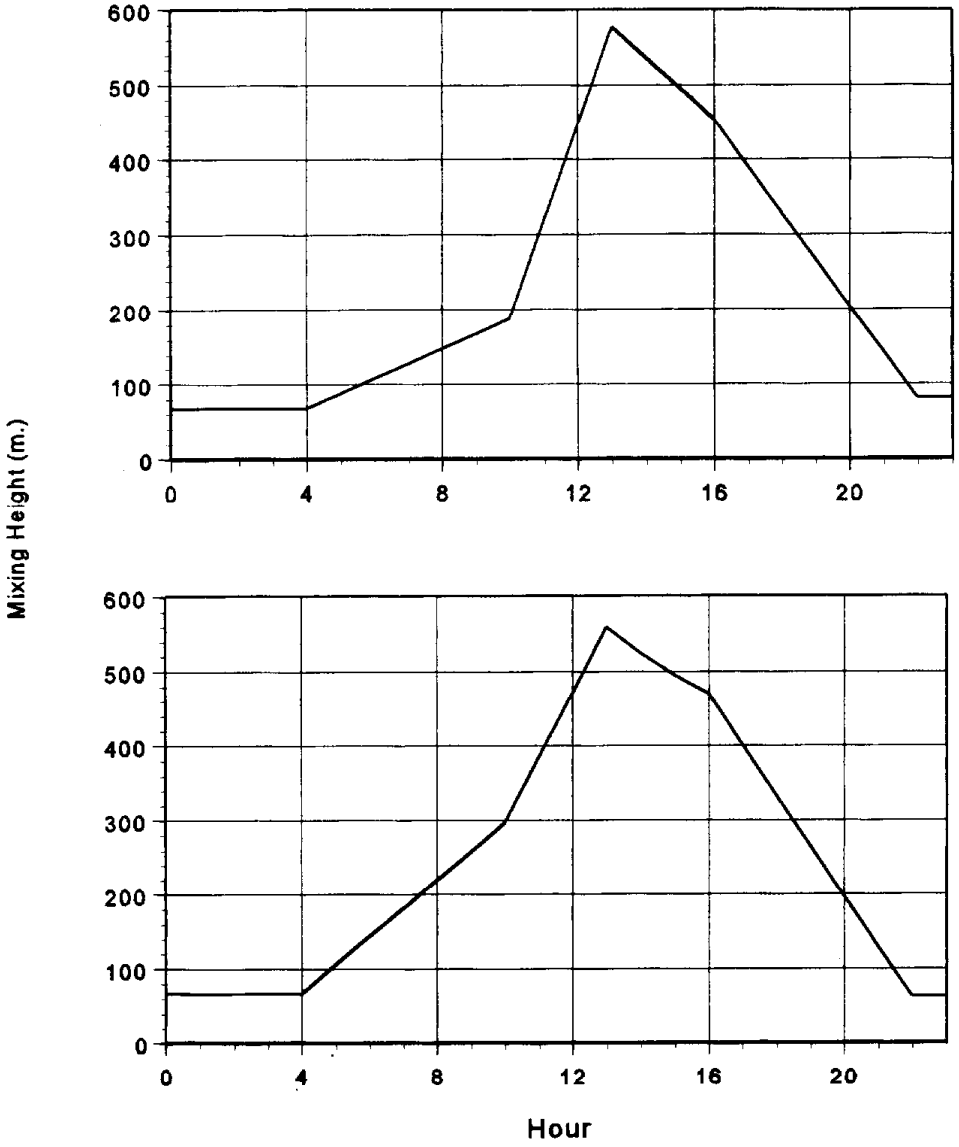

Figure 87. Diurnal mixing heights averaged over the period December 9, 1995-January 6, 1996 in Bakersfield (top) and Fresno (bottom).

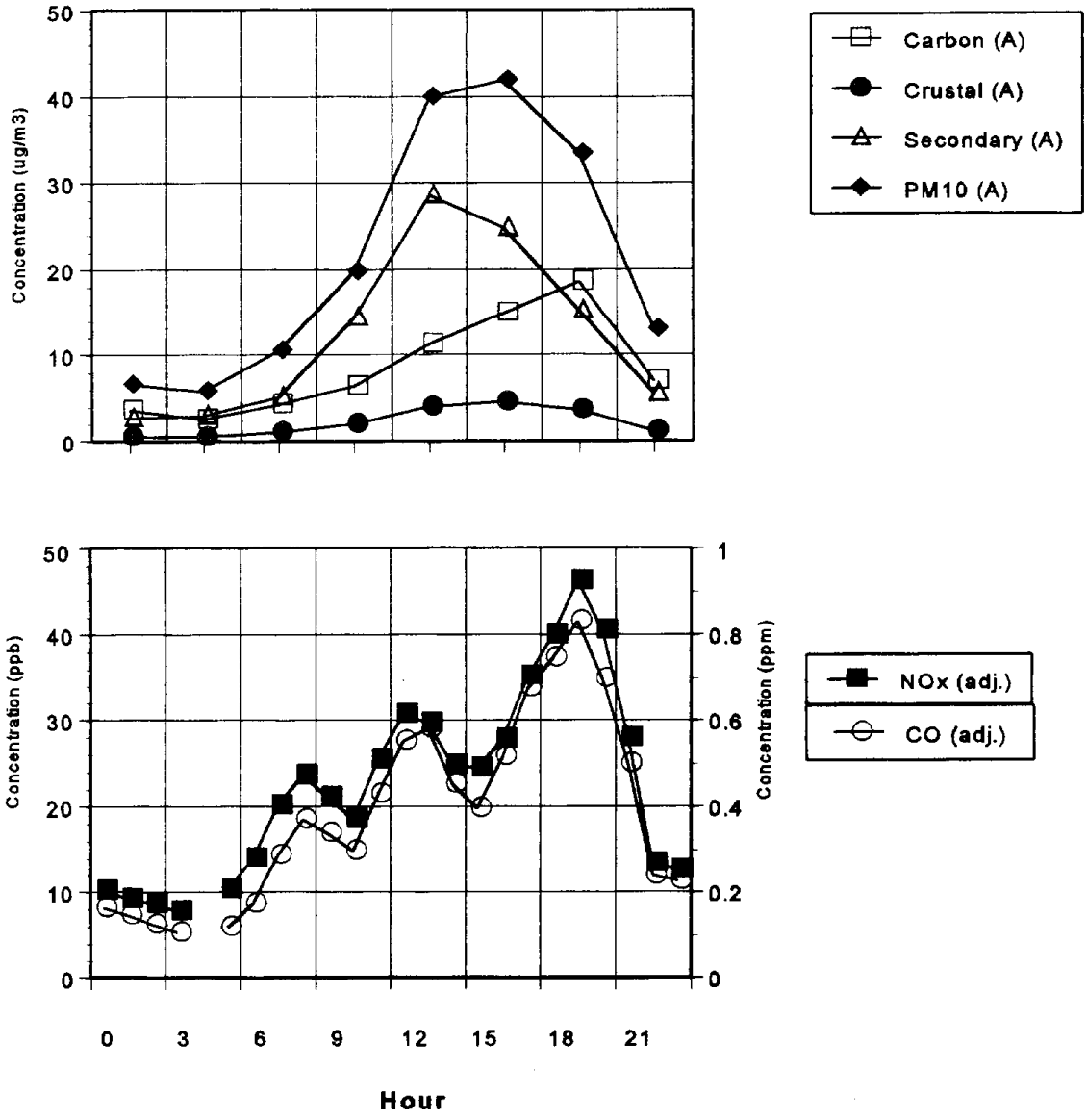

Figure 88. Diurnal concentrations averaged over the period December 9, 1995-January 6, 1996 in Bakersfield, adjusted for changes in mixing height.

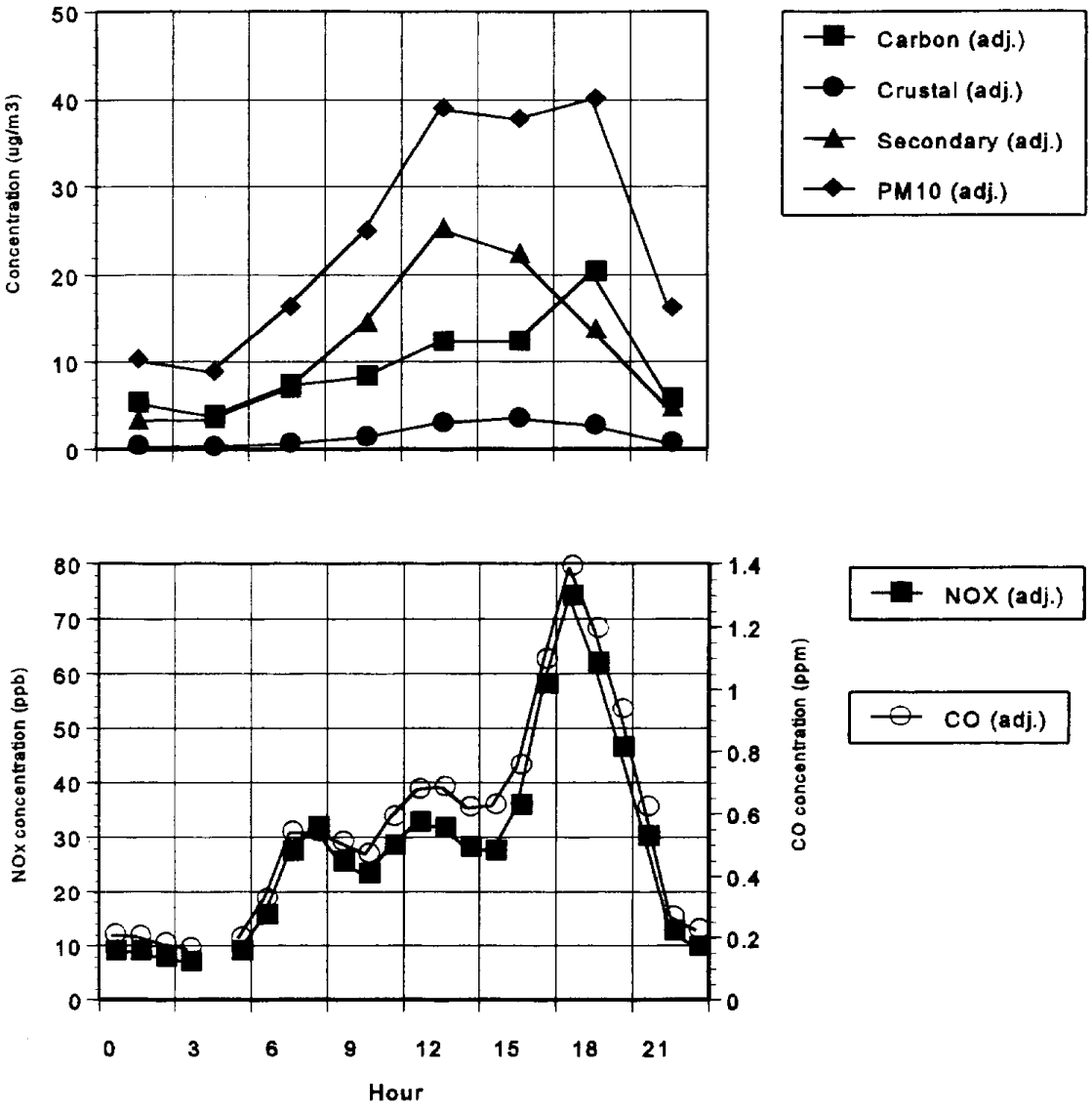

Figure 89. Diurnal concentrations averaged over the period December 9, 1995-January 6, 1996 in Fresno, adjusted for changes in mixing height.

Diurnal Patterns of Chemical Mass Balance Source Contributions

Chemical Mass Balance (CMB) analyses were obtained from the ARB and mean diurnal profiles were constructed for the predicted source contributions (see Figures 90 and 91). At the rural sites of Kern and Chowchilla, nitrate dominated the total, peaking between mid-morning and mid-afternoon. At Fresno and Bakersfield, the nitrate source contribution also exhibited daytime peaks and dominated between about 9 a.m. and 3 p.m. As noted earlier, such peaks are consistent with daytime photochemical production of nitric acid and subsequent rapid conversion to particulate nitrate via reaction with ammonia gas. The mean profiles of other components at Kern and Chowchilla showed little variation over the course of the day. In contrast, the carbon-related source contributors (motor vehicles, combustion, and the excess organic carbon not accounted for by motor vehicles or combustion) exhibited pronounced evening peaks at Bakersfield and Fresno. The combustion component exceeded the motor vehicle component on the samples collected beginning at 0, 3, 18, and 21 hours, in reasonable agreement with the diurnal profile of emissions (see Figure 75).

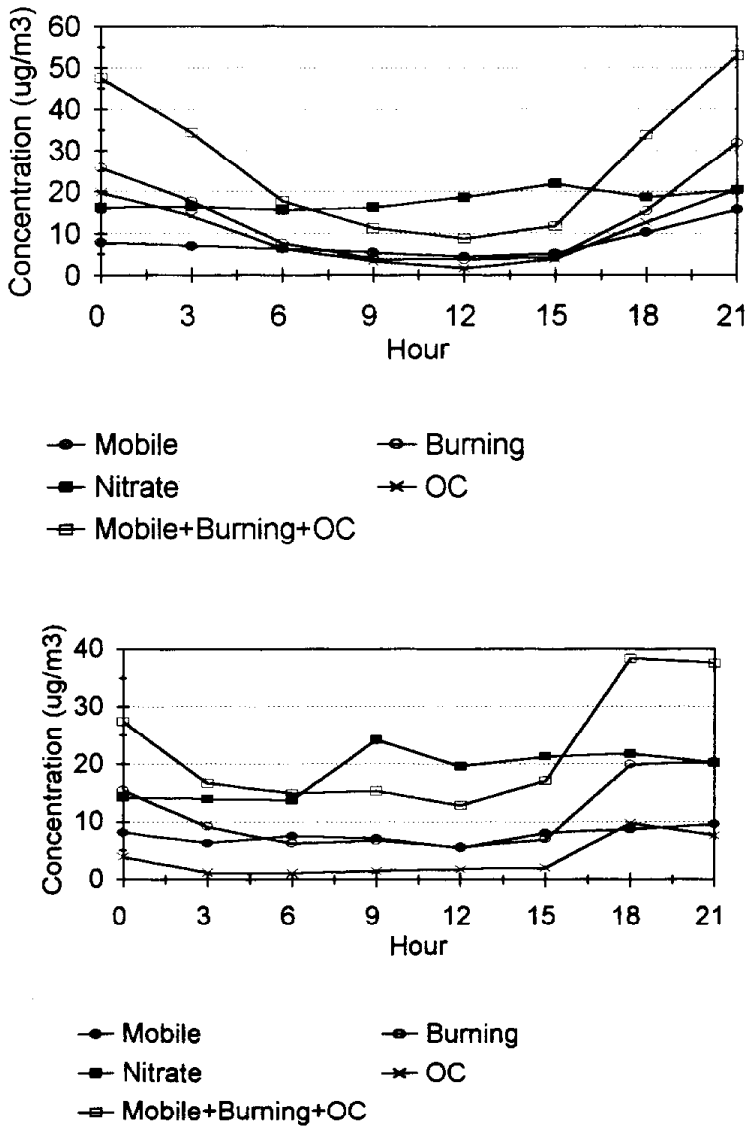

Figure 90. CMB-predicted source contributions averaged for available dates over the period December 9, 1995-January 6, 1996 for Fresno (top) and Bakersfield (bottom).

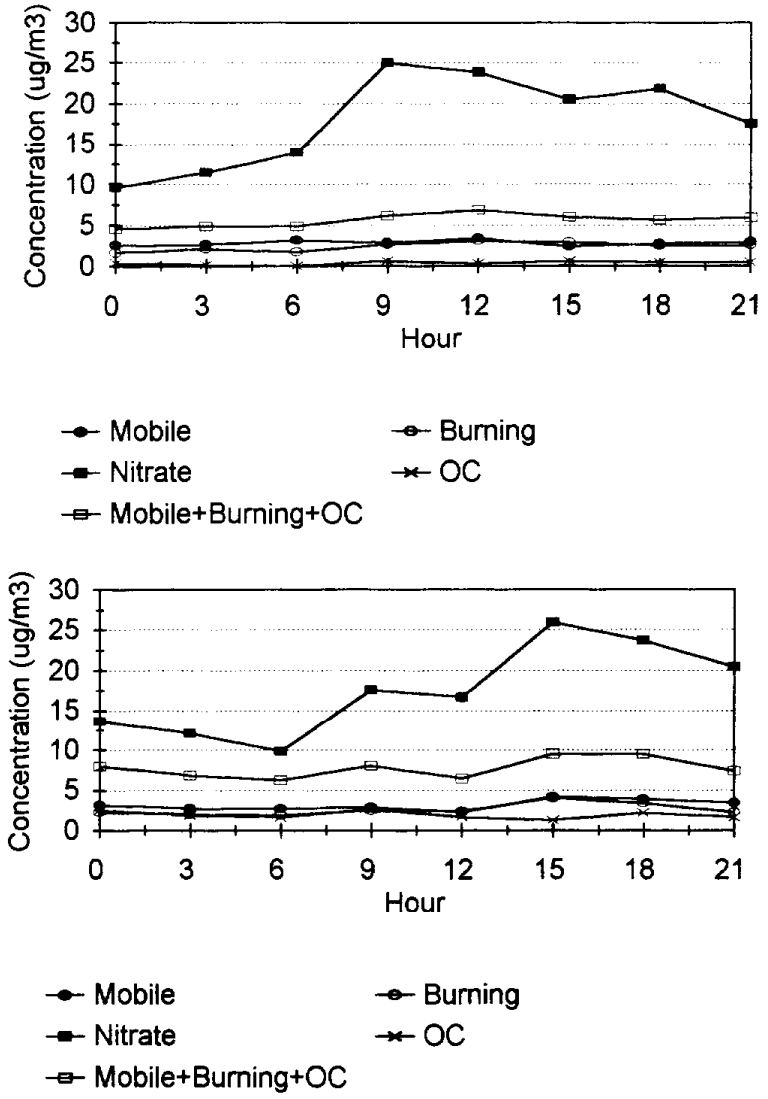

Figure 91. CMB-predicted source contributions averaged for available dates over the period December 9, 1995-January 6, 1996 for Kern (top) and Southwest Chowchilla (bottom).

CONCLUSION

In the winter study, diurnal profiles of emissions, ambient concentrations, and CMB source strengths showed generally consistent patterns (during fall, only 24-hour samples were collected). Evening peaks in PM mass coincided with both the afternoon decrease in mixing height and the late afternoon and early evening increases in motor vehicle emissions and fuel combustion.

At all four winter core sites (Bakersfield, Fresno, Chowchilla, and Kern), $PM_{2.5}$ mass was about 75 percent of the PM_{10} mass, on average. The $PM_{2.5}$ carbon and secondary (nitrate plus ammonium plus sulfate) concentrations were 80 to 100 percent of the PM_{10} carbon and secondary concentrations.

Both PM_{10} and $PM_{2.5}$ mass were dominated by the carbon and secondary components; however, the temporal patterns of carbon and secondary species differed. At all sites, secondary-species concentrations showed a daytime rise (about 5 to 15 $\mu g\ m^{-3}$). Bakersfield and Fresno showed mean evening rises of particulate carbon of about 30 $\mu g\ m^{-3}$. At Bakersfield and Fresno, secondary concentrations exceeded carbon concentrations during the day; carbon exceeded secondary at night. As a result, at Bakersfield and Fresno, both PM_{10} and $PM_{2.5}$ mass concentrations began to rise at about 3:00 p.m. (the 1500-1800 sample) and reached maxima between 1800 and midnight. The evening peaks in mass at Bakersfield and Fresno were driven by the carbon component. At Kern and Chowchilla, the secondary components also showed daytime peaks, but dominated during all hours. Consequently, at Kern and Chowchilla, PM mass peaks occurred during the day.

Organic carbon concentrations exceeded elemental carbon by factors of 2:1 to 3:1. At each site, both elemental and organic carbon followed the same diurnal profile, but the profiles at the urban sites (Bakersfield and Fresno) differed from those at the rural sites.

Regression analyses showed high correlations between particulate carbon and both CO and soluble potassium. These correlations were interpreted as indicating that motor vehicles and fuel combustion were the principal sources of particulate carbon, with the latter source being slightly larger. CMB analyses also allocate particulate carbon to motor vehicles and combustion, though a nontrivial fraction of organic carbon was unexplained by the CMB source contributions. The relative amounts of the carbon allocated to motor vehicles and combustion by the multiple regression and the CMB analyses were approximately consistent with emission inventory estimates.

Factor analysis was used to delineate chemical species that tended to covary. While the number of samples was limited, three distinct groups of species were delineated. Elemental and organic carbon were associated with CO, NO_x, alkenes (ethylene and acetylene), and aromatics (benzene, m-xylene, p-xylene). The second species group included C2-C5 alkanes (ethane, propane, i-butane, n-butane, i-pentane, n-pentane), and the third group included species having a photochemical source (formaldehyde, acetaldehyde, and acetone). Alkane concentrations were substantially greater at Bakersfield than at Fresno, with the ratio of ethane-to-acetylene being about 3:1 at Bakersfield and 1:1 at Fresno.

SECTION 8: CONCLUSION

TECHNICAL FINDINGS

The IMS95 was spatially extensive but temporally limited. The data may reflect meteorological and other conditions specific to the sampling period. The conclusions of this report are therefore specific to the study period, and their applicability to other time periods is not known.

Sampling and Measurements

The IMS95 saturation networks and core-site sampling produced a rich and informative data base. Overall, the measurements of PM mass and chemical composition were of reasonably high quality and consistency. However, because complete speciation was not carried out on some samples, it was not always possible to conduct some standard data validation tests, such as comparison of mass to the sum of species concentrations. Time series plots and spatial contour plots were used to supplement the standard validation tests.

The measurements were spatially dense but temporally limited, which limited the utility of some statistical procedures, such as principal components analysis, which require a large number of temporal replicates.

The comparison of measurements from collocated samplers captures sampling error as well as analytical error. Only two saturation sites were collocated. For most species, the uncertainties calculated from the differences between these two collocated sites were considerably higher than the analytical uncertainties listed in the data base.

Portable saturation samplers were collocated with the core-site sequential-filter samplers at Bakersfield, Fresno, Kern, and Corcoran. When the 3-hour measurements from the sequential-filter samplers were aggregated to match the 24-hour sampling

intervals of the saturation monitors, the agreement was very good. No offsets were evident and few substantial deviations occurred.

Classification of Site Characteristics

Three sites were located west of the western boundary of the IMS95 modeling domain (North Los Banos, Panoche Water District, and Candelabra Tower in Walnut Grove). The site designations of the other 81 chemistry sites were compared to information in the gridded land use, population, and emissions files, and to photos and videos of the sites. The sites' primary and secondary designations, which were made at the inception of the sampling program, were based upon emission source types and included the principal categories of agricultural, urban, transportation, residential, rural, industrial, and boundary, as well as numerous subcategories. For 57 of the sites, one or more items of conflicting information were found.

For 18 sites, emission source values in the gridded emissions inventory conflicted with the designated site characteristics. However, in only one case, confirmed by inspection of videos and photos, was the primary designation of the site apparently incorrect. For each of the remaining cases, site photos and videos indicated that the immediate environs of the site were of the same type as its classification. However, in each of these cases, emissions within the 4 km x 4 km cell containing the site in question were not dominated by the designated source type and were in fact substantially different than the emissions mix associated with other sites of the same designated type.

In addition, for thirty of the 42 residential or industrial sites, emissions within either a 4 km x 4 km or a 20 km x 20 km area were dominated by transportation or agricultural sources, rather than residential or industrial sources. However, as noted above, site photos and videos indicated in each case that the immediate environs of each such site were of the same type as its classification.

For ten other cases, some potential emission sources were observed in the videos or the photos, but had not been included among the secondary characteristics of the sites.

Thirty one (31) sites had designated characteristics that conflicted with the gridded land use files. In most cases, the land use was defined as agricultural, but the site characteristic was residential or urban. Inspection of photos and videos suggested that, in most cases, the land use files were inaccurate, of too coarse a resolution, or possibly outdated. As noted above for the emissions files, in some cases the site photos and videos indicated that the immediate environs of each such site were of the same type as its classification, though the larger surrounding area may have been different.

Fourteen (14) sites had designations that conflicted with the gridded population files. For 7 of these 14, the population appeared too small for a residential site. For the remaining seven sites, which were classified as either agricultural or industrial, the population appeared too large. The photos and videos again supported the existing site designations, suggesting that the gridded population file warrants investigation.

Site classifications, which were based on visual characterizations of site surroundings, did not predict emission source strengths on larger distance scales (4 to 20 km), which were found to be more characteristic of emission zopnes of influence. However, the site classifications were a useful indication of potential local emission sources, which in some cases were substantial.

Spatial Representativeness of the Monitoring Sites

The spatial representativeness (SR) of a monitoring site may be loosely defined as the area within which pollutant concentrations are approximately constant. The

more explicit definition that was used in this study is the percentage of the area of a saturation monitoring domain having concentrations within 20 percent of those recorded at the site under consideration. Population representativeness was defined as the percentage of domain population in areas having concentrations within 20 percent of those recorded at the site under consideration. The choice of 20 percent was based upon consideration of differences that would be expected to be judged significant from a health-effects perspective, the variation of concentrations across monitoring sites, measurement uncertainty, and an analysis of the sensitivity of the findings. Typically, PM concentrations varied across sites by about 50 percent on any day while sampling uncertainty for PM_{10} mass was about 10 $\mu g\ m^{-3}$, corresponding to about 10 to 20 percent of the typical mass concentrations recorded in the Fresno and Bakersfield areas.

To determine spatial representativeness, the monitoring data were interpolated to fine (0.1 km) grids for both the fall and winter saturation networks. The species analyzed were PM_{10} mass, the secondary component (sum of sulfate, nitrate, and ammonium), carbon (elemental plus organic), and the crustal component (the sum of aluminum, silicon, iron, manganese, calcium, and magnesium). The gridded values were then used to determine the portions of the monitoring domains having values within the specified percentage of those recorded at each individual site.

Spatial representativeness varied considerably among sites, days, and components. Averaging across days, the mean areal fractions of the saturation domains having PM_{10} concentrations within 20 percent of those recorded at the core sites were 65% for Bakersfield, 87% for Corcoran, 44% for Fresno, and 79% for Kern. Taking into consideration the areas of each monitoring domain, these values correspond to 195 km^2 for Bakersfield, 626 km^2 for Corcoran, 352 km^2 for Fresno, and 134 km^2 for Kern. In terms of distance, the values roughly correspond to about 10 to 20 km for the three winter networks and about 25 km for the fall Corcoran study. As noted,

considerable variation occurred among days and chemical species. Moreover, some sites, other than core sites, exhibited values representative of much smaller areas.

Population representativeness was always slightly greater or approximately equal to area representativeness. Monitoring sites generally had greater areas of representativeness for secondary species than for PM_{10} mass, and lesser areas for crustal and carbon components.

It was shown that at least 90 percent of each saturation monitoring domain would exhibit concentrations within 20 percent of those of the core site plus one or two additional sites. The most representative combinations of two to three sites were identified for each domain. While the core sites were shown to represent average domain concentrations well, they did not always represent the network maxima. In Corcoran, the maximum site exhibited PM mass concentrations up to 130 $\mu g\ m^{-3}$ greater than those of the core site. In Bakersfield and Fresno, the differences in concentration between the core and the maximum sites were less than 5 $\mu g\ m^{-3}$ on average.

Zones of Influence of Emissions

Three methods were employed to evaluate the zones of influence of emissions. First, gridded concentration fields were examined to identify concentration gradients. The gradients were qualitatively evaluated to identify approximate distances over which concentration peaks diminished to both urban and regional background levels. The gridded concentration fields were also compared with maps of emission densities. Second, a series of regressions of site concentrations versus emissions densities were carried out. Emission densities were determined for a variety of scales of spatial averaging and the averaging scales that provided the best fits between concentrations and emissions were identified. Finally, a dispersion model was used to estimate upwind areas of influence on the core sites.

The three methods yielded consistent results. The contour plots revealed neighborhood-scale (on the order of 1 km) influences in the Corcoran domain and urban-scale (5 to 15 km) influences for all saturation networks. In the fall Corcoran study, gradients of PM_{10} mass were 10 to 50 $\mu g\ m^{-3}\ km^{-1}$, implying that nearby emission sources often influenced site concentrations substantially. The distance scale for the decay from peak to urban background values was about 5 to 10 km in Corcoran and 10 to 15 km in the other domains. However, the range of influence of emission sources could have been greater than these scales since the network domains were not large enough to capture the decay from urban background levels to regional background levels.

The regression results indicated that transport and dispersion of emissions occurred on a scale of about 15 km (urban scale) during winter and about 40 km (regional scale) during fall. Local influences (neighborhood scale, 0.5 to 4 km) could have been superimposed upon the urban and regional-scale dispersion, as indicated by the scatter of concentrations within each saturation network, but the regressions were not capable of discerning such influences since the emissions grid-cell resolution was only 4 km x 4 km. The winter regressions are also consistent with regional dispersion of PM emissions on scales exceeding 15 to 20 km, since correlation coefficients remained high for scales exceeding the 14 km scale of the best fit regressions. The fall regression results showed no correlation between concentrations and emissions densities at scales less than 20 km because the urban sites (in Fresno and Bakersfield) showed lower PM_{10} concentrations than did the Corcoran sites, even though emission densities were greater in the urban areas. On a scale of about 40 km, though, the Corcoran concentrations were associated with higher emission densities, thus indicating the contribution of a regional background concentration to the overall values observed at the Corcoran sites.

The dispersion model calculations for the winter episodes showed substantial

source influence for locations within less than 5 to about 15 km of receptor sites and less influence, but geographically more widespread, from locations within about 15 to greater than 25 km. The results suggest a scale of significant emissions influence of a few up to about 15 km, and a scale of approximately 20 km or more over which emissions are more widely dispersed but still contribute to general background levels. Input data for the dispersion calculation were unavailable for the fall period.

In summary, it is possible to identify neighborhood-scale (about 1 km), urban-scale (about 15 to 20 km), and regional-scale (exceeding about 20 to 25 km) emission influences during both fall and winter. During winter, the neighborhood and urban scales dominated, with a mean urban background concentration of approximately 40 $\mu g\ m^{-3}$ in the Fresno and Bakersfield networks and mean peak-site values of about 60 to 80 $\mu g\ m^{-3}$. During fall, the mean regional background in the Corcoran network was about 100 $\mu g\ m^{-3}$, with neighborhood- and urban-scale influences increasing mean concentrations at the peak sites to about 130 to 190 $\mu g\ m^{-3}$.

Other Findings

In the winter study, diurnal profiles of emissions, ambient concentrations, and CMB source strengths showed generally consistent patterns (during fall, only 24-hour samples were collected). Evening peaks in PM mass coincided with both the afternoon decrease in mixing height and the late afternoon and early evening increases in motor vehicle emissions and fuel combustion.

At all four winter core sites (Bakersfield, Fresno, Chowchilla, and Kern), $PM_{2.5}$ mass was about 75 percent of the PM_{10} mass, on average. The $PM_{2.5}$ carbon and secondary (nitrate plus ammonium plus sulfate) concentrations were 80 to 100 percent of the PM_{10} carbon and secondary concentrations.

Both PM_{10} and $PM_{2.5}$ mass were dominated by the carbon and secondary

components; however, the temporal patterns of carbon and secondary species differed. At all sites, secondary-species concentrations showed a daytime rise (averaging about 5 to 15 $\mu g\ m^{-3}$). Bakersfield and Fresno showed mean evening rises of particulate carbon of about 30 $\mu g\ m^{-3}$. At Bakersfield and Fresno, secondary concentrations exceeded carbon concentrations during the day; carbon exceeded secondary at night. As a result, at Bakersfield and Fresno, both PM_{10} and $PM_{2.5}$ mass concentrations began to rise at about 3:00 p.m. (the 1500-1800 sample) and reached maxima between 1800 and midnight. The evening peaks in mass at Bakersfield and Fresno were driven by the carbon component. At Kern and Chowchilla, the secondary components also showed daytime peaks, but dominated during all hours. Consequently, at Kern and Chowchilla, PM mass peaks occurred during the day.

Organic carbon concentrations exceeded elemental carbon by factors of 2:1 to 3:1. At each site, both elemental and organic carbon followed the same diurnal profile, but the profiles at the urban sites (Bakersfield and Fresno) differed from those at the rural sites.

Regression analyses showed high correlations between particulate carbon and both CO and soluble potassium. These correlations were interpreted as indicating that motor vehicles and fuel combustion were the principal sources of particulate carbon, with the latter source being slightly larger. CMB analyses also allocate particulate carbon to motor vehicles and combustion, though a nontrivial fraction of organic carbon was unexplained by the CMB source contributions. The relative amounts of the carbon allocated to motor vehicles and combustion by the multiple regression and the CMB analyses were approximately consistent with emission inventory estimates.

Factor analysis was used to delineate chemical species that tended to covary. While the number of samples was limited, three distinct groups of species were delineated. Elemental and organic carbon were associated with CO, NO_x, alkenes

(ethylene and acetylene), and aromatics (benzene, m-xylene, p-xylene). The second species group included C2-C5 alkanes (ethane, propane, i-butane, n-butane, i-pentane, n-pentane), and the third group included species having a photochemical source (formaldehyde, acetaldehyde, and acetone). Alkane concentrations were substantially greater at Bakersfield than at Fresno, with the ratio of ethane-to-acetylene being about 3:1 at Bakersfield and 1:1 at Fresno.

RECOMMENDATIONS FOR FUTURE MONITORING STUDIES

Sample Collection and Measurements

Many aspects of the IMS95 sample collection and analysis should be retained for a future, expanded study, while a few should be re-examined. The portable saturation samplers performed well and yielded measurements that agreed well with collocated sequential filter samplers. Also, the design of the saturation domains generally yielded good estimates of the spatial patterns of the ambient concentrations. In a future study, though, the numbers of samplers and the dimensions of the networks should be reconsidered. In the Corcoran area, additional sites located around the industrial area would help to better define the steep concentration gradients observed there. In Bakersfield, no monitors were located south of the area having the highest emission density. All saturation domains were large enough to observe decreases from peak concentrations to urban background, but not to regional background levels.

In a future study, it would be desirable to develop a data-analysis plan prior to sampling. The questions to be addressed by the saturation networks might include revisiting those addressed by the present study as well as other questions of interest. The data-analysis plan could then be used to guide the design of the saturation networks. Results from the present study suggest expanding the spatial dimensions of the networks, as indicated above; to reduce the sampling requirements, it may be possible to reduce the density of monitoring sites in some areas. Although this study did not determine the effects of reduced density of sampling, it would be possible to do

so by reviewing the contour plots carefully and recomputing some of them by leaving out some of the more closely spaced sites. The data analysis plan should also specify the temporal duration of sampling. A more detailed study might commence in November and continue through January with saturation monitors operating continuously. However, both the temporal and spatial extent of sampling should be determined by the data-analysis methods to be used, taking into consideration the costs of sampling and analysis.

The time series of measurements clearly indicate the value of daily sampling, as opposed to sampling at intervals of three or six days. Longer-sampling intervals potentially miss the PM peaks. The 24-hour sample duration provided a good temporal resolution without requiring massive numbers of samples. However, complementing the 24-hour samplers with the more detailed 3-hour resolution from the sequential filter samplers at the core sites added useful insights. The addition of 3-hour, fine and coarse size resolution at the Corcoran site would be a valuable enhancement.

As indicated earlier, data validation could be more effective if all or most sites collected samples that were speciated and if more collocated samplers were employed.

Modeling

While the present project did not focus on PM modeling, it nevertheless made use of a number of the gridded modeling files, through comparison of grid-file information to photos and videos, and some issues appear to warrant further examination. First, the western boundary of the IMS95 domain would need to be shifted westward to encompass several monitoring sites, which had been established because they were considered critical for establishing boundary conditions. Second, the accuracy and resolution of the emissions, population, and land-use files should be reviewed. Discrepancies between site photos and videos, on the one hand, and the gridded values for population, land-use type, and emissions type, on the other, suggest

the existence of considerable sub-grid scale variability. The importance of such variability for the accuracy of modeling predictions appears to warrant consideration. In addition, the accuracy of some values, such as the locations of major point sources in the Corcoran area, should be reviewed.

Compliance Monitoring

The results obtained from the saturation networks have implications for PM compliance monitoring. The core sites in the Bakersfield and Fresno domains obtained maxima close to the network-wide maxima. However, because substantial percentages of those two domains often exhibited concentrations differing from those at the core sites by more than twenty percent, accurate estimation of network-wide outdoor PM exposure requires two to three sites in addition to the core site of each domain. In contrast, the Corcoran core site obtained values representative of much of the Corcoran area on all days but one; however, the domain maximum, which was highly localized, usually exceeded the core site value by substantial amounts.

REFERENCES

C. P. Calloway, S. Li, J. W. Buchanan, and R. K. Stevens. 1989. A refinement of the potassium tracer method for residential wood smoke. Atmos. Environ. 23: 67-69.

C. W. Lewis, R. E. Baumgardner, R. K. Stevens, L. D. Claxton, and J. Lewtas. 1988. Contribution of woodsmoke and motor vehicle emissions to ambient aerosol mutagenicity. Environ. Sci. Tech. 22 (8): 968-971.

K. L. Magliano. 1997. Chemical Mass Balance Modeling of Data From the 1995 Integrated Monitoring Study. Sacramento CA: California Air Resources Board.

W. B. Petersen and L. G. Lavdas. INPUFF 2.0 - A Multiple Source Gaussian Puff Dispersion Algorithm. EPA-600/8-86/024. Research Triangle Park NC: U.S. EPA, 1986.

P. A. Solomon, R. H. Thuillier, K. L. Magliano, A. J. Ranzieri, R. Hackney, E. Niccum, J. G. Watson, D. Lehrman, P, M. Roth, S. Ziman, F. Lurmann, G. Cass, and D. Alan Hansen. "1995 Integrated Monitoring Study: Study Objectives and Design". In: Proceedings of the 1996 U.S. EPA/A&WMA International Symposium on Measurement of Toxic and Related Air Pollutants. Pittsburgh, PA: Air and Waste Management Association, 1997a.

P. A. Solomon, J. C. Chow, J. G. Watson, J. Gillies, D. Egami, K. L. Magliano, P. Roberts, D. Wright, D. Crow, J. Newman, and C. Berkowitz. "1995 Integrated Monitoring Study: Spatial and Temporal Variability of PM10 During the Fall Saturation Study—Preliminary Results". In: Proceedings of the 1996 U.S. EPA/A&WMA International Symposium on Measurement of Toxic and Related Air Pollutants. Pittsburgh, PA: Air and Waste Management Association, 1997b.

APPENDIX A:
PLOTS OF COLLOCATED SATURATION AND CORE MEASUREMENTS

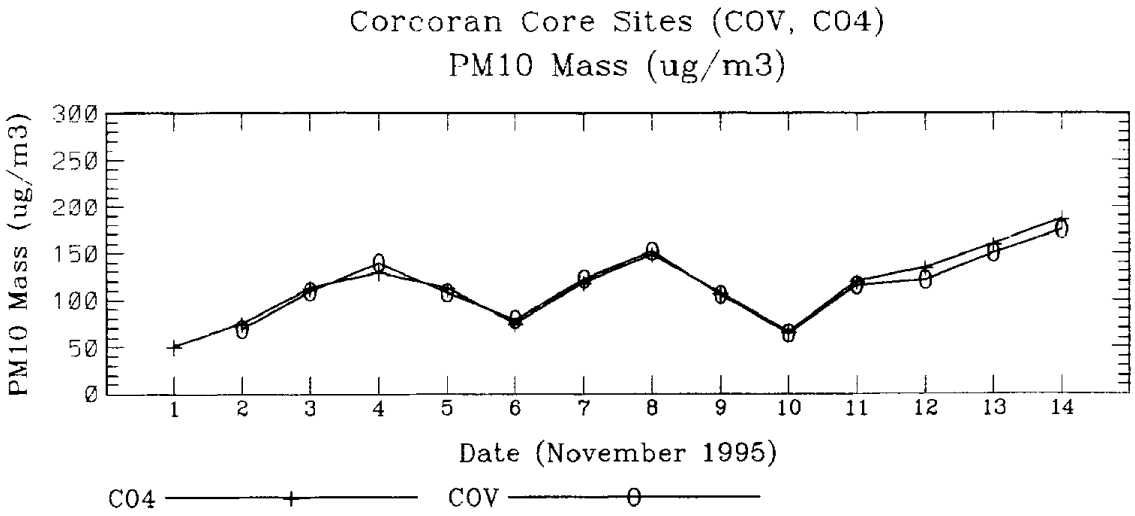
Corcoran Core Sites (COV, C04)
PM10 Mass (ug/m3)
PM10 Mass (ug/m3)
300
250
200
150
100
50
0
1 2 3 4 5 6 7 8 9 10 11 12 13 14
Date (November 1995)
C04
COV

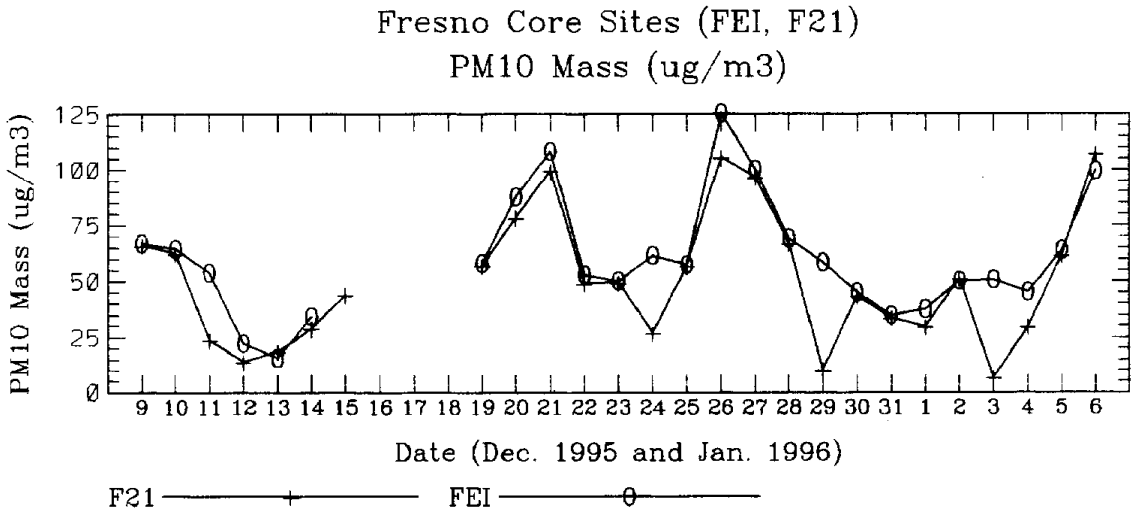
Fresno Core Sites (FEI, F21)
PM10 Mass (ug/m3)
PM10 Mass (ug/m3)
125
100
75
50
25
0
9 10 11 12 13 14 15 16 17 18 19 20 21 22 23 24 25 26 27 28 29 30 31 1 2 3 4 5 6
Date (Dec. 1995 and Jan. 1996)
F21
FEI

Kern Core Sites (KWR, K14)
PM10 Mass (ug/m3)

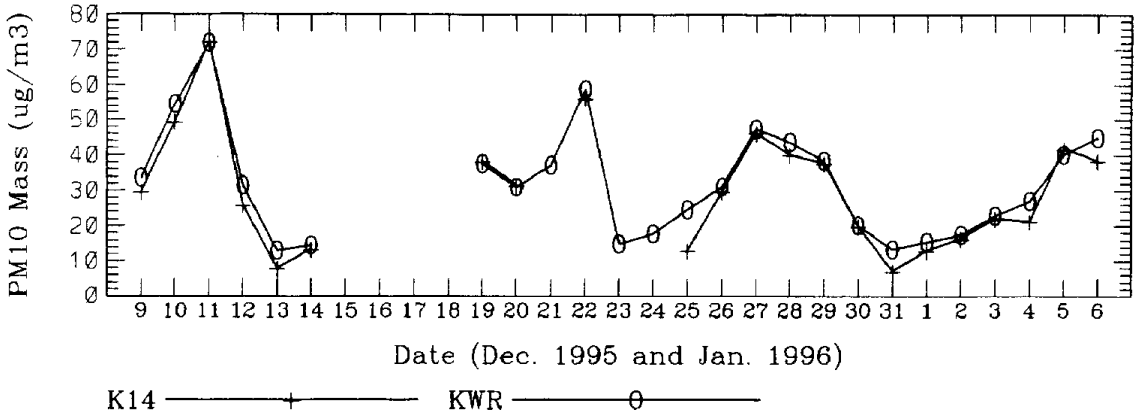

Bakersfield Core Sites (BFK, B01, B12)
PM10 Mass (ug/m3)

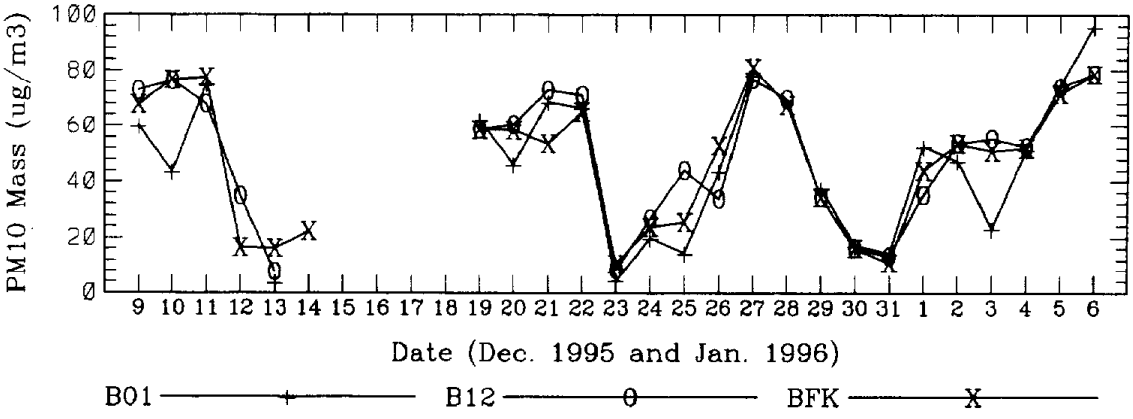

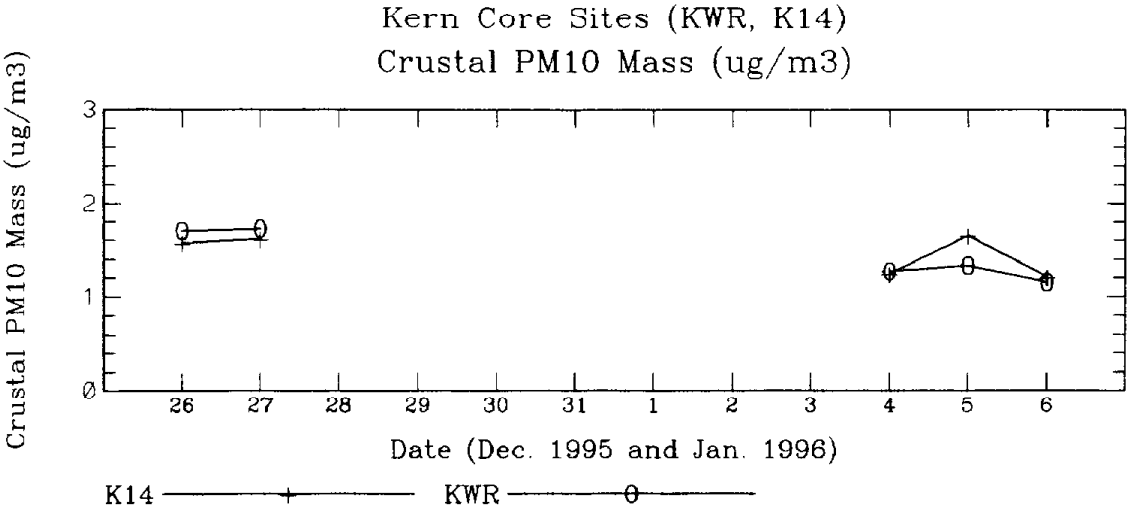
Kern Core Sites (KWR, K14)
Crustal PM10 Mass (ug/m3)
Crustal PM10 Mass (ug/m3)
3
2
1
0
26
27
28
29
30
31
1
2
3
4
5
6
Date (Dec. 1995 and Jan. 1996)
K14
KWR

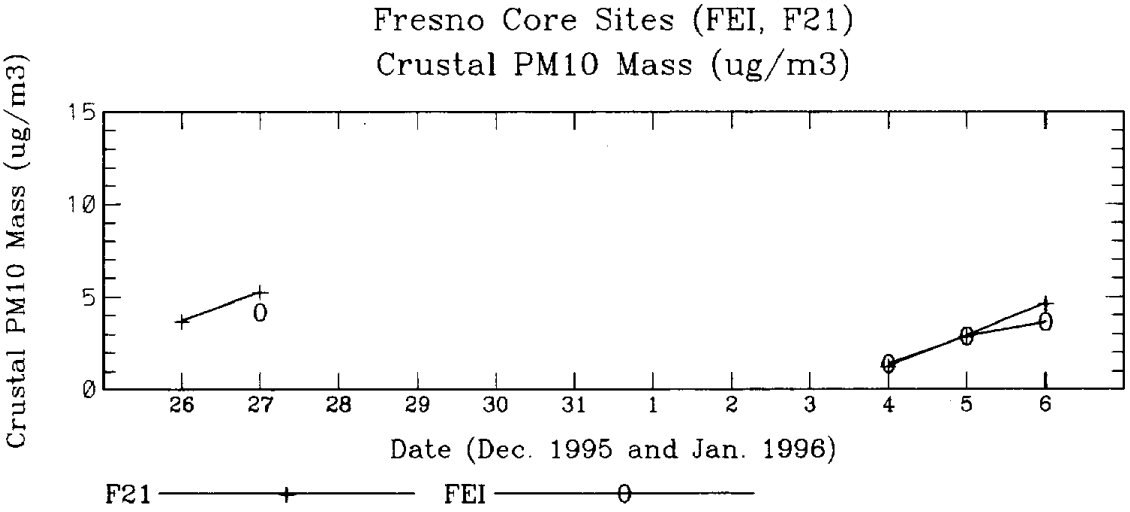
Fresno Core Sites (FEI, F21)
Crustal PM10 Mass (ug/m3)
Crustal PM10 Mass (ug/m3)
15
10
5
0
26
27
28
29
30
31
1
2
3
4
5
6
Date (Dec. 1995 and Jan. 1996)
F21
FEI

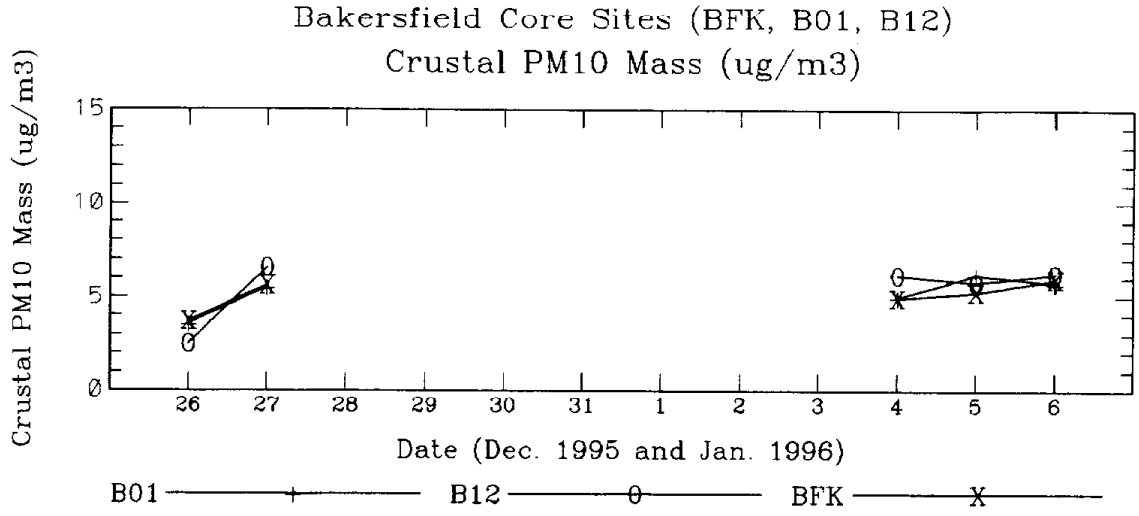
Bakersfield Core Sites (BFK, B01, B12)
Crustal PM10 Mass (ug/m3)
Crustal PM10 Mass (ug/m3)
15
10
5
0
26
27
28
29
30
31
1
2
3
4
5
6
Date (Dec. 1995 and Jan. 1996)
B01
B12
BFK

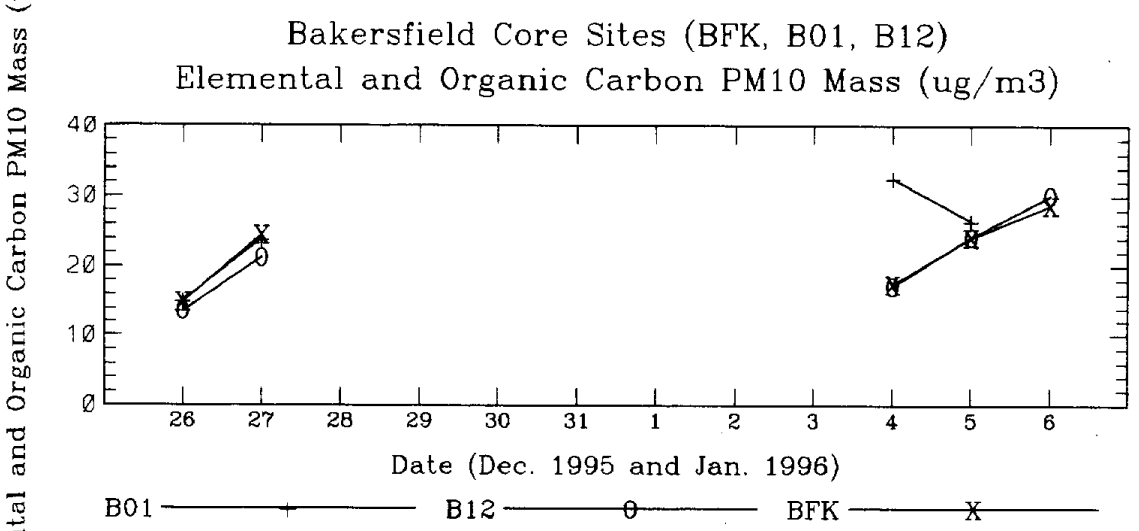
Bakersfield Core Sites (BFK, B01, B12)
Elemental and Organic Carbon PM10 Mass (ug/m3)
Elemental and Organic Carbon PM10 Mass (ug/m3)
40
30
20
10
0
26
27
28
29
30
31
1
2
3
4
5
6
Date (Dec. 1995 and Jan. 1996)
B01
B12
BFK

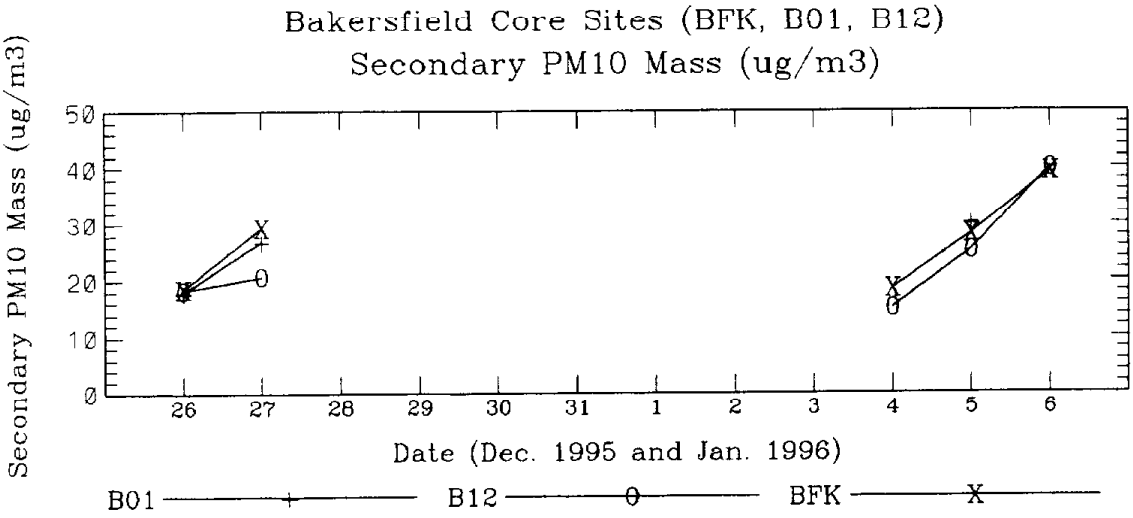
Bakersfield Core Sites (BFK, B01, B12)
Secondary PM10 Mass (ug/m3)
Secondary PM10 Mass (ug/m3)
50
40
30
20
10
0
26
27
28
29
30
31
1
2
3
4
5
6
Date (Dec. 1995 and Jan. 1996)
B01
B12
BFK

APPENDIX B: SITE CHARACTERISTICS

Site	Site Type	Site Characteristic	CD-ROM vs. Characteristic	Land Use vs. Characteristic	Population vs. Characteristic	Emissions vs. Characteristic
BFK	CORE/WNTR	UrbGen, ResGen, UrbCom, TransMix, IndOil	OK	Agri, not urb or res	OK	OK
COA	BOUNDARY	BndSide, ResGen, IndOil, AgNative	No resid on CD	Wrong - mixed range, not res or ind	Pop too small for res, but OK for ag	OK
CHO	BNDRY/FLUX	ThruVal, AgNative	-	OK	OK	Ag very low
COP	CORE/FALL	ResGen, UrbGen	OK	Agri, not res or urb	Pop too small for res at 244 km^2	OK
DEV	BNDRY/FLUX	ThruCen, RurGen, AgNative	OK	OK	OK	OK
ERL	BNDRY/FLUX	BndSide, RurGen, AgGen, IndOil	No ind oil on CD	OK	OK	OK
FEI	CORE/WNTR	UrbGen, ResGen, ResWood, TransRes, TransMix	OK	Agri, not urb or res	OK	OK
FEL	WSO/MET	IndOil, AgGen, AgCrop	-	OK	OK	MV & Pt high
FRI	BNDRY/FLUX	ThruNor, RurGen, AgNative	OK	OK	OK	Ag low, MV & Res high fits neither Ag nor Rural profile
KRN	WSO/MET	IndOil, AgGen, AgCrop	OK	OK	OK	OK
KWR	CORE/WNTR	RurGen	OK	OK	OK	OK
LBS	BNDRY/FLUX	ThruNor, AgGen, ThruCen, AgNative	-	-	-	-
LOO	BOUNDARY	BndClean, AgNative	OK	OK	OK	Ag very low (Jan only)

Site	Site Type	Site Characteristic	CD-ROM vs. Characteristic	Land Use vs. Characteristic	Population vs. Characteristic	Emissions vs. Characteristic
MKR	BNDRY/UAME	BndSide, AgCrop	OK	OK	OK	OK
REY	BOUNDARY	ThruVal, RurGen, AgNative	OK	OK	OK	OK
SPR	BNDRY/FLUX	ThruCen, ResWood, AgNative	OK	Agri only, no Res	Pop too small for res, but OK for Ag	OK
SWC	CORE/WNTR	ThruNor, AgGen, IndAgr, AgCrop	-	OK	OK	OK
TEH	BOUNDARY	ThruVal, AgNative	-	OK	OK	Ag low in Jan - missing key source?
01B	WNTR/SATUR	Collocated	OK	Agri, not urb or res	OK	OK
02B	WNTR/SATUR	Collocated, UrbGen, ResGen, UrbCom, TransMix	OK	Agri, not urb or res	OK	OK
03B	WNTR/SATUR	ResGen, ResWood, TransRes	Ind (N) not in Tbl 4	Agri, not res	OK	OK
04B	WNTR/SATUR	TransMix, UrbGen	OK	Agri, not urb	OK	OK
05B	WNTR/SATUR	IndOil, IndGen	OK	Agri, not ind	OK but pop may be too high for ind	OK
06B	WNTR/SATUR	AgCrop, AgGen, AgNative, Interstitial	-	OK	OK	Ag low in Jan - missing key source?
07B	WNTR/SATUR	IndOil, UrbGen, IndGen, UrbCom	OK	Agri, not urb or ind	OK	OK
08B	WNTR/SATUR	AgCrop, AgGen, TransRR	OK	OK	OK	Ag low in Jan - missing key source?
09B	WNTR/SATUR	AgGen, AgGen, AgCrop, AgNative	OK	OK	OK	Ag very low

Site	Site Type	Site Characteristic	CD-ROM vs. Characteristic	Land Use vs. Characteristic	Population vs. Characteristic	Emissions vs. Characteristic
10B	WNTR/SATUR	Interstitial, ResGen, TransRes, IndOil	OK	Agri, not res	OK	OK
11B	WNTR/SATUR	ResWood, ResGen	OK	Agri, not res	OK	OK
12B	WNTR/SATUR	Collocated	OK	Agri, not urb, resid or com	OK	OK
01C	FALL/SATUR	ResGen	OK	Agri, not res	OK	OK
02C	FALL/SATUR	AgNative, RurGen	Water (E) not in Tbl 4	OK	OK	OK
03C	FALL/SATUR	AgCrop, TransRR	Transp is a dirt road	OK	OK	OK
04C	FALL/SATUR	ResGen, UrbGen, Collocated	OK	Agri, not res	OK	OK
05C	FALL/SATUR	IndAgr, IndGen, TransRR	Res (W) not in Tbl 4	OK	OK	Pt very low (Nov only), Ag high
06C	FALL/SATUR	IndGen, TransRR	Res (S,W) not in Tbl 4	Agri, not ind	OK	Pt very low (Nov only), Ag high
07C	FALL/SATUR	Interstitial, AgCrop	Res (S) not in Tbl 4	OK	OK	OK
08C	FALL/SATUR	ResGen, IndAgr	OK	Agri, not res, but 2nd purpose OK	Pop too small for res	OK
09C	FALL/SATUR	Interstitial, ResGen, AgCrop	OK	Agri, not res	Pop too small for res, but 2nd purpose OK	OK
10C	FALL/SATUR	ResGen, Interstitial	OK	Agri, not res	Pop too small for res	OK
11C	FALL/SATUR	AgDairy	Res (NW) and prison not in Tbl 4	OK	OK	OK

Site	Site Type	Site Characteristic	CD-ROM vs. Characteristic	Land Use vs. Characteristic	Population vs. Characteristic	Emissions vs. Characteristic
12C	FALL/SATUR	IndAgr, ResGen, TransRR	OK	OK	OK but 2nd purpose wrong - pop too small	Pt very low (Nov only), Ag high
13C	FALL/SATUR	AgDairy, AgCrop	-	OK	OK	OK
14C	FALL/SATUR	AgPoultry	-	OK	OK	OK
15C	FALL/SATUR	IndWaste, IndAgr	Res (NW) not in Tbl 4	OK b/c ind small area	OK	Pt very low (Nov only), Ag high
16C	FALL/SATUR	IndAgr, ResGen, TransRR, Interstitial	OK	OK	Pop too high for indagr, too small for res	Pt very low (Nov only), Ag high
17C	FALL/SATUR	ResGen, AgGen, Interstitial	OK	Agri, not res, but 2nd purpose OK	Pop too small for res	OK
18C	FALL/SATUR	AgCrop	-	OK	OK	OK
19C	FALL/SATUR	IndWaste, TransRR, AgCrop	OK	OK b/c ind small area	OK but pop may be too big for ind	OK
20C	FALL/SATUR	AgNative, RurGen	OK	OK	OK	OK
21C	FALL/SATUR	AgCrop	OK	OK	OK	OK
22C	FALL/SATUR	AgDairy, AgCrop	-	OK	OK	OK
18F	WNTR/SATUR	IndConst, AgGen, AgCrop	CD does not show ind constr, only agri and sewage trtmnt plant	OK	OK	Pt low, Ag very high
19F	WNTR/SATUR	TransRes, ResGen	Ind (lumber plant) (SW) not in Tbl 4	OK	OK	OK
20F	WNTR/SATUR	ResGen, ResWood, TransRes	OK	Agri, not res	OK	OK
21F	WNTR/SATUR	Collocated	OK	OK	OK	OK

Site	Site Type	Site Characteristic	CD-ROM vs. Characteristic	Land Use vs. Characteristic	Population vs. Characteristic	Emissions vs. Characteristic
22F	WNTR/SATUR	Interstitial, ResGen, AgCrop	No agri, res (NW) only, remainder ind and constr	Agri, not res but 2nd purpose OK	OK	OK
23F	WNTR/SATUR	UrbCom, IndGen, TransMix	Res not in Tbl 4	Agri, not urb or ind	OK	OK
24F	WNTR/SATUR	ResWood, ResGen, TransRes, IndConst	OK	Agri, not res	OK	OK
25F	WNTR/SATUR	UrbCom, ResGen, TransMix	OK	Agri, not urb or res	OK	OK
26F	WNTR/SATUR	ResGen, TransRes	Agri not in Tbl 4	Agri, not res	OK	OK
27F	WNTR/SATUR	TransMix, ResGen	OK	OK	OK	OK
28F	WNTR/SATUR	UrbCom, TransMix	OK	OK	OK	Ag low, Pt high
29F	WNTR/SATUR	ResWood, ResGen, TransRes	OK	Agri, not res	OK	OK
30F	WNTR/SATUR	TransRR, UrbGen	OK	OK	OK	OK
31F	WNTR/SATUR	UrbCom, UrbGen, TransMix	OK	Agri, not urb	OK	OK
32F	WNTR/SATUR	ResWood, ResGen, TransRes	OK	Agri, not res	OK	OK
33F	WNTR/SATUR	AgGen, ResGen, UrbCom, TransRes, AgDairy	OK	OK	Pop too big for agr, but 2nd & 3rd purposes OK	OK
34F	WNTR/SATUR	Collocated, AgGen, AgDairy	-	OK	OK	OK
35F	WNTR/SATUR	AgDairy	OK	OK	Pop too big for agr	OK

Site	Site Type	Site Characteristic	CD-ROM vs. Characteristic	Land Use vs. Characteristic	Population vs. Characteristic	Emissions vs. Characteristic
36F	WNTR/SATUR	AgCrop	OK	OK	OK	OK
37F	WNTR/SATUR	---	--	Agri, not urb	OK	OK
38F	WNTR/SATUR	TransMix, ResGen, UrbCom	OK	OK	OK	OK
39F	WNTR/SATUR	IndAgr, IndGen	CD shows more urb agri & trucks than ind agri	OK	OK	OK
40F	WNTR/SATUR	IndGen, AgCrop	OK	OK	Pop too big for agri	OK
41F	WNTR/SATUR	ResWood, ResGen, TransRes	OK	Agri, not res	Pop too small for res	OK
42F	WNTR/SATUR	AgDairy, AgGen	OK	OK	Pop too big for agri	Ag very low
43F	WNTR/SATUR	IndConst, AgGen, TransRes	No agri	OK - ind const small area	Pop too big for agri	OK
13K	WNTR/SATUR	RurGen, ThruCen, AgNative	OK	OK	OK	OK
14K	WNTR/SATUR	Collocated, RurGen, ThruCen, AgNative	OK	OK	OK	OK
15K	WNTR/SATUR	RurGen, ThruCen, AgNative	OK	OK	OK	OK
16K	WNTR/SATUR	RurGen, ThruCen, AgNative	OK	OK	OK	OK
17K	WNTR/SATUR	RurGen, ThruCen, AgNative	OK	OK	OK	OK

APPENDIX C: CONTOUR PLOTS OF AVERAGE CONCENTRATIONS

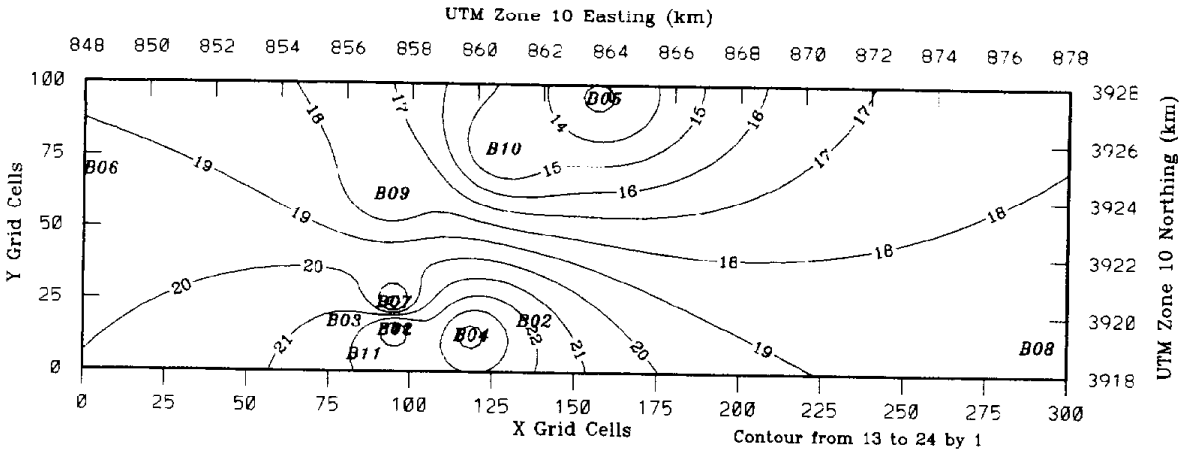

Bakersfield Saturation Sites, Domain: bkf1, dx = 0.1 km
Contours of Elemental and Organic Carbon PM10 Mass (ug/m3)
Averaged Over Dec. 26-27 and Jan. 4-6

IMS95 Data Analysis

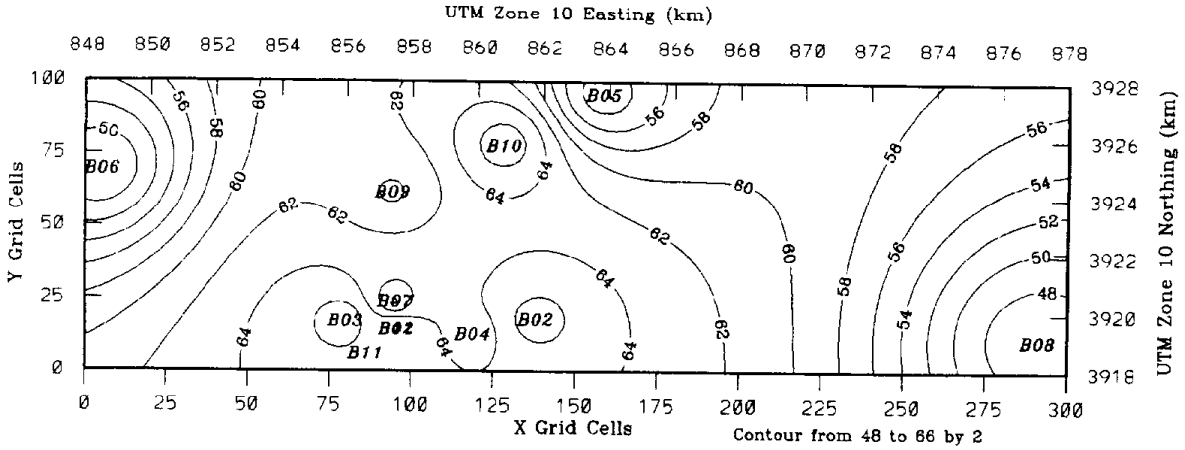

Bakersfield Saturation Sites, Domain: bkf1, dx = 0.1 km
Contours of PM10 Mass (ug/m3)
Averaged Over Dec. 9–10, 26–28, and Jan. 4–6

IMS95 Data Analysis

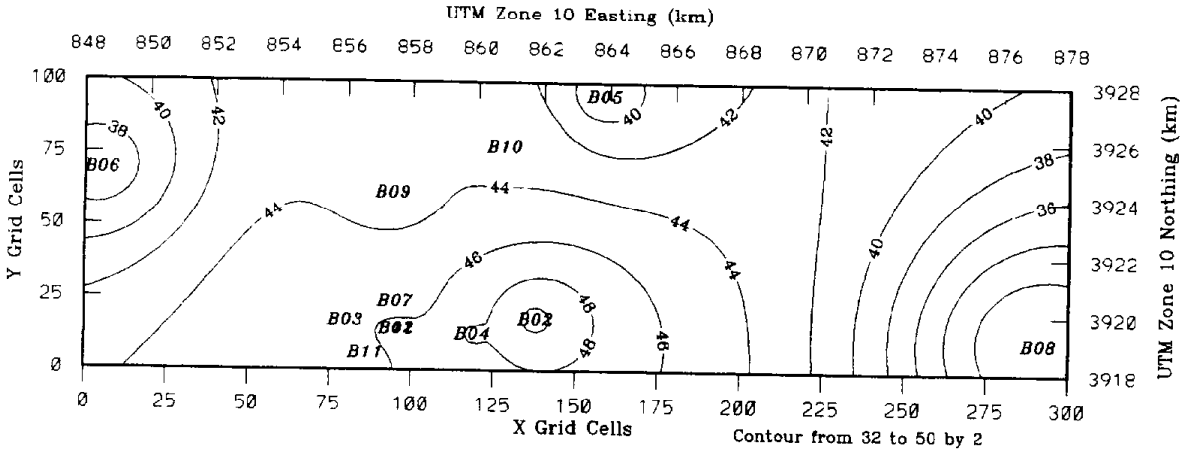

Bakersfield Saturation Sites, Domain: bkf1, dx = 0.1 km
Contours of PM10 Mass (ug/m3)
Averaged Over Dec. 9-14, 19-31, Jan. 1-6

IMS95 Data Analysis

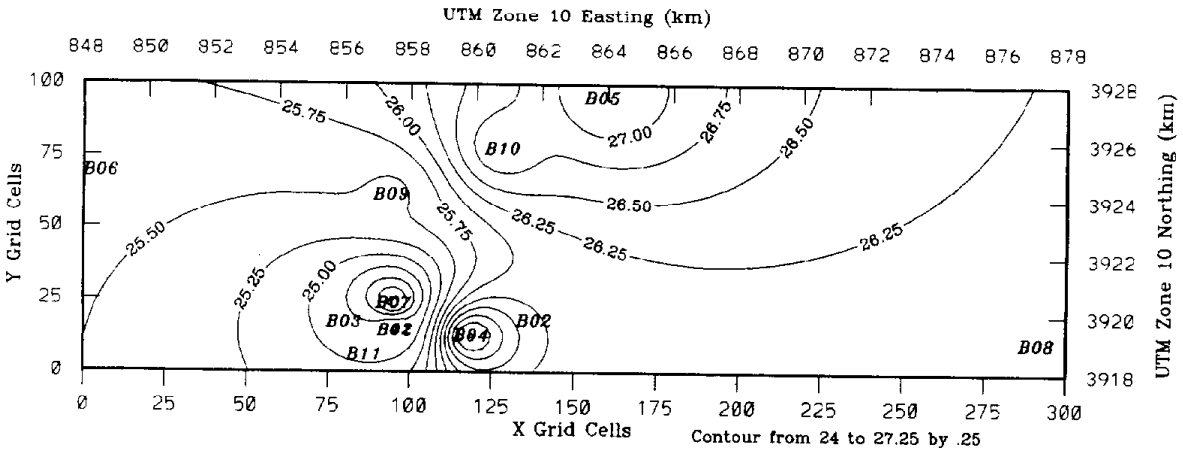

Bakersfield Saturation Sites, Domain: bkf1, dx = 0.1 km
Contours of Secondary PM10 Mass (ug/m3)
Averaged Over Dec. 26-27 and Jan. 4-6

IMS95 Data Analysis

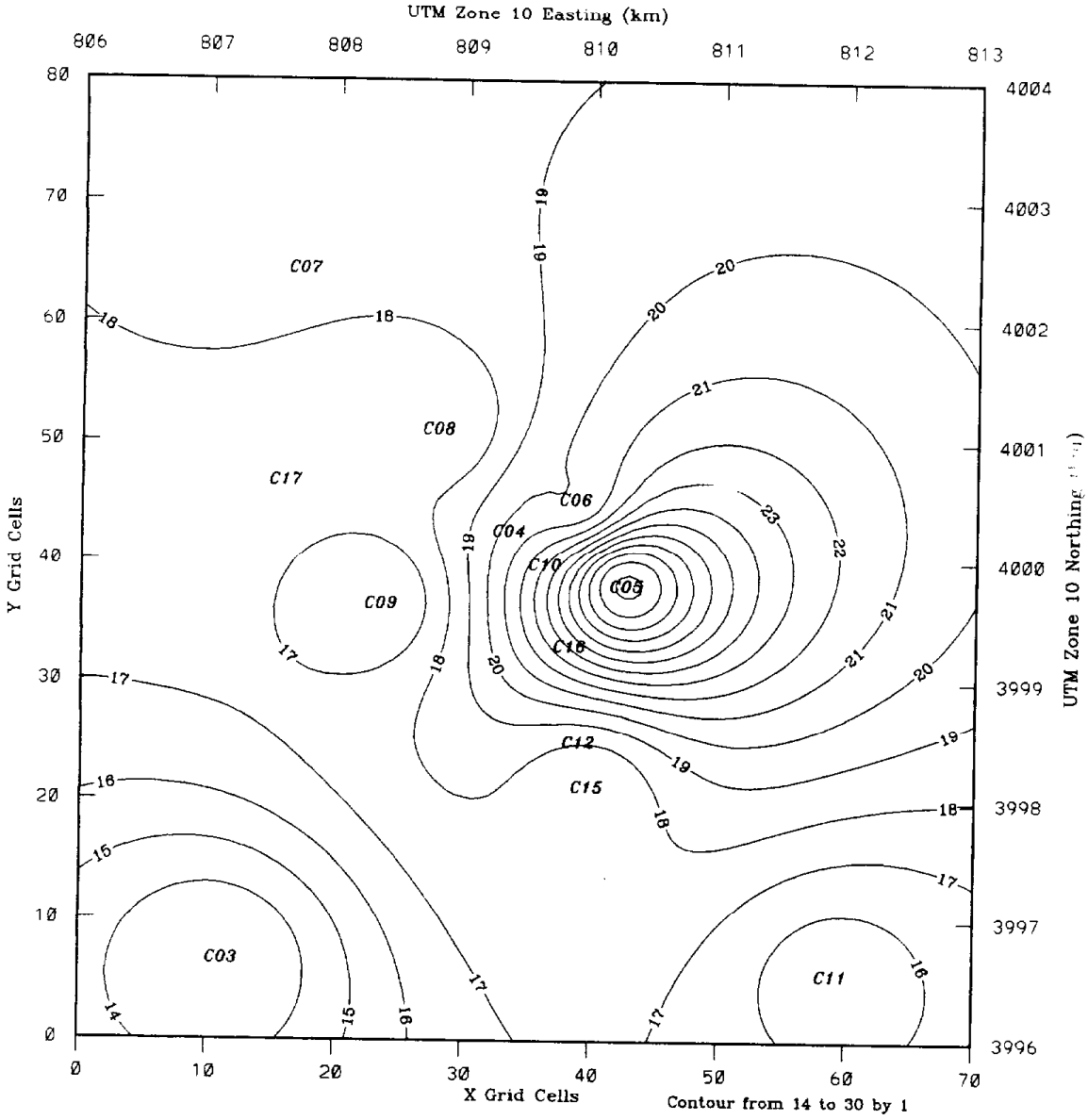

Corcoran Saturation Sites, Subdomain: cor2, dx = 0.1 km
Contours of Elemental and Organic Carbon PM10 Mass (ug/m3)
Averaged Over Nov. 1–14

IMS95 Data Analysis

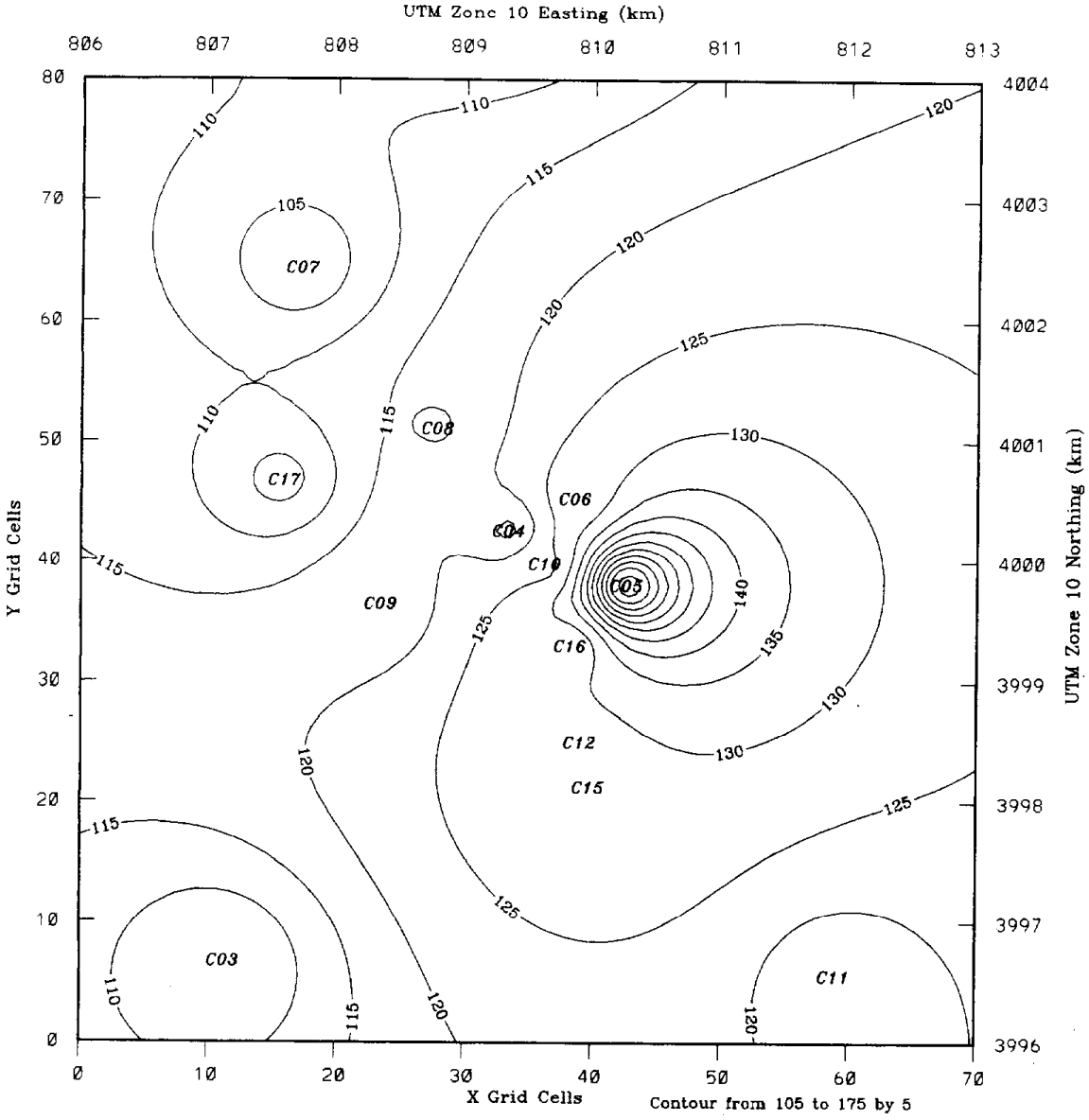

Corcoran Saturation Sites, Subdomain: cor2, dx = 0.1 km
Contours of PM10 Mass (ug/m3)
Averaged Over Nov. 1-14

IMS95 Data Analysis

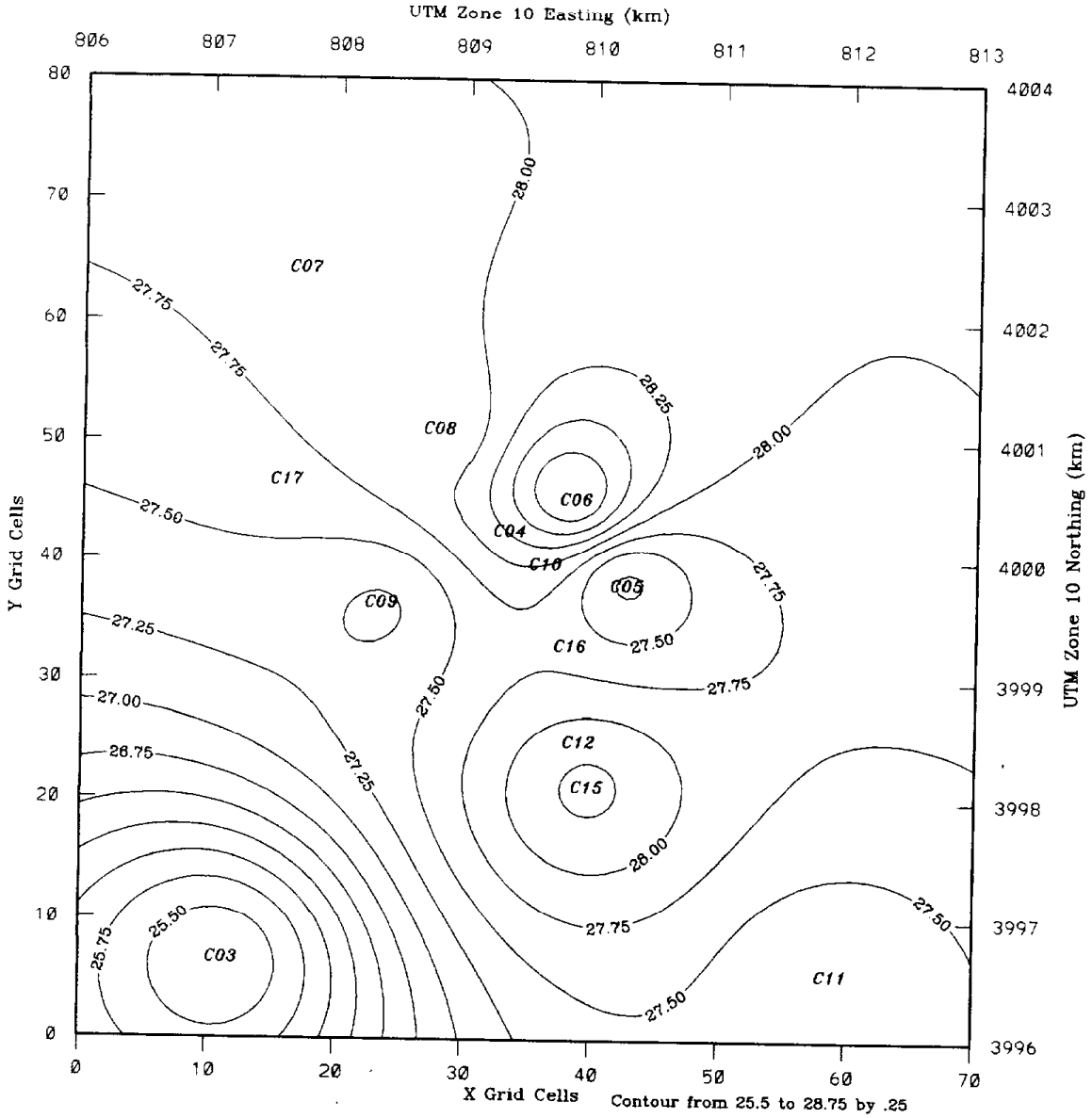

Corcoran Saturation Sites, Subdomain: cor2, dx = 0.1 km
Contours of Secondary PM10 Mass (ug/m3)
Averaged Over Nov. 1-14

IMS95 Data Analysis

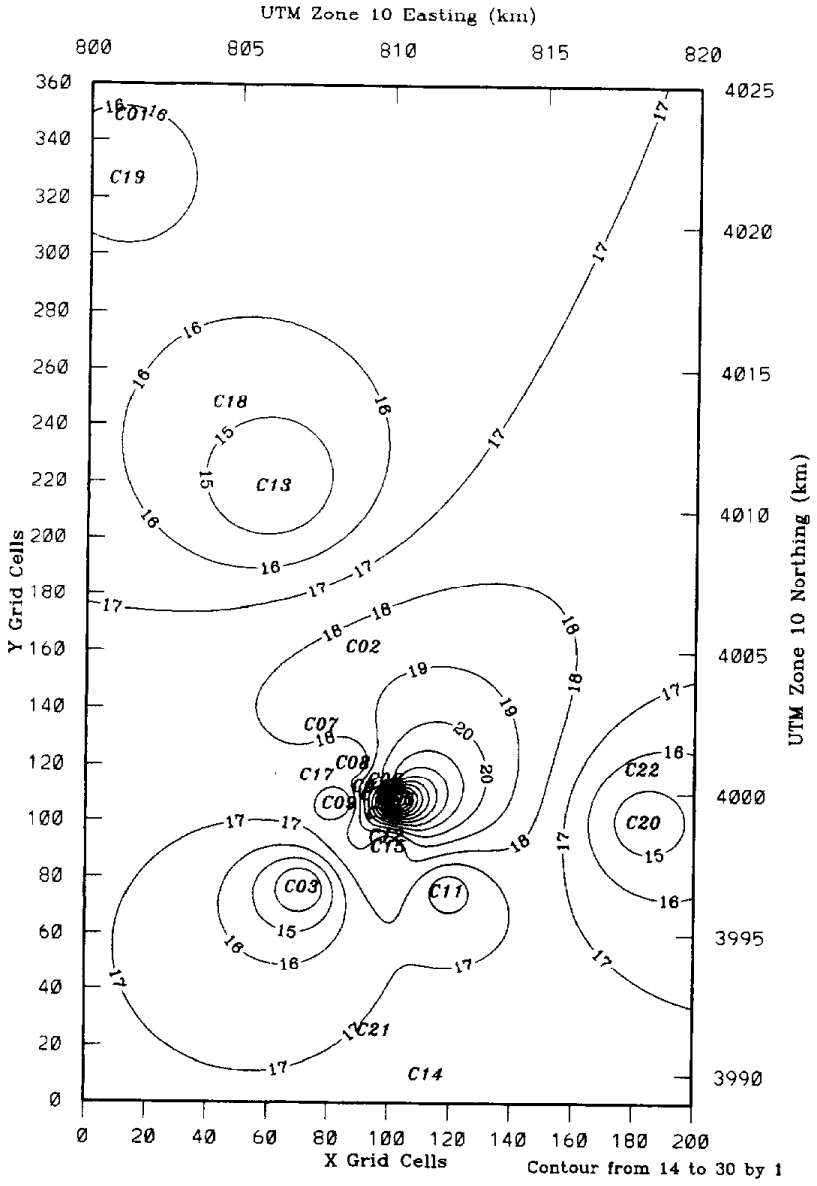

Corcoran Saturation Sites, Domain: cor1, dx = 0.1 km
Contours of Elemental and Organic Carbon PM10 Mass (ug/m3)
Averaged Over Nov. 1–14

IMS95 Data Analysis

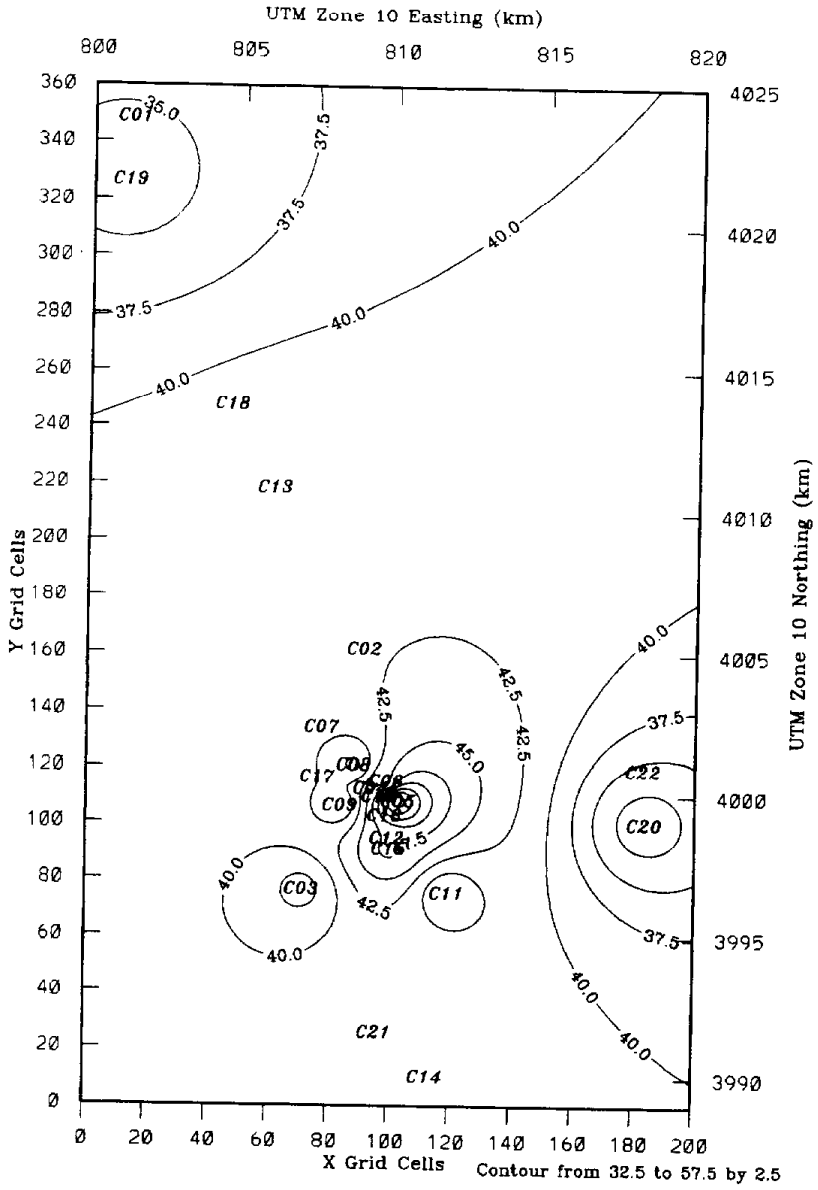

Corcoran Saturation Sites, Domain: cor1, dx = 0.1 km
Contours of Crustal PM10 Mass (ug/m3)
Averaged Over Nov. 6–14

IMS95 Data Analysis

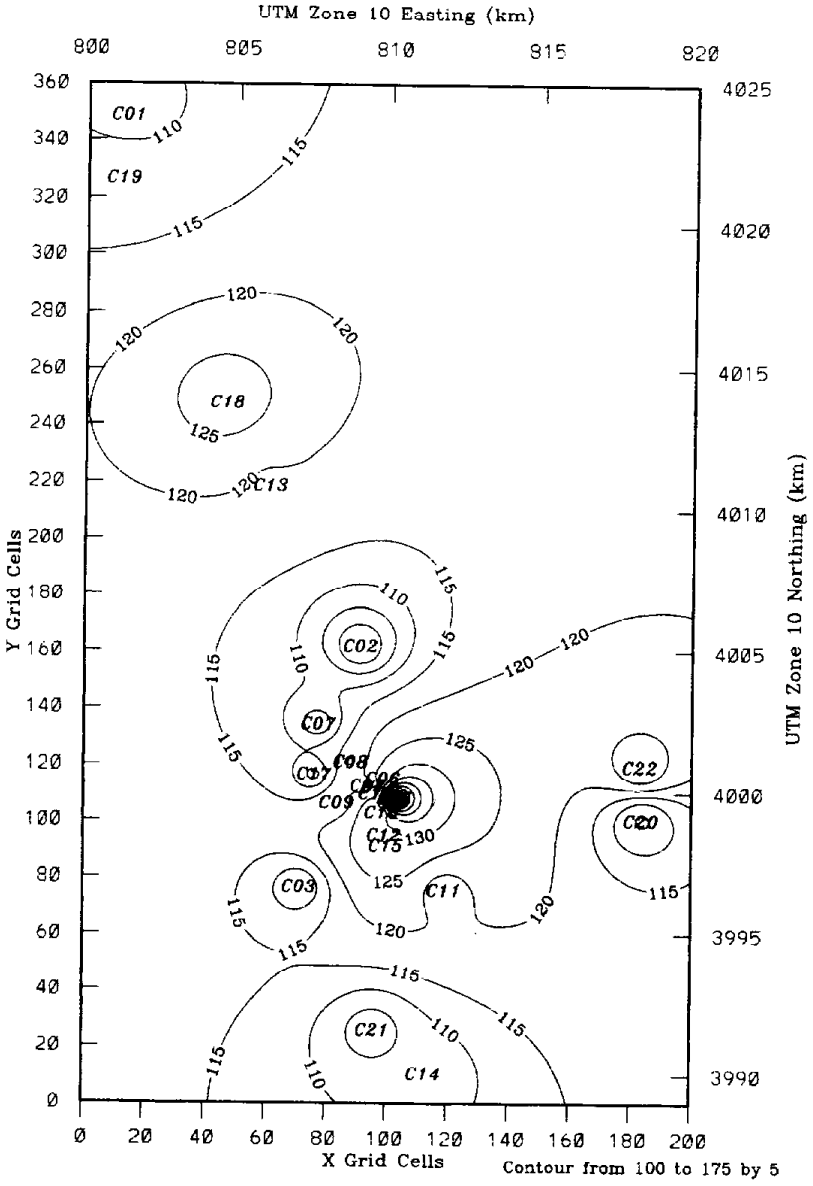

Corcoran Saturation Sites, Domain: cor1, dx = 0.1 km
Contours of PM10 Mass (ug/m3)
Averaged Over Nov. 1–14

IMS95 Data Analysis

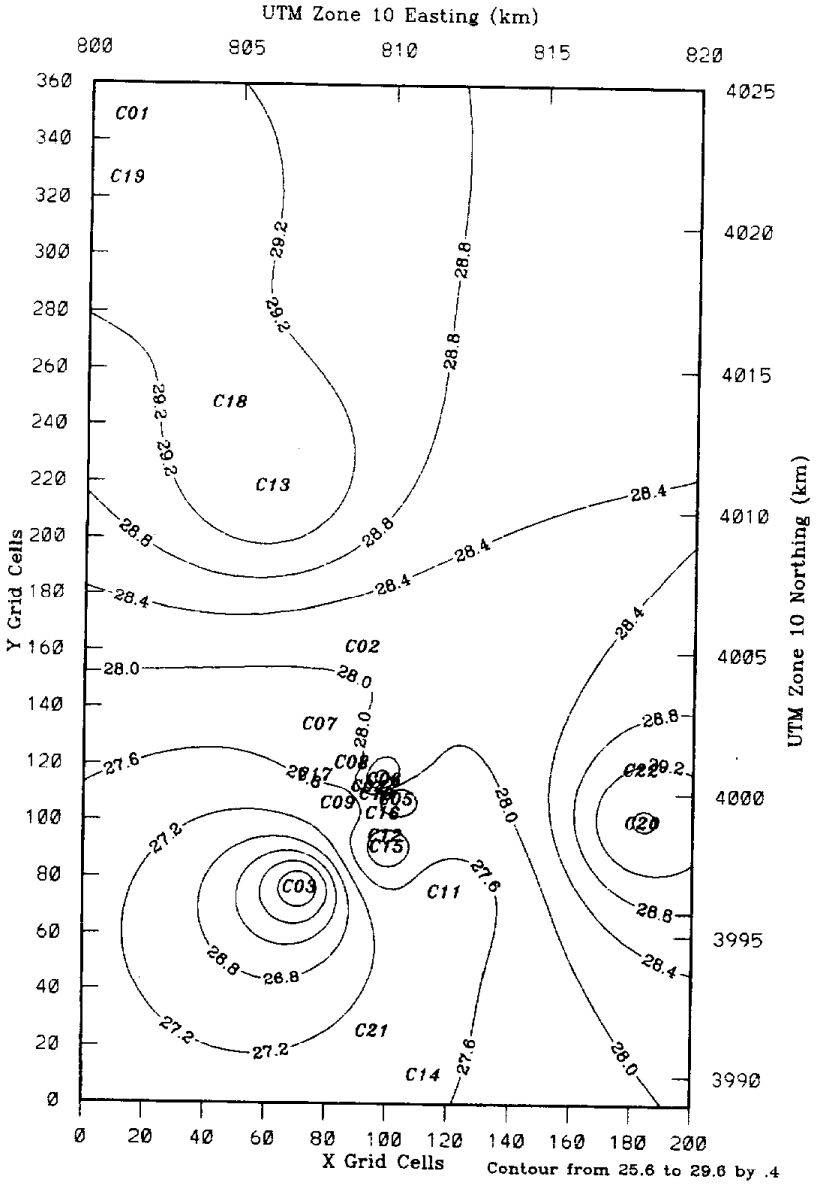

Corcoran Saturation Sites, Domain: cor1, dx = 0.1 km
Contours of Secondary PM10 Mass (ug/m3)
Averaged Over Nov. 1–14

IMS95 Data Analysis

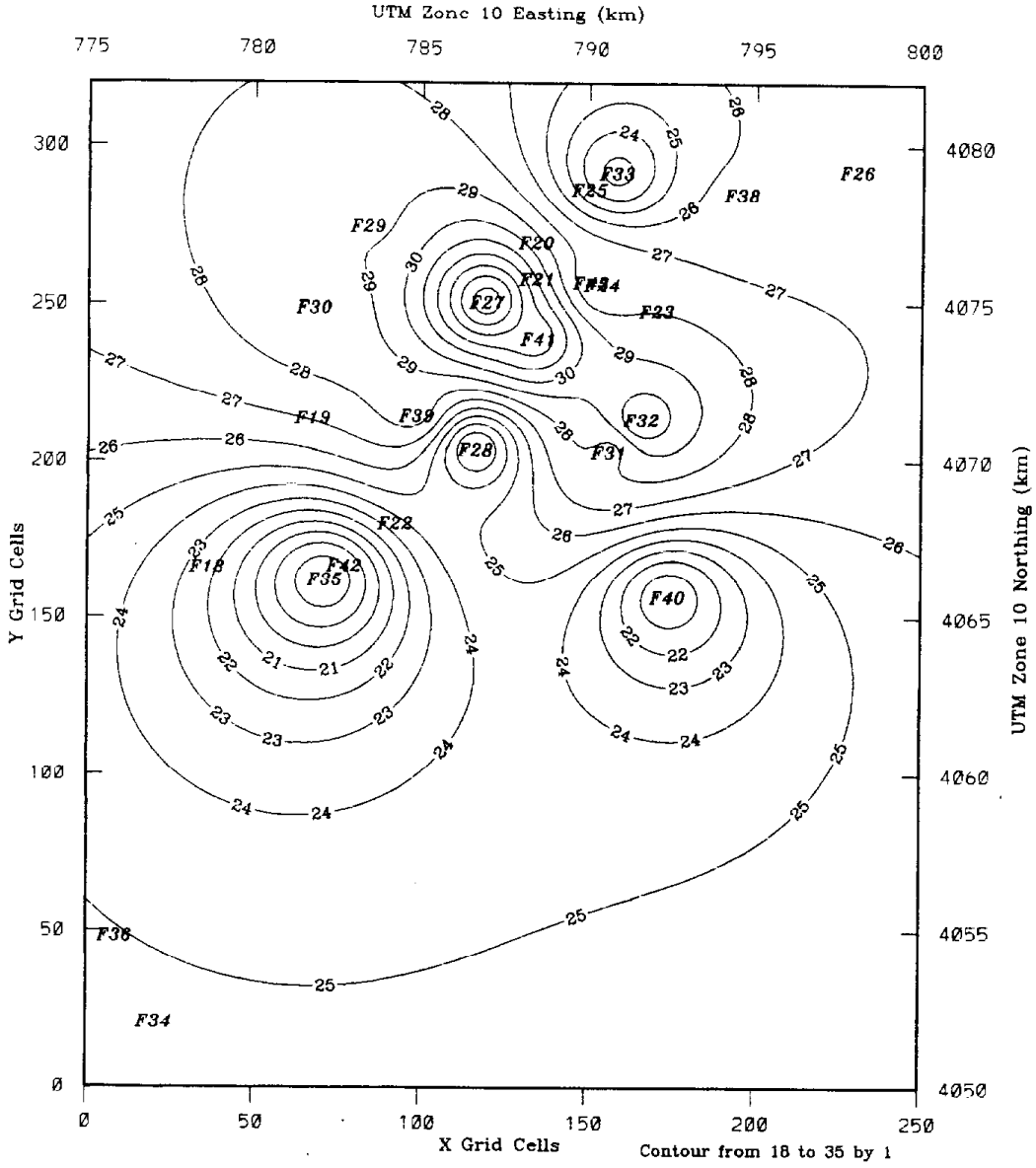

Fresno Saturation Sites, Domain: frs1, dx = 0.1 km
Contours of Elemental and Organic Carbon PM10 Mass (ug/m3)
Averaged Over Dec. 26-27 and Jan. 4-6

IMS95 Data Analysis

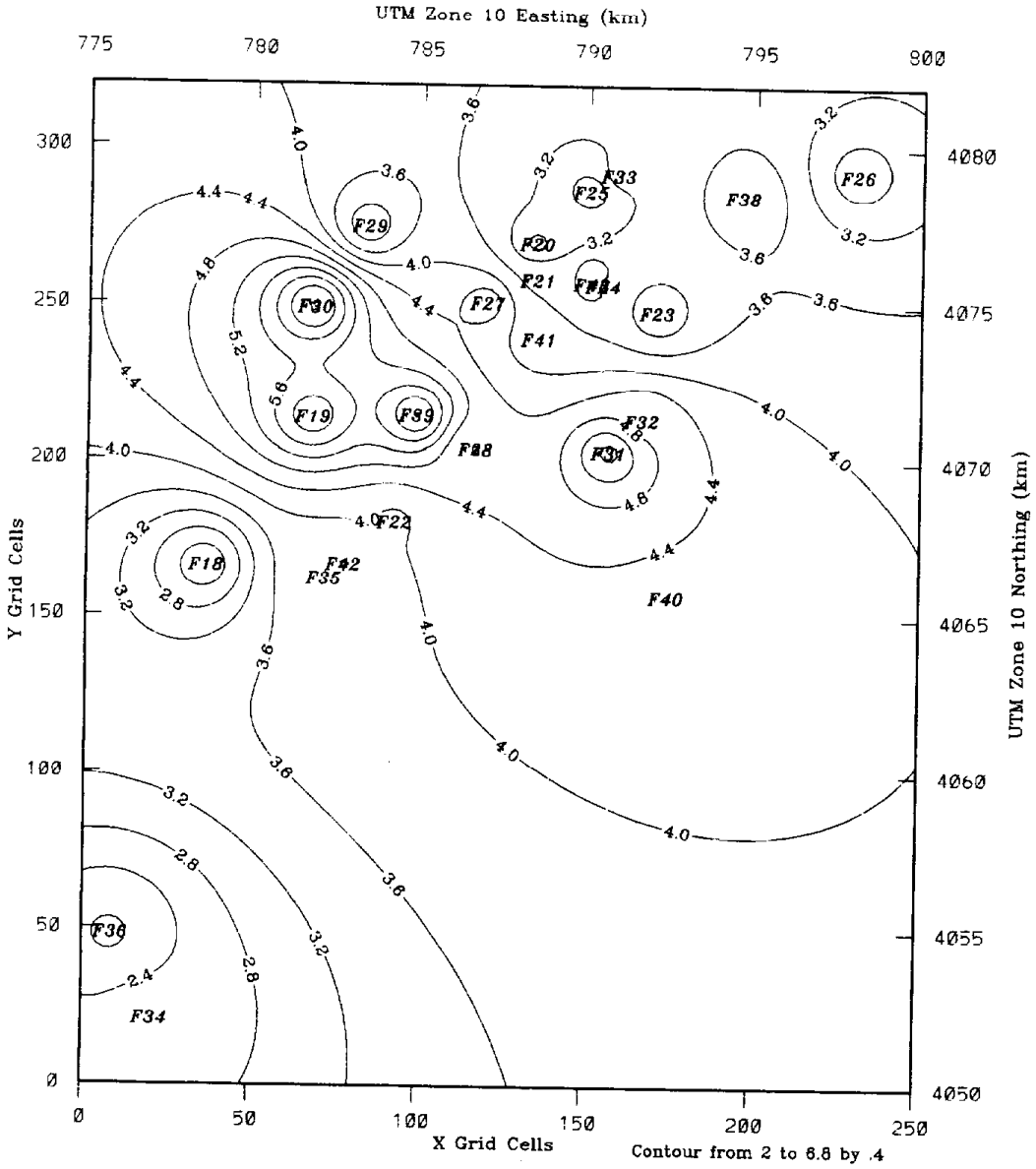

Fresno Saturation Sites, Domain: frs1, dx = 0.1 km
Contours of Crustal PM10 Mass (ug/m3)
Averaged Over Dec. 26-27 and Jan. 4-6

IMS95 Data Analysis

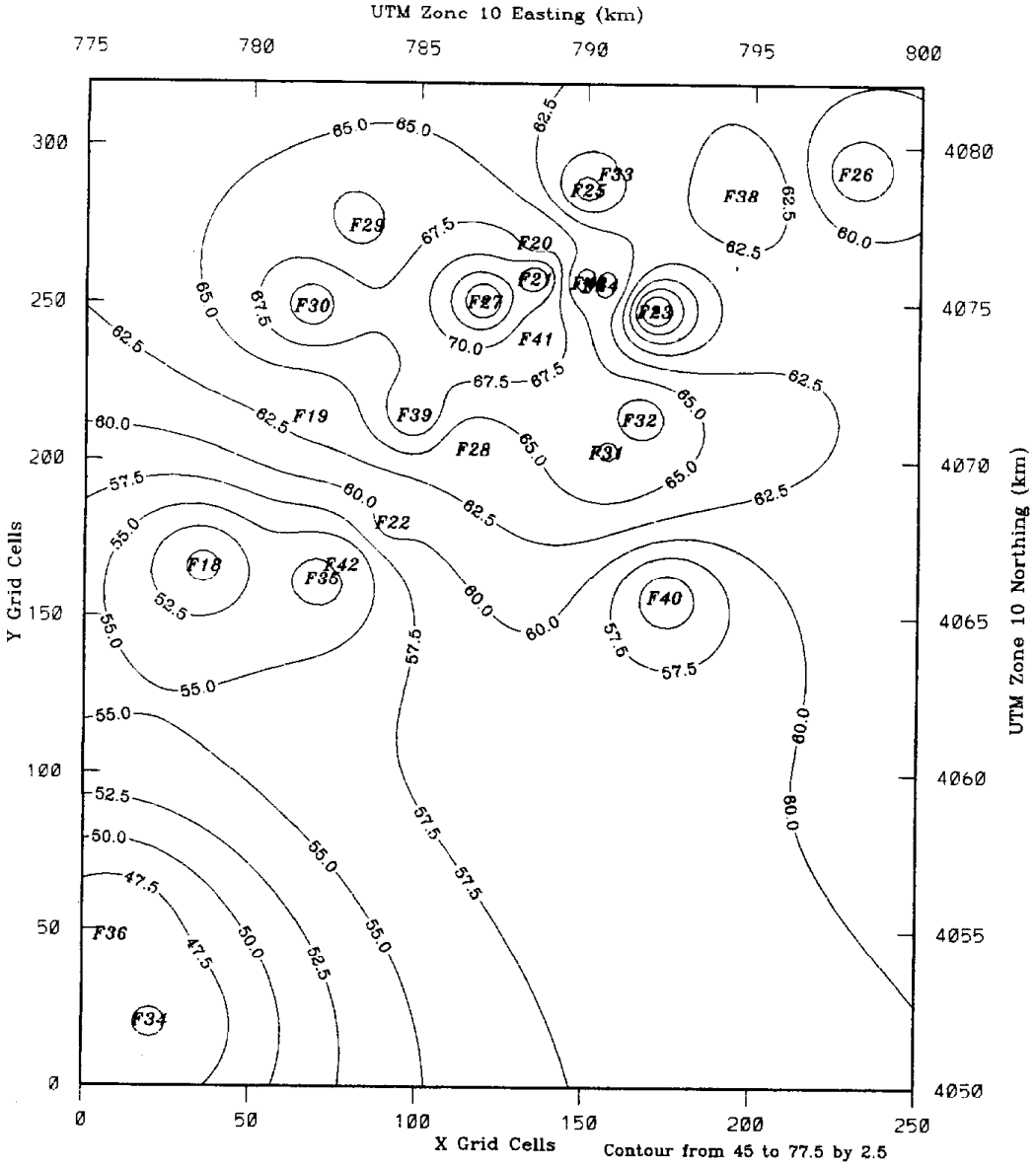

Fresno Saturation Sites, Domain: frs1, dx = 0.1 km
Contours of PM10 Mass (ug/m3)
Averaged Over Dec. 9–10, 26–28, and Jan. 4–6

IMS95 Data Analysis

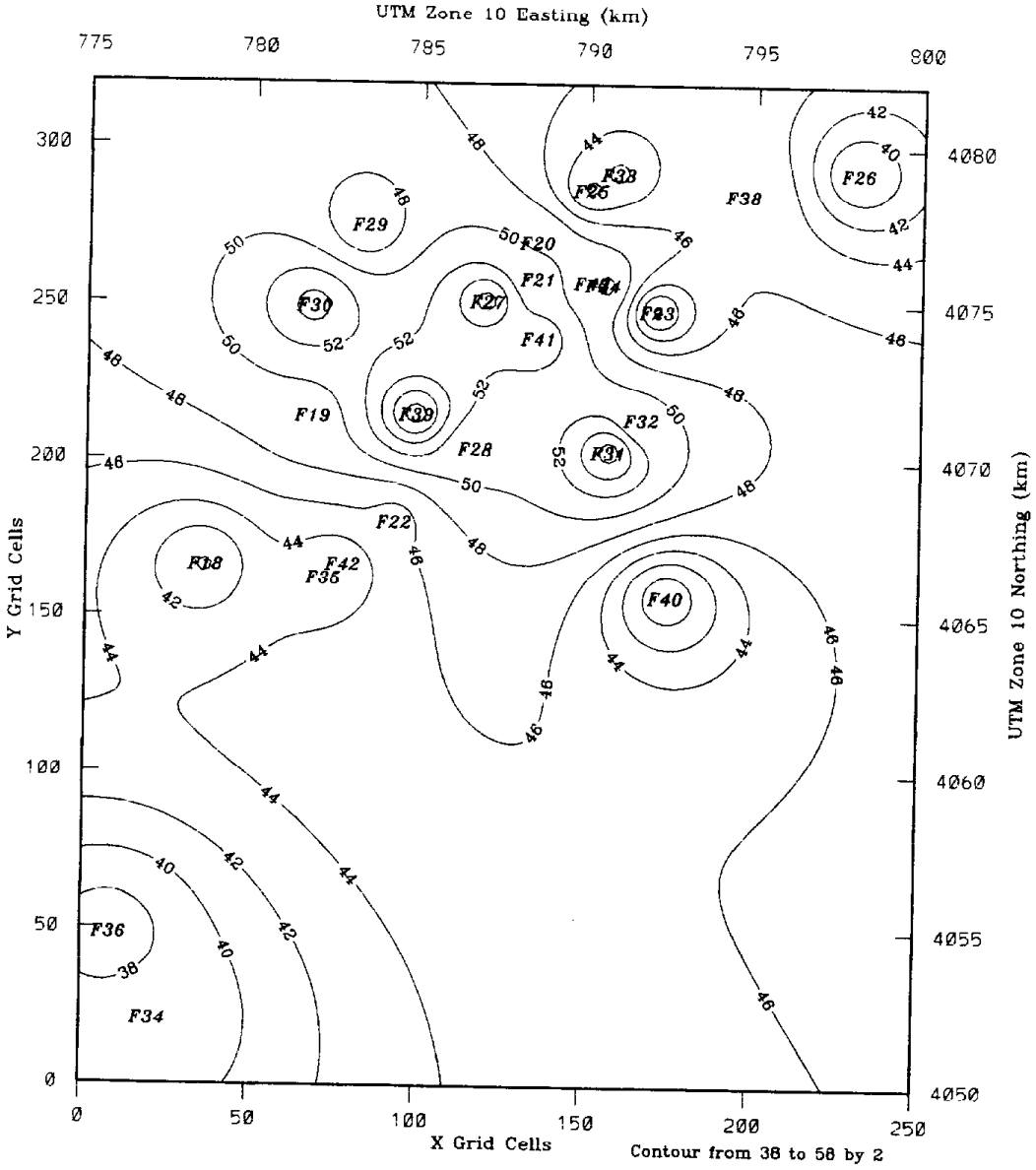

Fresno Saturation Sites, Domain: frs1, dx = 0.1 km
Contours of PM10 Mass (ug/m3)
Averaged Over Dec. 9–15, 19–31 and Jan. 1–6

IMS95 Data Analysis

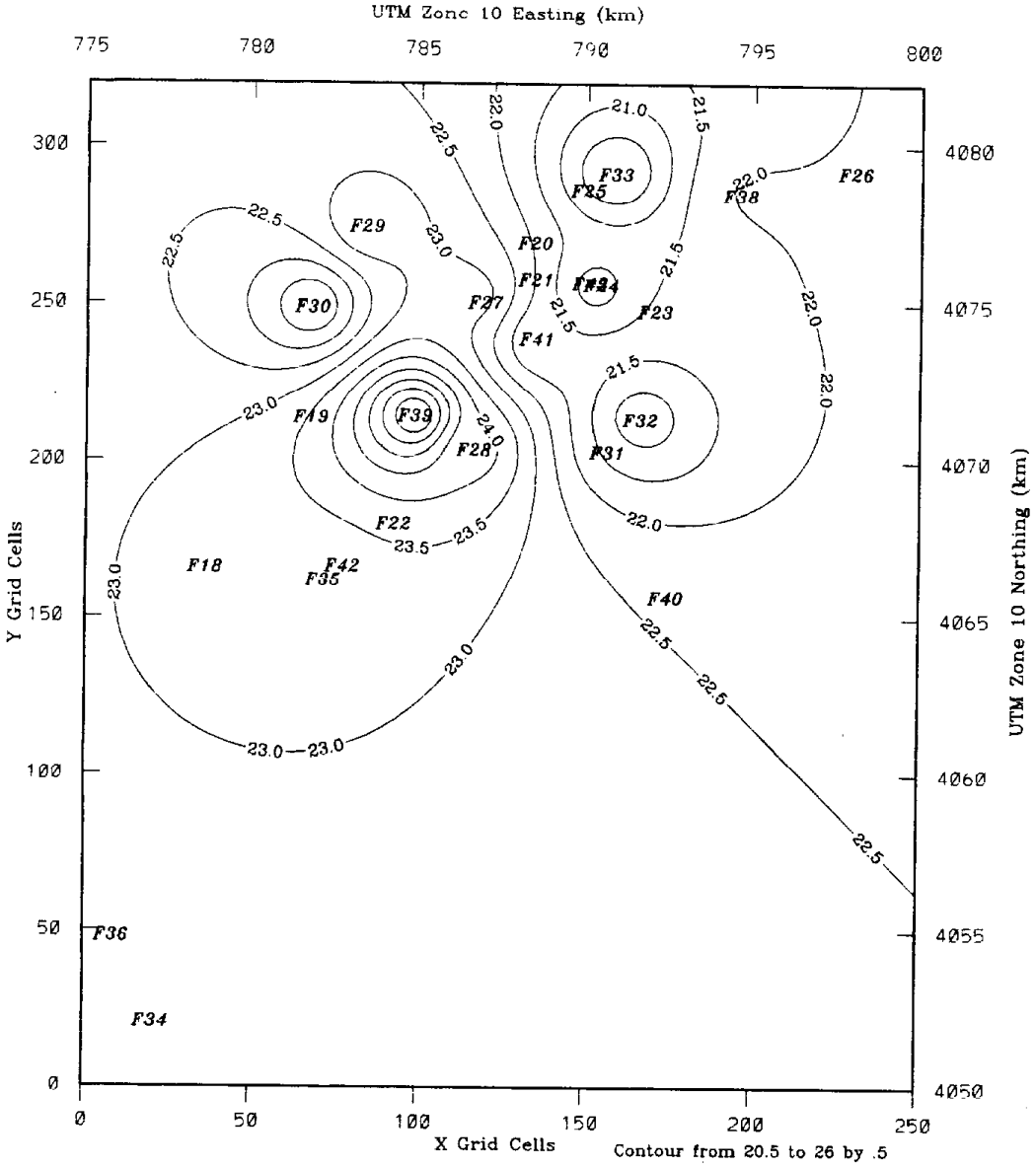

Fresno Saturation Sites, Domain: frs1, dx = 0.1 km
Contours of Secondary PM10 Mass (ug/m3)
Averaged Over Dec. 26-27 and Jan. 4-6

IMS95 Data Analysis

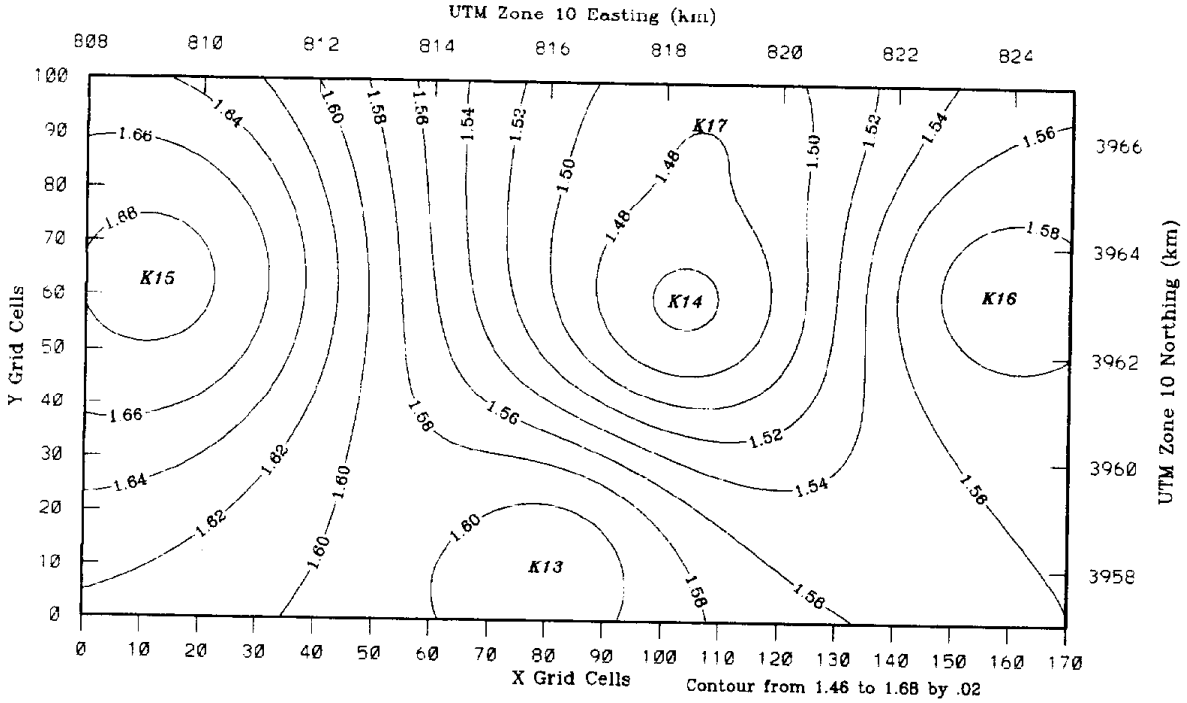

Kern Wildlife Refuge Saturation Sites, Domain: krn1, dx = 0.1 km
Contours of Crustal PM10 Mass (ug/m3)
Averaged Over Dec. 26-27 and Jan. 4-6

IMS95 Data Analysis

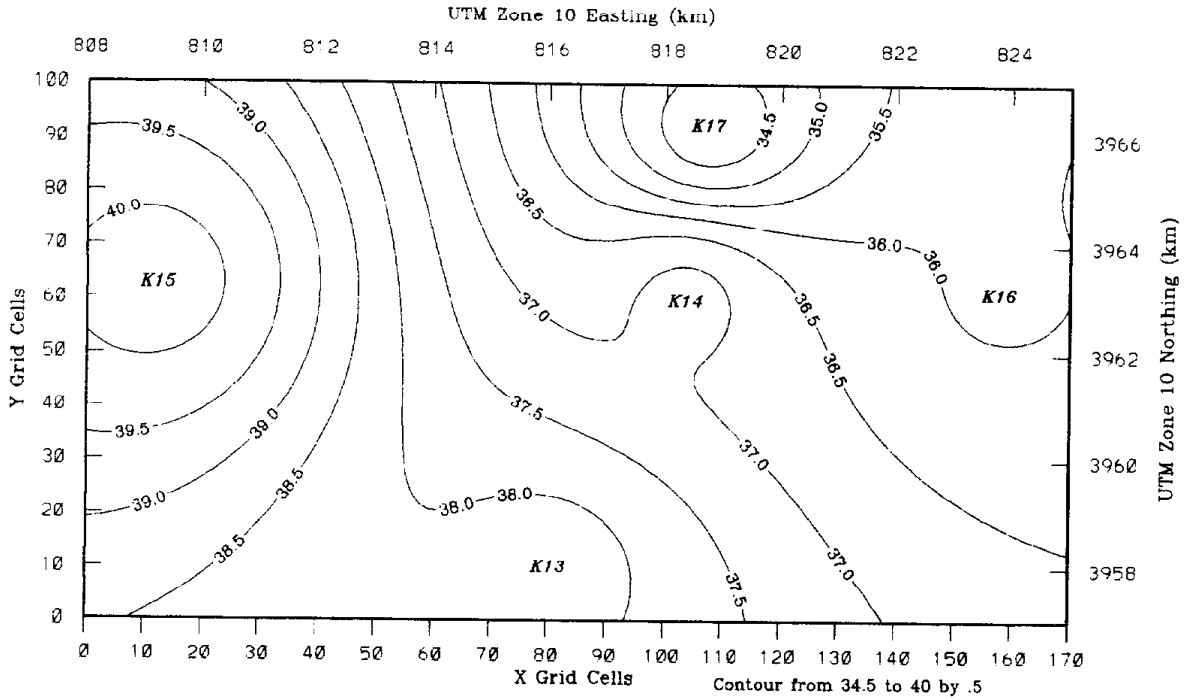

Kern Wildlife Refuge Saturation Sites, Domain: krn1, dx = 0.1 km
Contours of PM10 Mass (ug/m3)
Averaged Over Dec. 9–10, 26–28, and Jan. 4–6

IMS95 Data Analysis

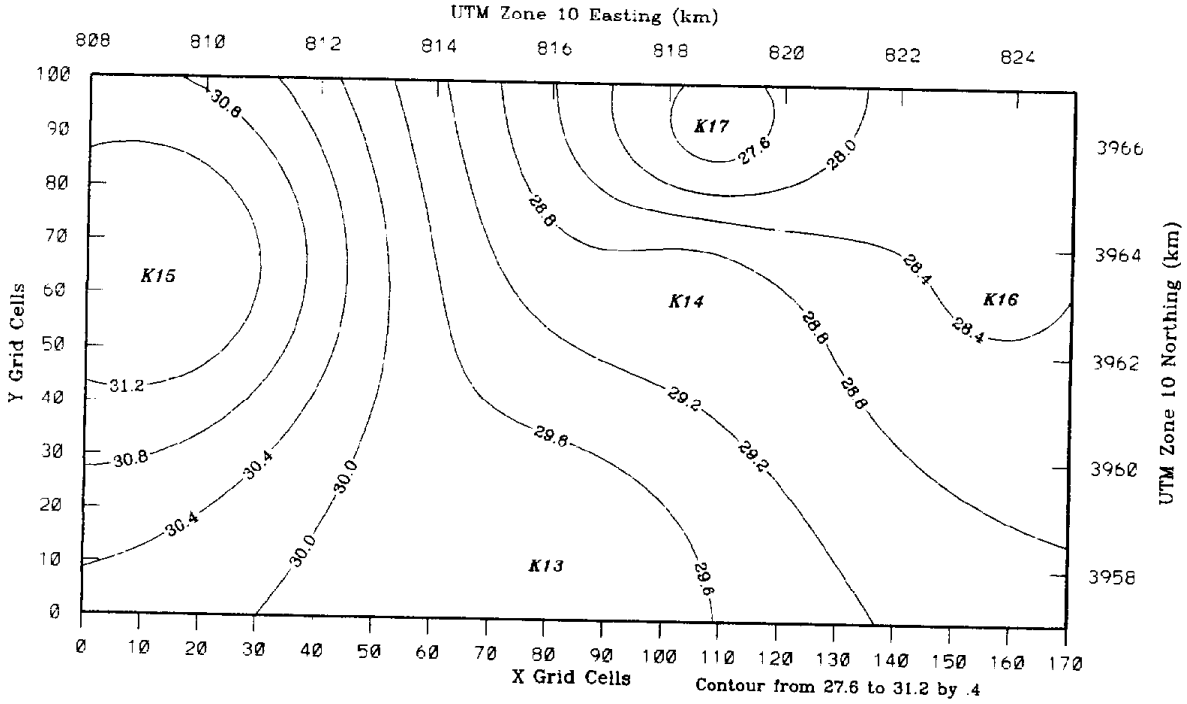

Kern Wildlife Refuge Saturation Sites, Domain: krn1, dx = 0.1 km
Contours of PM10 Mass (ug/m3)
Averaged Over Dec. 9–14, 19–31, Jan. 1–6

IMS95 Data Analysis

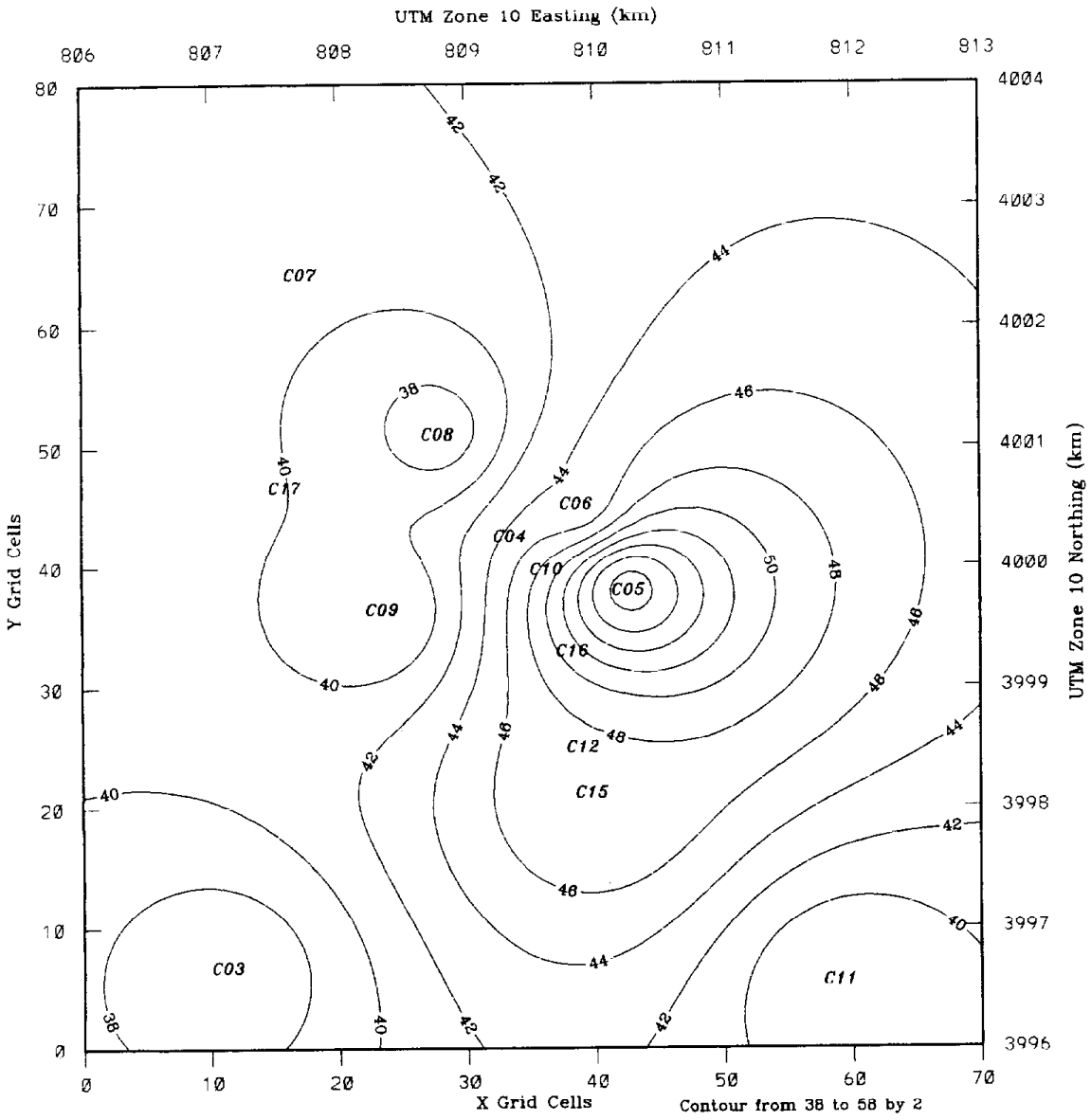

Corcoran Saturation Sites, Subdomain: cor2, dx = 0.1 km
Contours of Crustal PM10 Mass (ug/m3)
Averaged Over Nov. 6–14

IMS95 Data Analysis

APPENDIX D: MAPS OF EMISSION DENSITIES

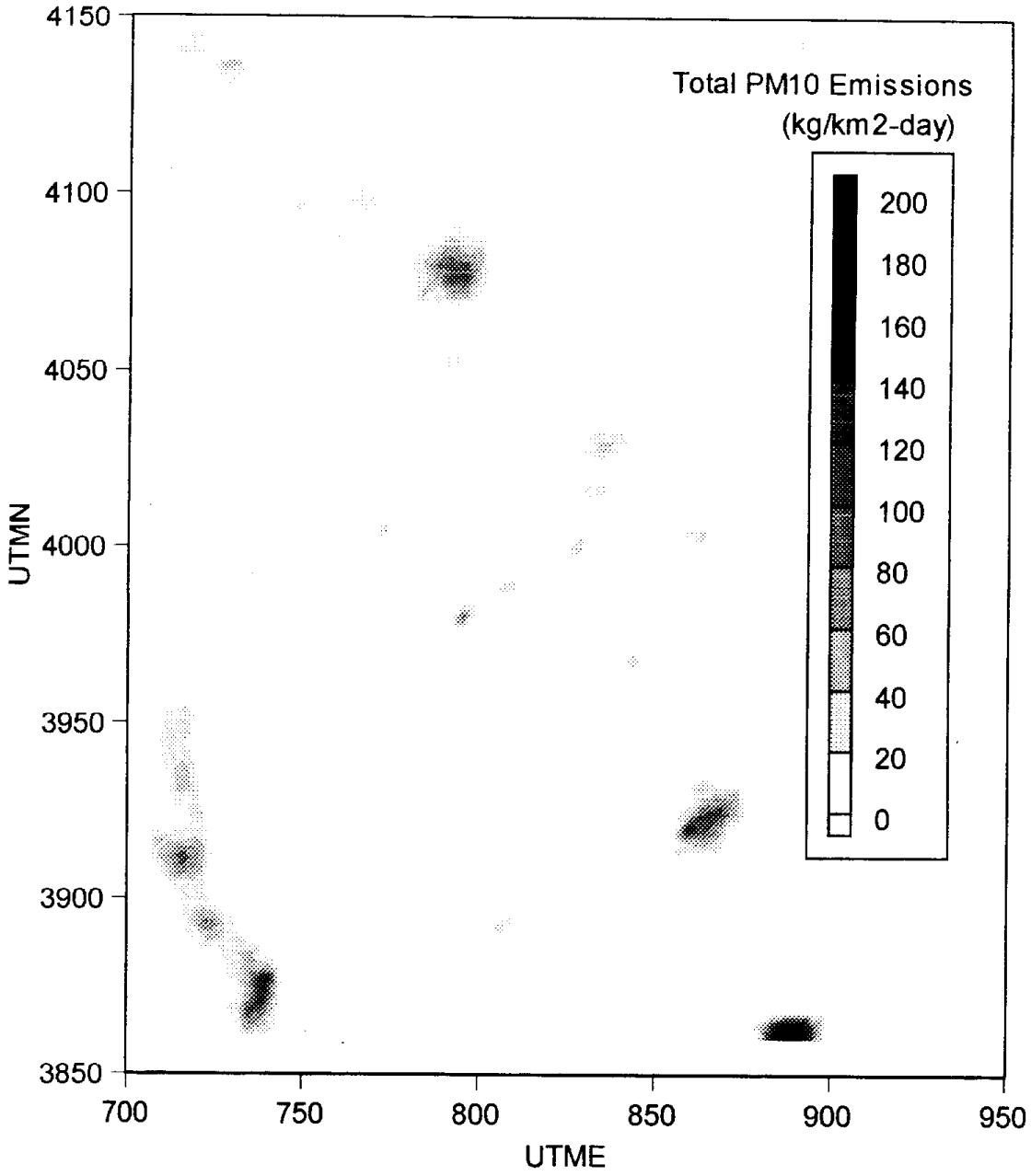

Figure 1. Total PM_{10} emissions (kg km^{-2} day^{-1}) in the IMS95 domain, January 5, 1996.

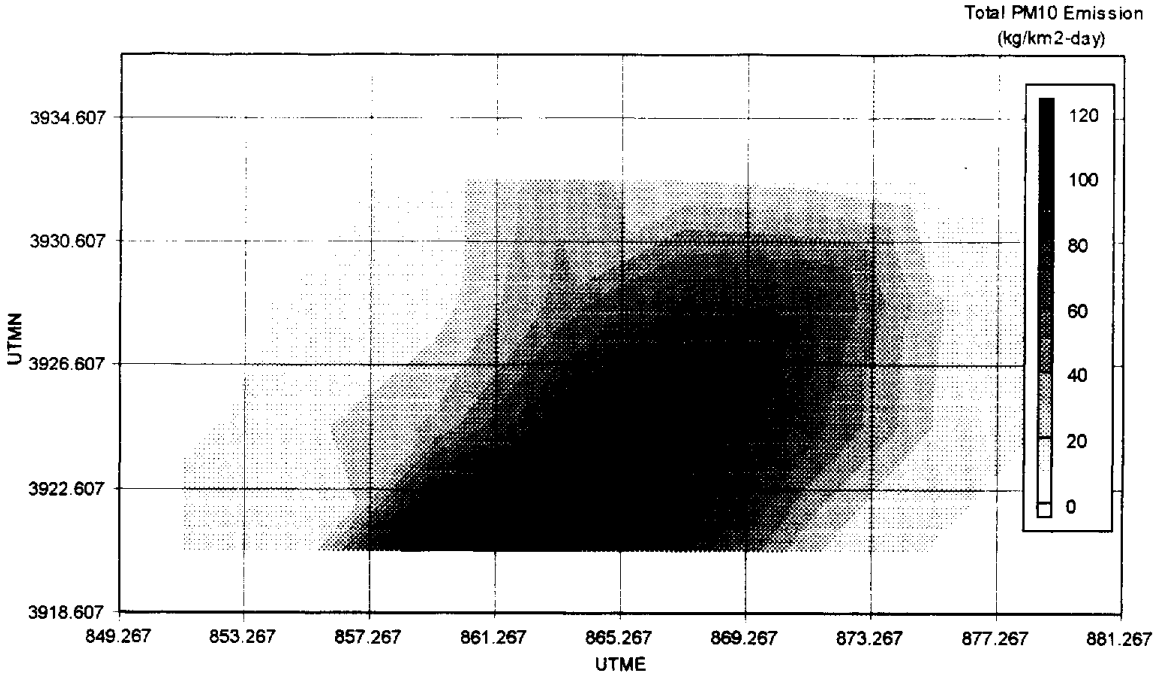

Figure 2. Total PM_{10} emissions(kg km^{-2} day^{-1}) in the Bakersfield area, January 5, 1996.

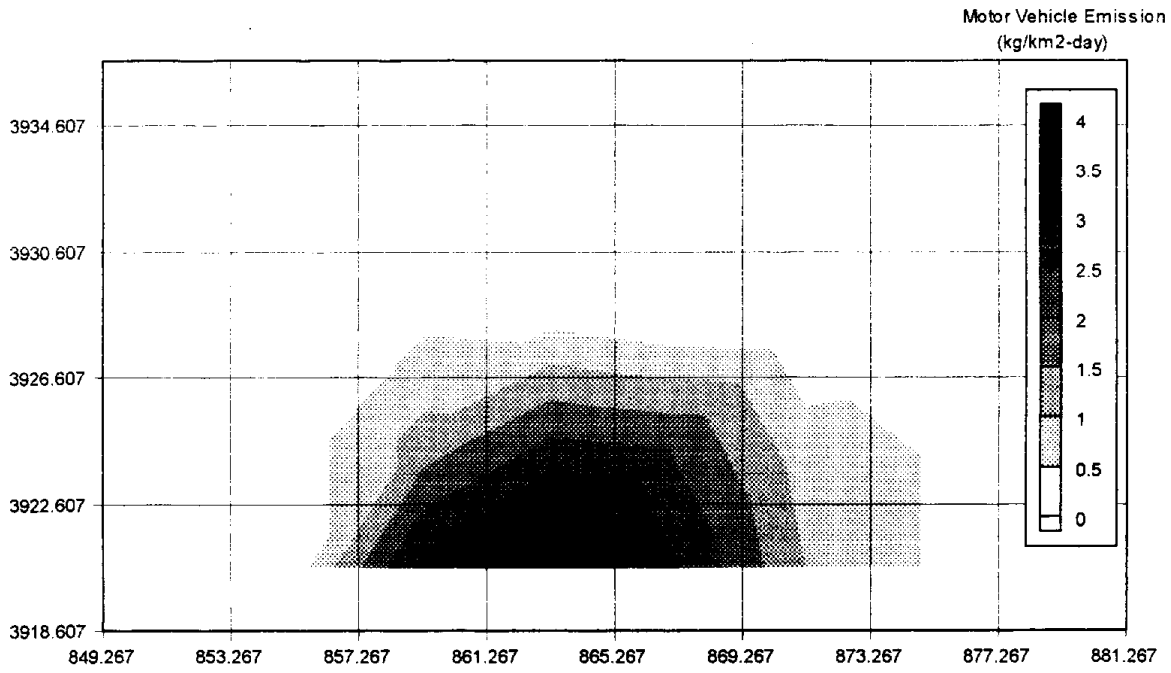

Figure 3. Total motor vehicle emissions(kg km^{-2} day^{-1}) in the Bakersfield area, January 5, 1996.

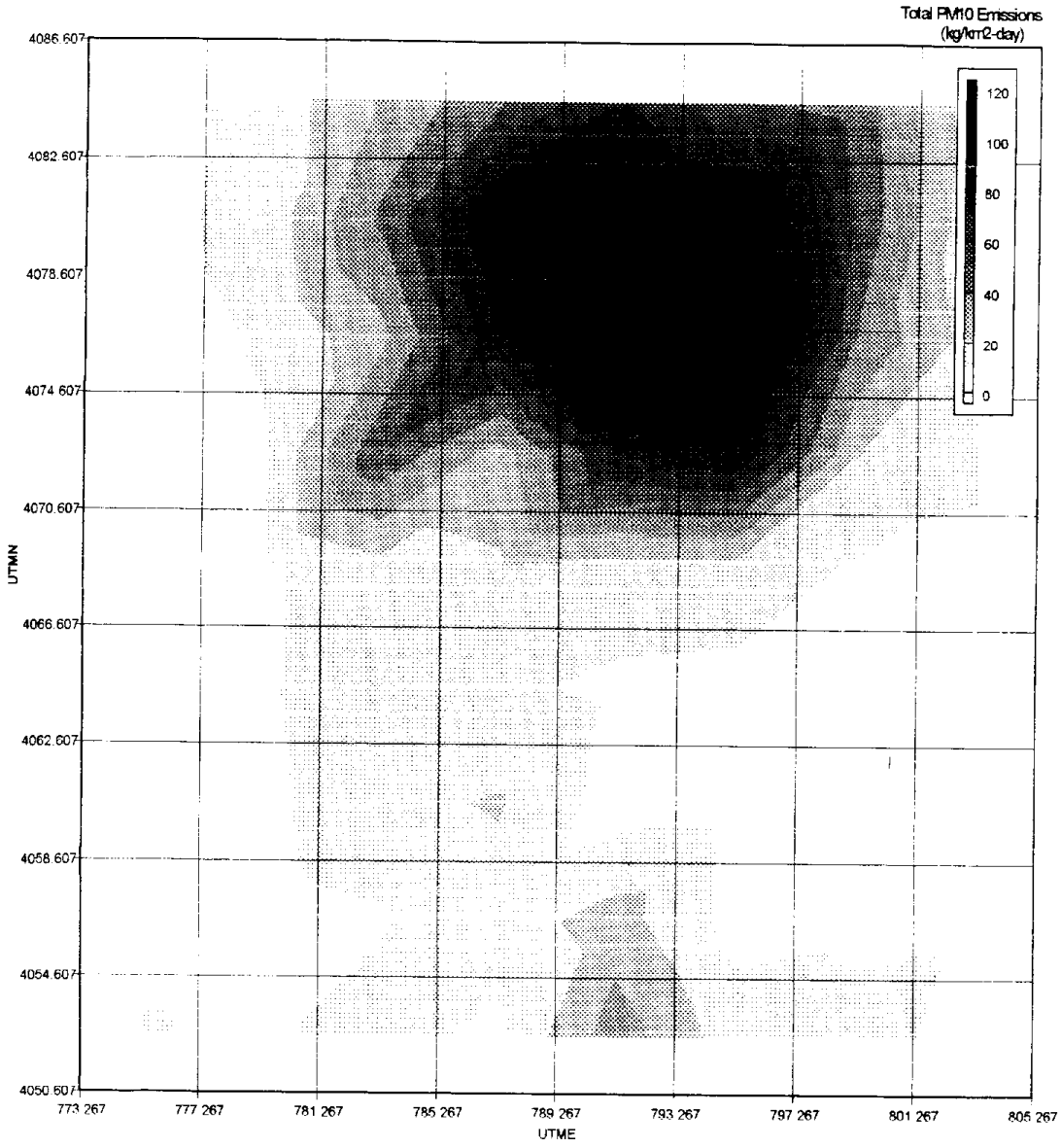

Figure 4. Total PM_{10} emissions(kg km^{-2} day^{-1}) in the Fresno area, January 5, 1996.

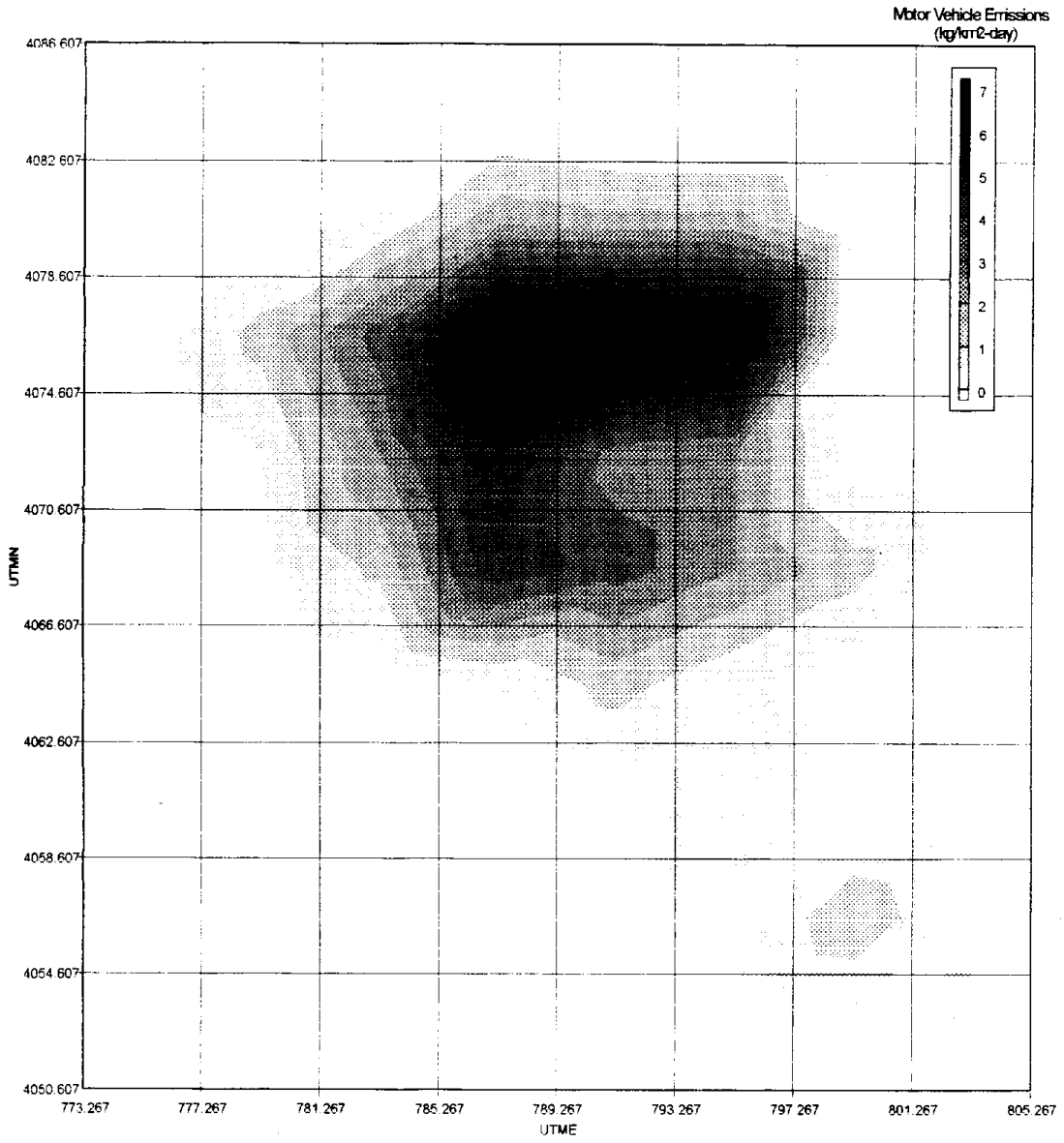

Figure 5. Motor vehicle emissions (kg km^{-2} day^{-1}) in the Fresno area, January 5, 1996.

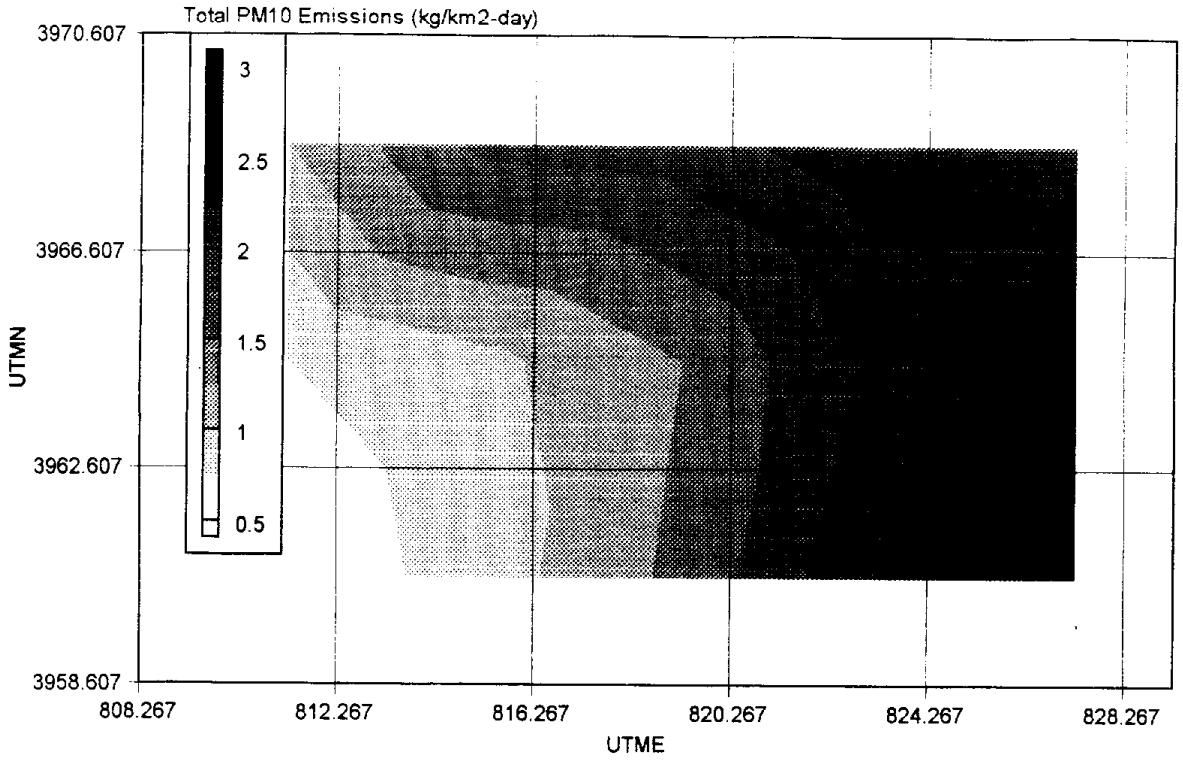

Figure 6. Total PM_{10} emissions (kg km^{-2} day^{-1}) in the Kern Wildlife Refuge, January 5, 1996.

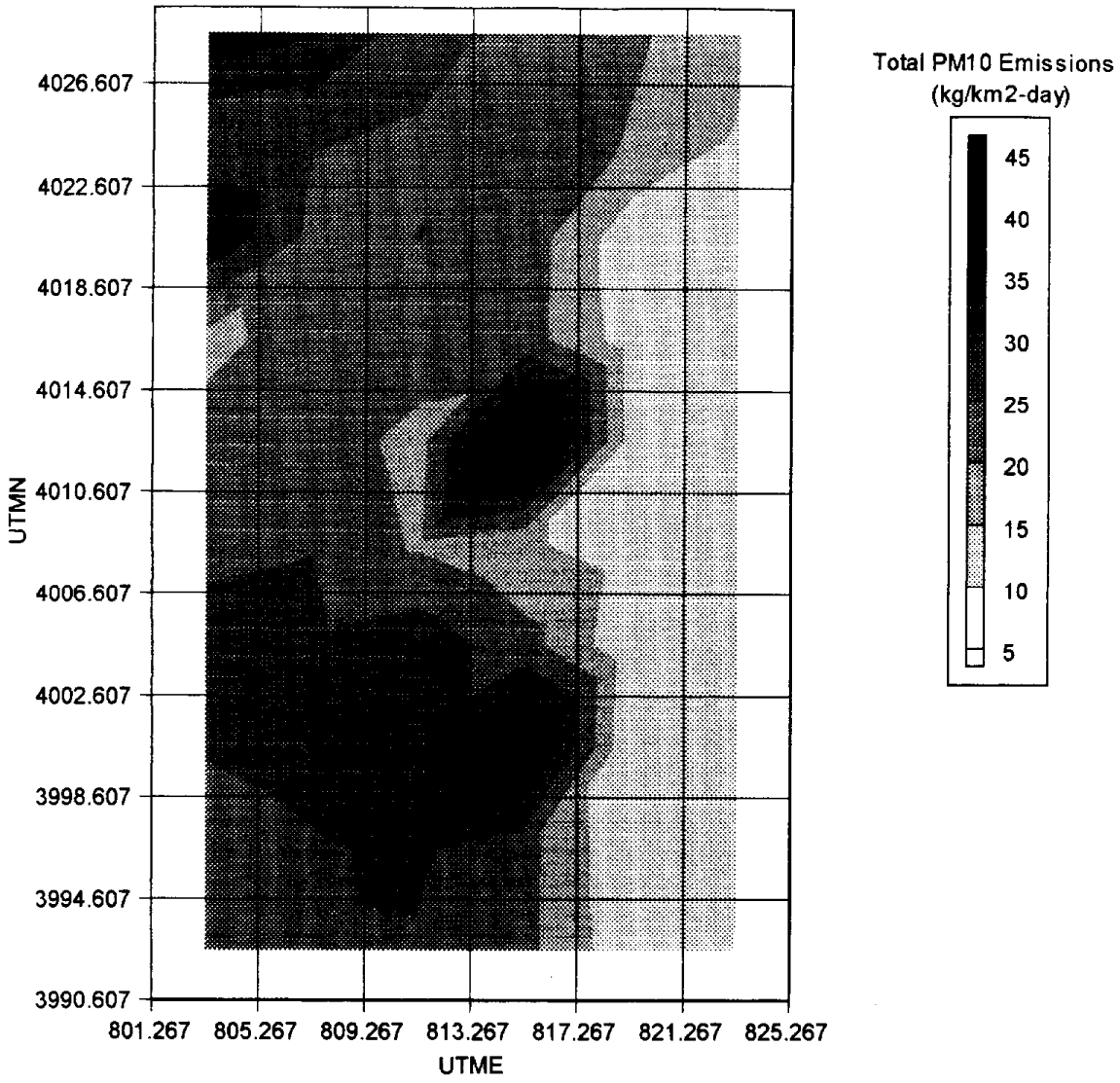

Figure 7. Total PM_{10} emissions (kg km^{-1} day^{-1}) in the Corcoran area, November 13, 1995.

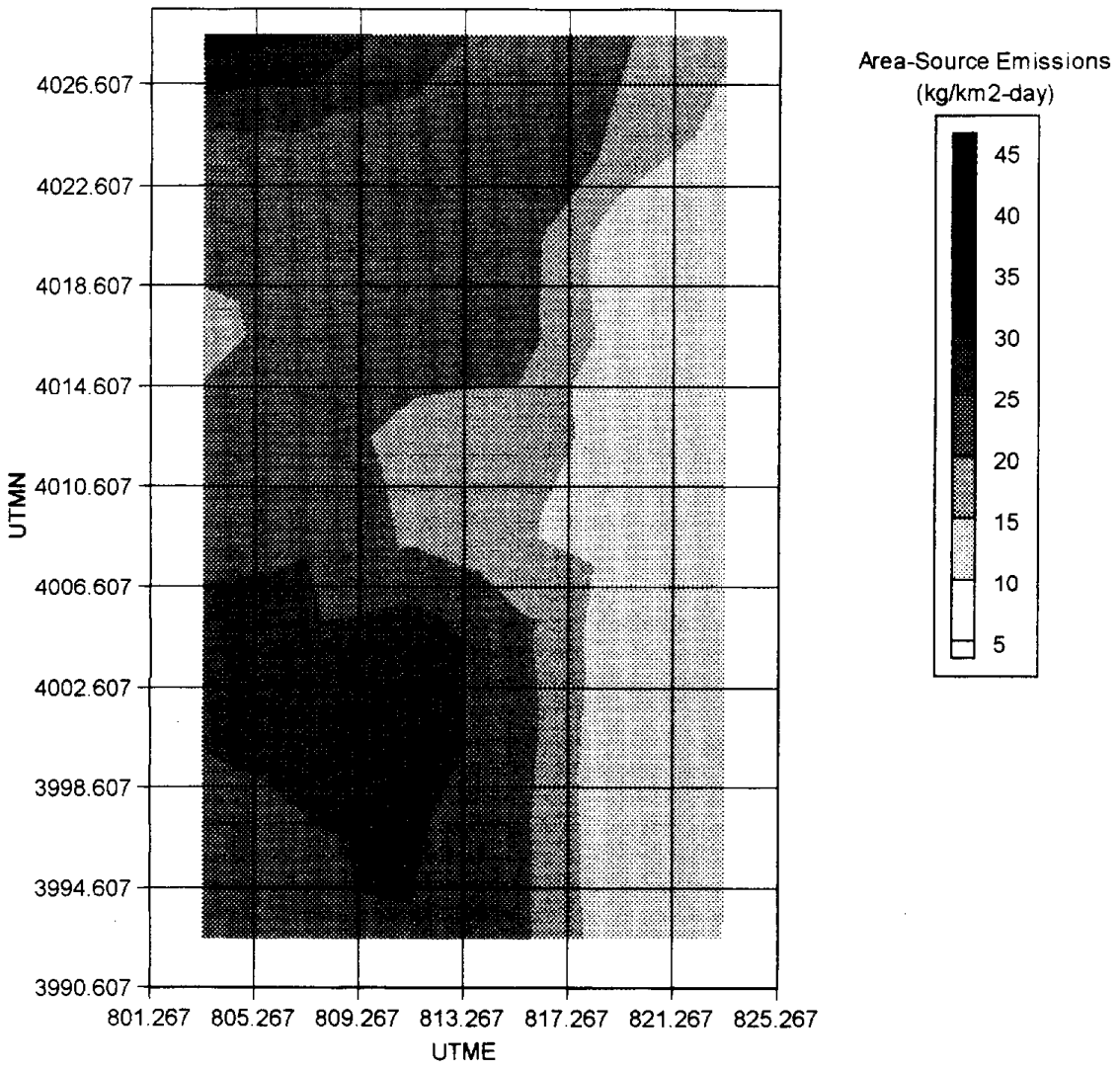

Figure 8. Area-source emissions (kg km^{-2} day^{-1}) in the Corcoran area, November 13, 1995.